Plan optimization for stereotactic radiotherapy

ISBN: 978-90-8559-406-2
Druk: Optima Rotterdam
©Copyright: 2004 American Association of Physicists in Medicine (chapter 2)
2006 Elsevier Inc. (chapter 3)
2007 Elsevier Inc. (chapter 4)
2008 Elsevier Inc. (chapter 6,7)

Plan Optimization for Stereotactic Radiotherapy

Plan optimalisatie voor stereotactische radiotherapie

Proefschrift

ter verkrijging van de graad van doctor aan de
Erasmus Universiteit Rotterdam
op gezag van de rector magnificus

Prof. dr. S.W.J. Lamberts

en volgens besluit van het College voor Promoties.

De openbare verdediging zal plaatsvinden op
16 oktober 2008 om 16:00 uur
door

Jacobus Abraham de Pooter

geboren te Terneuzen.

Promotiecommissie

Promotor:	Prof. dr. B.J.M. Heijmen
Overige leden:	Prof. dr. P.C. Levendag
	Prof. dr. J.N.M. IJzermans
	Prof. dr. M. Verheij

This thesis has been prepared at the Department of Radiation Oncology,
Erasmus MC - Daniel den Hoed Cancer Center, Rotterdam, The Netherlands.

Address for correspondence:
J.A. de Pooter
NMi-VSL
Thijsseweg 11
2629 JA Delft
Tel. +31-15 269 1623
E-mail: jdpooter@nmi.nl

Machtig zijn de werken van de Heer,
wie ze liefheeft, onderzoekt ze.
Psalm 111:2

Aan: Lycia, Simon en Mathias

Contents

Chapter 1

Introduction

1.1 Stereotactic radiotherapy

Cancer is one of the leading causes of death in the world. Next to surgery and chemotherapy, radiotherapy is one of the most used treatment modalities for cancer. About 50% of the patients with cancer will be treated with radiotherapy during the management of their disease.

In radiotherapy, ionizing radiation is used to kill proliferating tumor cells. As an unwanted (but sometimes unavoidable) side-effect, delivery of ionizing radiation to the patient may also lead to damage to healthy tissues. Generally, the total dose is delivered in a number of daily fractions. In between fractions, the healthy tissues can often more effectively repair part of the damage than tumors. Hence, the cumulative damage to tumor tissue is higher than for normal tissue when exposed to the same total dose in a large number of fractions. For most tumors and healthy tissues, this differential repair effect is enhanced with higher numbers of fractions.

Apart from fractionation, the balance between eradication of tumor cells and treatment related toxicity is also dependent on the accuracy of daily tumor localization at the treatment unit, and on the quality of the delivered dose distribution, preferentially with low volumes of critical organs irradiated to high doses. In external beam radiotherapy (EBRT), the tumor dose is delivered with a linear accelerator, using a set of treatment beams that enter the patient from different directions. For each direction, the beam is shaped according to the projection of the tumor. Beam shaping is performed with a multi-leaf collimator (MLC). In 3D conformal radiotherapy (3D-CRT), the applied beam profiles are flat or wedge shaped. In intensity modulated radiotherapy (IMRT) the beam intensity profiles are customized to optimally focus the radiation on the tumor. EBRT dose distributions are usually designed by a dosimetrist, using treatment planning software and a planning CT-scan of the patient. During treatment planning, all treatment parameters, such as the number of beams, the beam directions, intensity modulation, and beam shapes are defined.

In contrast to more conventional 3D-CRT or IMRT, for stereotactic radiotherapy the total dose is delivered in one or a small number of fractions with a high dose per fraction, resulting in a much higher biological effective dose to the tumor. For example, a fractionation schedule consisting of 3 fractions of 20 Gy, as often applied in stereotactic lung treatments, has the same biological effect as a dose of 150 Gy delivered in fractions of 2 Gy. In the latter case, 75 fractions are needed, which is generally considered too high. Therefore, stereotactic radiotherapy is well suited for treatment of tumors that are highly insensitive to radiation.

Another characteristic of stereotactic treatments is the high dosimetrical and geometrical precision. Because of the low number of fractions, the differential inter-fraction repair effect as discussed above may be much reduced in stereotactic treatments. The higher chance on toxicity related to the applied low number of fractions is counteracted by more focused dose distributions, and the increment in geometrical and dosimetrical precision, which allows for smaller target volumes yielding smaller volumes of normal tissue receiving a high dose. The focused dose distributions for stereotactic radiotherapy are characterized by a high conformality of the dose distribution to the target volume, a high dose fall-off between target volume and normal tissue, and minimization of the dose to organ at risk (OAR), which is

accomplished by advanced dose delivery techniques and optimization of the planned dose distribution.

Initially, stereotactic radiotherapy was developed for tumors inside the skull (intracranial stereotactic radiotherapy). Later on, the technique has been copied for treatment of extra-cranial tumors (stereotactic body radiation therapy, SBRT[1,2].

1.2 Outline of this thesis

This thesis discusses several techniques for more focused stereotactic irradiation of intracranial (chapter 2) and extra-cranial (liver) tumors (chapters 3 to 7). Chapter 2 investigates the advantages and feasibility of partial cone blocking in (static) arc therapy for small intracranial lesions.

Chapter 3 describes adaptations to the in-house developed beam direction and beam weight optimization algorithm ('Cycle') for SBRT. Important extensions of Cycle for SBRT are the inclusion of beam shape optimization, and the inclusion of non-coplanar beam orientations (i.e., outside the axial plane of the patient). In chapters 3 and 6, it is investigated whether automated non-coplanar beam direction optimization with the extended Cycle algorithm improves the therapeutic ratio for SBRT of liver patients treated with 3D-CRT or IMRT, respectively.

In chapter 4, Cycle is used to compare liver SBRT based on dose prescription at the surrounding 65% isodose with dose prescription at 80%. Both strategies are often encountered in literature[1,3]. In chapter 5, using Cycle, treatment plans are generated with a maximized generalized equivalent uniform dose (gEUD) for the PTV, and compared with the strategies using 65% or 80% dose prescription.

Clinical introduction of improved treatment technologies, such as daily 4D-CT image guidance for SBRT of liver tumors, may allow the use of smaller CTV-PTV margins. In chapter 7, the effect of smaller margins on the treatment planning is investigated.

Bibliography

[1] Blomgren H, Lax I, Naslund I, et al. Stereotactic high dose fraction radiation therapy of extracranial tumors using an accelerator. Clinical experience of the first thirty-one patients *Acta Oncol.* 1995;34:861–870.

[2] Timmerman RD, Kavanagh BD. Stereotactic body radiation therapy *Curr Probl Cancer.* 2005;29:120–157.

[3] Schefter TE, Kavanagh BD, Timmerman RD, et al. A phase I trial of stereotactic body radiation therapy (SBRT) for liver metastases *Int J Radiat Oncol Biol Phys.* 2005;62:1371–1378.

Chapter 2

Stereotactic arc therapy for small elongated tumors using cones and collimator jaws; dosimetric and planning aspects

JA de Pooter, M Essers, PJCM Nowak, C de Pan, BJM Heijmen, PC Levendag,
Med Phys. 2004;**31**:3444 - 51

Abstract

Purpose:
Stereotactic arc treatment of small intra-cranial tumors is usually performed with arcs collimated by circular cones, resulting in treatment volumes which are basically spherical. For non-spherical lesions this results in a sub-optimal dose distribution. Multiple isocenters may improve the dose conformity for these lesions, at the cost of large overdosages in the target volume. To achieve improved dose conformity as well as dose homogeneity, the linac jaws (with a minimum distance of 1.0 cm to the central beam axis) can routinely be used to block part of the circular beams. The purpose of this study was to investigate the feasibility of blocking cones with diameters as small as 1.0 cm and a minimum distance between the jaw and the central beam axis of 0.3 cm.
Materials and methods:
First, the reproducibility in jaw positioning and resulting dose delivery on the treatment unit were assessed. Second, the accuracy of the TPS dose calculation for these small fields was established. Finally, clinically applied treatment plans using non-blocked cones were compared with plans using the partially blocked cones for several treatment sites.
Results and conclusion:
The reproducibility in dose delivery on our Varian Clinac 2300 C/D machines on the central beam axis is 0.8% (1 SD). The accuracy of the TPS dose calculation algorithm is critically dependent on the used fits for the penumbra and the phantom scatter. The average deviation of calculated from measured dose on the central beam axis is -1.0%$\pm$1.4% (1 SD), which is clinically acceptable. Partial cone blocking results in improved dose distributions for elongated tumors, such as vestibular schwannoma and uveal melanoma. Multiple isocenters may be avoided. The technique is easy to implement and requires no additional workload.

2.1 Introduction

Small intra-cranial tumors are often treated with linac based stereotactic radiosurgery (SRS) and radiotherapy (SRT)[1] using multiple arcs with circular collimators, resulting in treatment volumes which are basically spherical. However, in general the shape of the lesion (GTV) and the Planning Target Volume (PTV) are non-spherical.

Therefore, to improve the dose conformity to the target volume, arcs with multiple isocenters, each using a smaller cone size for collimation, are often applied clinically. A disadvantage of this technique is the increase in dose inhomogeneity in regions where arcs with different isocenters overlap. Large overdosages in the PTV, and perhaps in small areas of normal tissue, will be present[2]. Other disadvantages of using multiple isocenters are the geometrical set-up inaccuracy introduced when changing from one isocenter to the other, and the increase in treatment time.

By partially blocking the circular collimator opening with the collimator jaws, the dose distribution becomes more elliptical[1]. This solution is routinely available in the Radionics XKnife software* for cones having a diameter of 2.0 cm and larger, and jaw positions equal to or larger than 1.0 cm from the central beam axis. Bellerive et al.[1] compared dose distributions for arc treatments with circular cones using either single or multiple isocenters with arc treatments using partially blocked cones. They concluded that by using partially blocked cones for lesions greater than 3.0 cm in maximum extent, the dose homogeneity in the target volume was increased, while the dose delivered to healthy tissue was reduced. Hacker et al.[3] compared single isocenter stereotactic arc treatment plans using cones, four independent static jaws (i.e., without a cone) and an 'ideal' collimator.

The latter collimator adjusts its shape continuously in such a way, that its projection in the beams eye view (BEV) always matches the projection of the PTV in the BEV. For tumors with a maximum extent larger than 3.5 cm, the dose conformity to the target volume using four independent jaws was much better than using cones. The mean volume of involved normal tissue at the prescription dose was reduced by 57% if the collimation was performed either with four independent jaws or with an 'ideal' collimator instead of a cone. For lower doses, the volume of involved normal tissue was further reduced by using the 'ideal' collimator instead of the jaws. In a modeling study, Nedzi et al[4] compared several dynamic (i.e., the collimator shape changes during the arc) field shaping devices, including both an 'ideal' collimator and a cone dynamically blocked with the jaws, with a conventional cone, for tumors with a maximum dimension between 2.0 and 4.2 cm. The treatment volume ratio (TVR; target volume divided by the treatment volume at the prescription dose) was increased from 37% for a conventional cone to 44% for the dynamic jaw collimator and to 55% for the 'ideal' collimator.

Miniature Multileaf Collimators (MMLC), having leaf widths of 3-5 mm at isocenter[2,5,6] can also be used for the stereotactic treatment of intra-cranial lesions, either using multiple static beams[2,5], using dynamic arcs[7] or using static intensity modulated beams[5,7] Their usefulness in improving target conformity has especially been demonstrated for lesions

*Radionics, Thyco Healthcare, Burlington, MA

$>$ 3 cm. Techniques using dynamic arcs and IMRT beams are more complicated and require a more extensive quality assurance than techniques using cones.

In this paper, we investigate the feasibility of using partially blocked cones with diameters as small as 1.0 cm, and with a minimum jaw position of 0.3 cm from the central beam axis, to improve target conformity for small elongated tumor volumes. Because the fields are very small, a small deviation in jaw position may introduce considerable deviations in the delivered absolute dose value, and the total high dose volume. Therefore, the reproducibility in jaw positioning and resulting dose delivery of these small fields was investigated. Second, the accuracy of the treatment planning system (TPS) dose calculation was investigated for these small fieldsizes. The calculations of the TPS were compared with absolute measured dose values on the central beam axis, and with measured profiles. Finally, several clinical treatment plans were compared with plans using partially blocked cones. The presented tumor sites are a vestibular schwannoma and a uveal melanoma.

2.2 Materials and methods

2.2.1 Treatment Unit

In our institution, stereotactic arc treatments are performed using the 6 MV beam of a Varian Clinac 2300 C/D[†] accelerator. Circular collimators (Radionics) (cones) are available with diameters ranging from 0.5 cm to 5.0 cm at isocenter, with an increment in diameter of 0.25 cm. Partial blocking of the cones is performed using the four independent jaws of the accelerator. With these jaws, any rectangular field can be set, with a resolution in jaw position of 1.0 mm. Any jaw that is not used to block part of the cone is set at a distance of 3.0 cm from the central beam axis.

2.2.2 Treatment Planning System

The XKnife TPS is used for treatment planning[8] The dose, D, for a partially blocked field in a point x,y,z is calculated using the following algorithm:

$$\begin{aligned} D(d,s_{jaw},s_{net},x,y,z) =& M \times S_c(s_{jaw}) \times S_p(s_{net}) \\ & \times \mathrm{TMR}(d,s_{net}) \times \Phi(x_0,y_0) \times \frac{\mathrm{SAD}^2}{(\mathrm{SAD}-z)^2} \qquad (2.1) \\ \text{with } \Phi(x_0,y_0) =& \mathrm{OAR}(x_0,y_0) \times P_{x_1} \times P_{x_2} \times P_{y_1} \times P_{y_2} \end{aligned}$$

The factor M relates the reference field in XKnife to the linac calibration field. S_c is the collimator scatter factor as a function of the equivalent square field width, s_{jaw}, of the jaw field (the cone is ignored in the calculation of s_{jaw} because its influence on the collimator scatter can be neglected). S_p is the phantom scatter factor as a function of the equivalent square field width, s_{net}, of the field shaped by the jaws and the cones at the patient skin. The Tissue Maximum Ratio, TMR, is a function of s_{net} and the depth in the patient, d. Φ accounts for the off-axis dose distribution by multiplication of the OAR, the off-axis ratio measured

[†] Varian Assoc., Palo Alto, CA

for the cone, with the product of the jaw penumbra factors, P_{x_1}, P_{x_2}, P_{y_1}, P_{y_2} [9]. x_0 and y_0 are the lateral coordinates x,y scaled to the isocenter plane. SAD is the Source to Axis Distance and z is the coordinate along the central beam axis in the direction of the linac isocenter.

Measured S_c and S_p data are fitted to a simple function with the variable s as the width of the equivalent square field.

$$S_{c,p}(s) = a_{c,p} - b_{c,p}\exp(-c_{c,p}s) \tag{2.2}$$

The algorithm (Eq. 2.1) uses these fitted functions to determine S_c and S_p by substituting their corresponding equivalent square field width.

Penumbra Factor

Fits to the penumbras of the measured inline and crossline profiles for a 4 cm square field are required to determine the penumbra factors, P_{x_1}, P_{x_2}, P_{y_1}, P_{y_2}. The penumbra of the actual profile has to be fitted to the following equation:

$$P = \begin{cases} 1 - 0.5\exp(-a_{in}|x|) & \text{for } x < 0 \text{ (inside the field)} \\ T_0 + (0.5 - T_0)\exp(-a_{out}|x|) & \text{for } x > 0 \text{ (outside the field)} \end{cases} \tag{2.3}$$

T_0 is the jaw transmission factor, a_{in} and a_{out} are the penumbra fit parameters, respectively inside and outside the field. The 50% value of each penumbra factor coincides with the edge (at $x = 0$) of the corresponding jaw.

For jaw settings smaller than 1.0 cm from the central beam axis the influence of the penumbra on the central axis dose increases. Because the accuracy of the algorithm is assessed for these jaw settings, it is crucial that the correct penumbra fit is applied. The penumbra profile was determined using a diode with an effective detection diameter of 2.5 mm. This measured profile is a convolution of the actual profile with the response kernel of the diode detector[10]. The smoothing effect of the diode on the measured profile was eliminated by fitting the convolution of the penumbra factor function (Eq. 2.3) with the gaussian response kernel of the diode detector[11] to the measured profile using the least squares method. The parameters a_{in}, a_{out} and T_0 resulting from the best fit, determine the deconvolved penumbra fit. The deconvolved penumbra fit results in a reduction of 0.6 mm of the 20%/80% penumbra width, from 3.1 mm to 2.5 mm (Fig. 2.1), which agrees with previous investigations[11,12] where a reduction of 0.5 mm in the 20%/80% penumbra was observed using a diode with a diameter of the sensitive volume of 2.5 mm. As shown in Fig. 2.1, for jaw settings closer than 0.8 cm to the central beam axis, it is important to apply a deconvolution to the measured profile, otherwise large inaccuracies in calculated dose values on the central beam axis can be present: e.g., at 3 mm from the field edge, the deconvolved fit is about 3% higher than the measured fit.

Phantom Scatter

S_p is measured directly, using a constant linac collimator opening of 6.0×6.0 cm^2 (resulting in a constant collimator scatter, S_c), and only changing the cone diameter (Fig. 2.2). These measured S_p values are fit to the function in Eq. 2.2, using the relation $s = 0.891 \cdot d$ for the

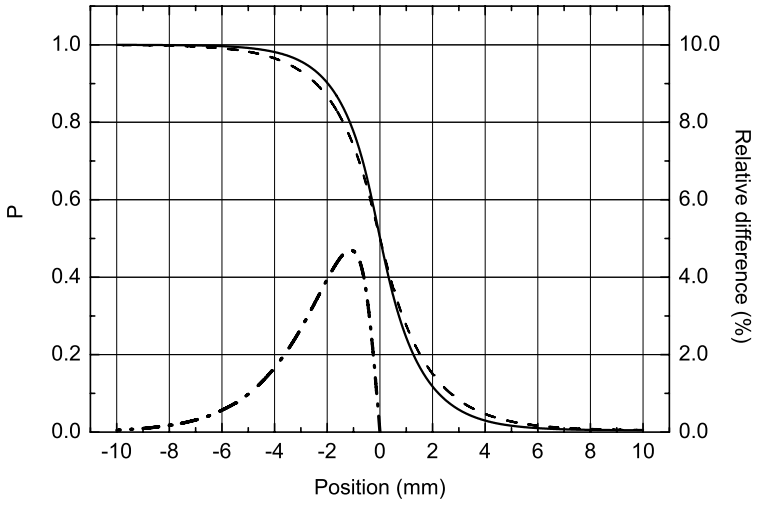

Figure 2.1: Penumbra fits based on a measured profile for a 4 × 4 cm^2 field; including the spatial smearing of the detector (dashed line), and after applying a deconvolution to eliminate the spatial influence of the diode detector (solid line), and the relative difference between both fits (dash-dotted line).

equivalent square field width of a circular field[13] where d is the diameter of the circular field.

For circular fields with a diameter less than 2.0 cm, the dose on the central beam axis is highly influenced by lateral electron disequilibrium[14]. Therefore the phantom scatter cannot be measured directly for these fields. Our investigations demonstrate that a fit based on measurements for field diameters of 2.0 cm and larger corresponded very well to the data of Bjärngard et al.[14], who determined the phantom scatter as a function of field diameter for a clinical 6 MV beam using Monte Carlo simulations (Fig. 2.2). In the TPS algorithm (Eq. 2.1), the electron disequilibrium on the central beam axis caused by small jaw settings is taken into account by the penumbra factors (Eq. 2.3).

2.2.3 Measurements and calculations

Reproducibility in jaw positioning and dose delivery

The reproducibility in jaw positioning and resulting dose delivery was determined for a set of 15 square and rectangular fields. The minimum distance of each jaw to the central beam axis was 0.3 cm. Realized jaw positions were measured using the light field of the linac, as well as using X-ray films (Kodak X-Omat V). The dose measurements were performed at the isocenter at the depth of dose maximum with a diode in a water phantom[‡] To determine the short term reproducibility, the set of fields was set up five times in random order and the jaw

[‡]Wellhöfer-Scanditronix, IBA, Husbyborg, Uppsala, Sweden

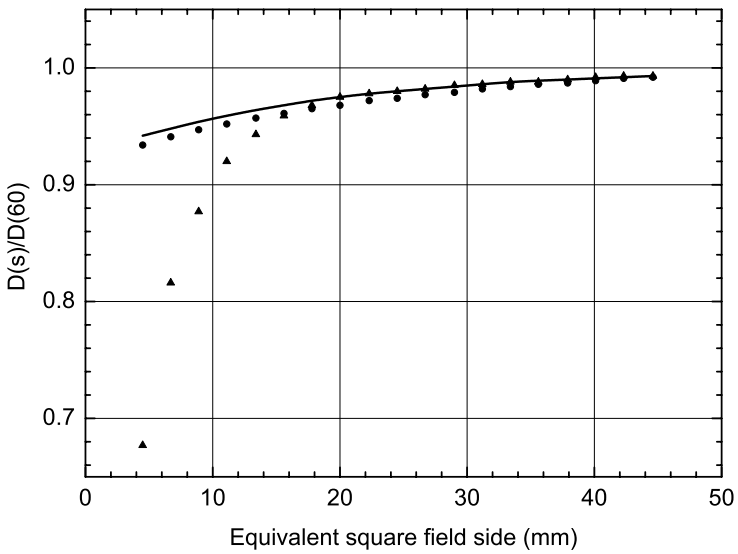

Figure 2.2: Central axis ionization measurements (triangles) at depth=d_{max} for cones with the collimator jaws fixed at 6.0 × 6.0 cm^2 plotted against the equivalent square field width, s. The measurements are normalized to the measurement for a 6.0 × 6.0 cm^2 open field. The corrected values (solid line) based on a fit to the measured data for cone diameters of 2.0 cm and larger, and the Monte Carlo derived S_p data by Bjärngard et al.[14] (circles) are plotted. The equivalent square field width, s, is related to the diameter, d, of the cones by $s = 0.891 \cdot d$[13].

positions as well as the dose delivery were measured. To check the long term stability, the measurements were repeated during a period of 2 months.

Accuracy of the dose calculation algorithm

Clinically, the TPS dose calculation algorithm is used for blocked cones with a minimum distance between the jaw edge and the central beam axis of 1.0 cm. To investigate the accuracy of the dose calculations for jaw positions closer to the central beam axis, with a minimum distance of 0.3 cm, absolute and relative dose calculations were compared with measurements.

First, the absolute dose at the central beam axis at 1.5 cm depth was measured to assess the accuracy of the absolute dose calculations for a set of 60 symmetric rectangular fields with dimensions between 0.6 × 0.6 cm^2 and 6.0 × 6.0 cm^2. In addition, the absolute dose at the central beam axis was measured for a set of 290 fields shaped by partially blocked cones (with diameters of 1.0, 1.5, 2.0, 3.0 and 4.0 cm). Symmetric and asymmetric jaw settings were applied. The absolute dose measurements for the partially blocked cones were performed at four depths: 1.5, 5, 10 and 15 cm. The measurements were normalized to the value measured at d_{max}(= 1.5 cm) for a 10 × 10 cm^2 field at a source to skin distance of 100 cm. This field is the calibration field of the linac, for which 1 monitor unit equals 1 cGy.

Second, measured and calculated profiles in the X and Y direction at different depths (1.5–15 cm) were compared for a set of partially blocked fields with cone diameters ranging from 1.0 to 3.0 cm and with varying jaw settings. The isocenter was positioned either at 1.5 or 5.0 cm depth. All measurements were performed using the same shielded diode and water phantom used to acquire the input data for the TPS.

2.3 Results and discussion

2.3.1 Reproducibility

Our investigations demonstrate that the short and long term reproducibility in jaw positioning of our Varian 2300 C/D machines is 0.3 mm (1 SD), independent of fieldsize, gantry angle and collimator angle. For rectangular fields larger than 0.8×0.8 cm^2, the short and long term dosimetric reproducibility was within 0.4% (1 SD). For fields with a width of 0.6 cm, the reproducibility in delivered dose was within 0.8% (1 SD). Using the dose calculation algorithm (Eq. 2.1), the variation in dose delivery resulting from the variation in jaw positioning was estimated, and turned out to be of the same order as the actually measured dose reproducibility. It is important to note that in our experience the actual reproducibility in jaw positioning is much better than 1.0 mm which is specified by the Varian Acceptance Procedure. These results indicate that the Varian 2300 C/D machine is suitable for accurate and reproducible dose delivery using very small fields[15] with a minimum fieldside of 6 mm.

Cone Diameter (cm)	d (cm)	X (%)	S (%)	Max (%)
1.0	1.5 and 10	1.0	1.9	4.3
1.5	1.5	0.3	1.3	2.3
1.5	10.0	-0.1	1.2	2.2
2.0	1.5	-0.8	1.1	2.9
2.0	5.0	-1.5	0.8	2.7
2.0	10.0	-1.8	0.9	3.8
2.0	15.0	-2.2	0.9	3.8
3.0	1.5	-1.2	1.0	2.9
3.0	10.0	-2.2	1.5	3.5
4.0	1.5	-1.3	0.6	2.4
all cones	all depths	-1.0	1.4	4.3

Table 2.1: Average deviation, X, of calculated from measured dose on the central beam axis, spread, S, around this average, given as one standard deviation, and maximum deviation, Max, for a large set of partially blocked fields, for several cone diameters and depths. The results for the 1.0 cm cone are combined for both depths, because the number of partially blocked fields that can be set up is small for this cone.

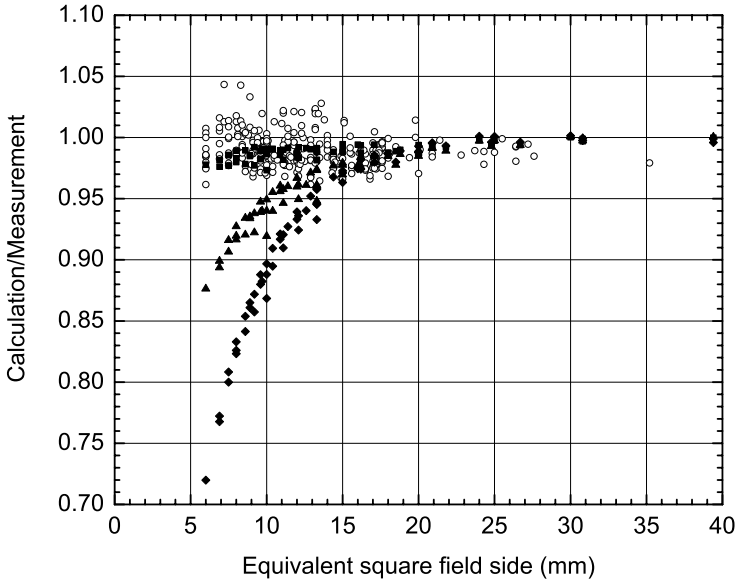

Figure 2.3: Ratio of calculated and measured dose on the central axis, for partially blocked cones (open circles), and symmetric rectangular fields at depth=1.5 cm (squares). For symmetric rectangular fields calculations were also performed using the non-deconvolved penumbra fit (triangles), and using the S_p fit, based on measured data, that are not corrected for electron disequilibrium, at depth=1.5 cm (diamonds).

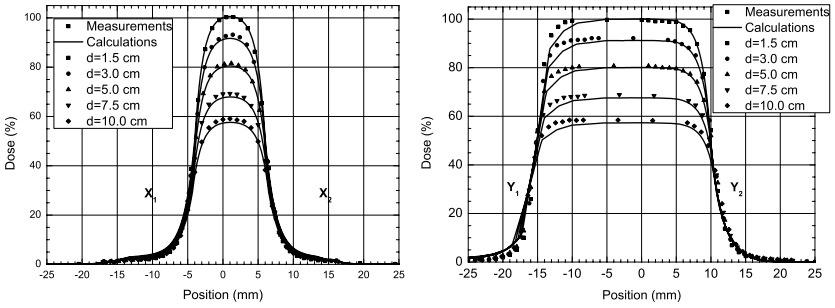

Figure 2.4: Profiles for a partially blocked cone at different depths (1.5, 3.0, 5.0, 7.5 and 10 cm) in (a) the X-direction and (b) the Y-direction, for a 3.0 cm diameter cone, blocked with the collimator jaws X_1 at 0.4 cm, X_2 at 0.6 cm and Y_2 at 1.0 cm from the central beam axis.

2.3.2 Dose calculation accuracy of the treatment planning system

Dose calculation on the central beam axis

Measurements and calculations were compared for partially blocked fields with diameters ranging from 1 to 4 cm, at 1.5, 5.0, 10 and 15 cm depth. Many asymmetric jaw positions were investigated. Using the S_p fit corrected for electron disequilibrium, and the deconvolved penumbra fit, the average deviation of the calculated from the measured central axis dose for the complete set (for all depths and cone diameters) of partially blocked fields was -1.0%±1.4% (1 SD), see Fig. 2.3. The deviations for different cone diameters and depths are summarized in Table 2.1. For the set of rectangular fields (i.e. without cone) the accuracy of the calculated central axis dose at a depth of 1.5 cm was -1.2%±0.6% (1 SD), see Fig. 2.3.

The importance of using the deconvolved penumbra fit is demonstrated in Figs. 2.1 and 2.3. Using the measured non-deconvolved penumbra fit, the calculations indicate an increasing deviation from measurements with decreasing field size. In the algorithm, the penumbra factors of four jaws are multiplied, which explains the $4 \times 3\% = 12\%$ difference in deviation for a 0.6×0.6 cm^2 field, when the non-deconvolved fit is used in the calculation (Fig. 2.1). Therefore the deconvolved fit has been demonstrated to provide a superior fit.

As shown in Figs. 2.2 and 2.3, it is also important to use the correct S_p fit, where the influence of electron disequilibrium is eliminated. If the actual measured data for field diameters smaller than 2.0 cm would have been used to determine the S_p fit, the penumbra influence would have been taken into account twice (by the S_p and the penumbra factor), resulting in very large deviations of the calculated from the measured dose.

Relative dose calculations

Examples of measured and calculated profiles are shown in Figs. 2.4 (three jaws are used to block the cones) and 2.5 (only the X-jaws are used to block the cone). In these examples, the isocenter is situated at 1.5 cm depth (Fig. 2.4), and at 5 cm (Fig. 2.5). The normalization point is situated on the central beam axis at depth=1.5 cm, where the measured profiles are normalized at 100%, and the calculated dose is 100% multiplied by the ratio between the calculated and the measured absolute dose. In this way, the absolute dose deviation is given for all positions.

In the shown examples as well as in all other investigated situations, the geometrical deviation in penumbra position is less than 1.0 mm on the sides that are blocked by a jaw. On the sides that are not blocked by one of the jaws, the maximum geometrical deviation in penumbra position is 1.5 mm. The sides that are blocked by the jaws show a deviation in absolute dose of 2% for all off-axis positions. The largest dose deviations are observed at the sides that are not blocked by the jaws (Y_1 in Fig. 2.4(b), and Y_1 and Y_2 in Fig. 2.5(b)). The maximum deviation between the calculated and measured dose was 5%.

The 5% deviation in absolute dose occurs for off-axis positions at larger depth (7.5-15 cm) on the profile parallel to the jaw edge. This is explained by the following: with decreasing field width normal to the profile direction, the shape of the profile becomes more flat (Fig. 2.6(a)). Compared to the open cone, the reduction in dose due to electron disequilibrium is higher on the central beam axis (point C, Fig. 2.6(b)) than at off-axis positions (e.g. point P),

because the latter were already closer to the field edge. The algorithm uses the OAR for an open cone, and does not correct for this flattening effect, which results in larger deviations from the actual measured data. For a clinical treatment plan, the largest deviation of the sum of all arcs will be much smaller. Therefore the dose calculation accuracy for these small fields is sufficient for clinical use.

2.3.3 Comparison of clinical treatment plans

Case 1: Vestibular Schwannoma

In our institute, vestibular schwannomas are treated either with stereotactic radiosurgery or with stereotactic radiotherapy. Most schwannomas have an elongated shape, so multiple isocenters often have to be applied. With stereotactic radiosurgery the target receives a dose of at least 12 Gy in a single fraction. Critical structures located close to this benign lesion are the brain stem and the trigeminal nerve. The maximum delivered dose to these structures should be below 10 Gy and 8 Gy, respectively. Moreover, the vestibulocochlear and facial nerves are located inside the target volume. To preserve the function of these nerves, high overdosages (larger than 15 Gy) should be avoided. Typically, in treatment plans with multiple isocenters the maximum dose is 150% of the prescription dose; in our case 18 Gy. If patients have functional hearing, fractionated stereotactic radiotherapy is applied, using 12 fractions of 2.8 Gy.

For the presented vestibular schwannoma patient, the original plan consisted of two isocenters, with a 1.5 cm cone and a 0.75 cm cone. For the plan that uses partially blocked cones, one isocenter was applied using a 2 cm partially blocked cone. The original plan resulted in a large dose inhomogeneity in the PTV, up to 175% of the prescribed dose (Fig. 2.7). Because the patient had functional hearing, he was originally treated with fractionated stereotactic radiotherapy with 12 fractions of 2.8 Gy. For comparison purposes the dose volume histograms for the original plan are displayed (Fig. 2.7) with a normalization of

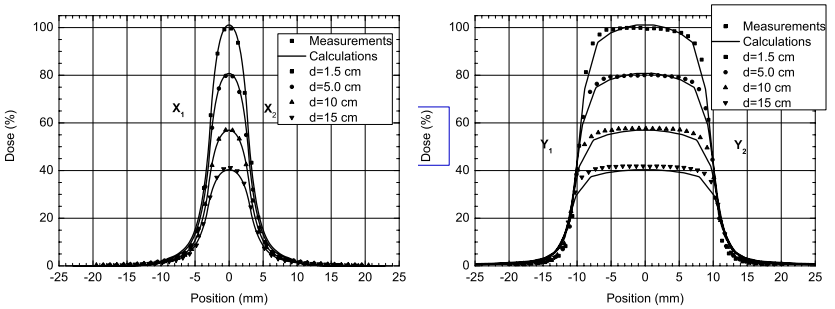

Figure 2.5: Profiles for a partially blocked cone at different depths (1.5, 5.0, 10 and 15 cm): in (a) the X-direction and (b) the Y-direction, for a 2.0 cm diameter cone, blocked with the collimator jaws X_1 at 0.3 cm and X_2 at 0.3 cm from the central beam axis.

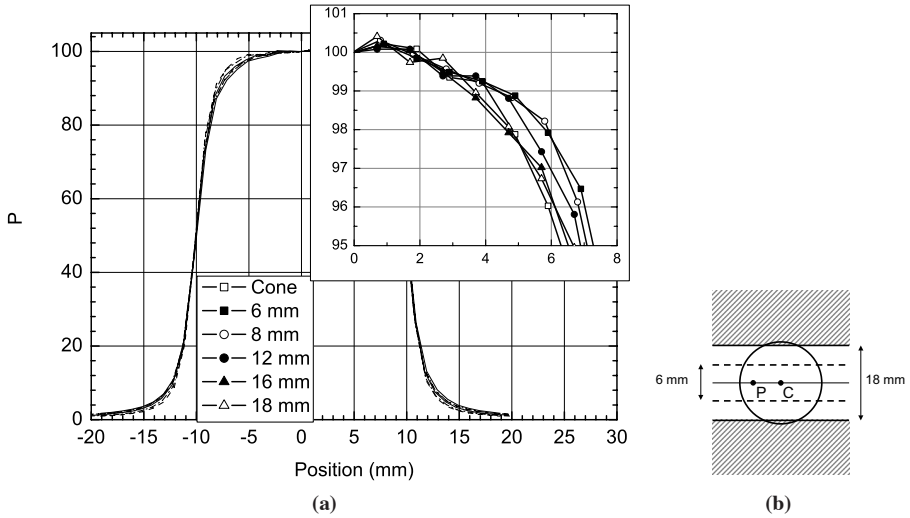

Figure 2.6: (a) Profiles in the Y-direction for a 2 cm cone, normalized to 100% at the central beam axis, with different jaw settings in the X-direction. (b) Diagram of the situation for the profile measurements in (a). The profiles are measured along the line PC.

12 Gy to the prescription isodose. Because one isocenter could be applied in the partially blocked plan, the overdosage in the PTV was reduced from 21 Gy to 15 Gy. The maximum dose in the trigeminal nerve was reduced by 1.3 Gy, from 6.5 Gy to 5.2 Gy. The small part of the brain stem that receives a high dose is reduced in the plan that uses the partial blocked cone. PITV (the ratio between the volume covered by the prescription isodose contour and the target volume) was almost the same for both plans; 2.67 for the original plan and 2.73 for plan that uses partially blocked cones. Thus the dose inhomogeneity was largely improved, without a loss in conformity. As a result of partial cone blocking, it would have been possible to treat this patient with one fraction of 12 Gy instead of 12 fractions of 2.8 Gy.

Case 2: Uveal Melanoma

In our institution, uveal melanoma are irradiated to a total dose of 50 Gy in 5 fractions. Important critical structures are the optic nerve and the ciliary body. Our dose limits per fraction are 4 Gy and 2.5 Gy, respectively. In addition to the stereotactic frame for the head fixation, a non-invasive eye fixation camera system is used[16] comparable to the system described by Dieckman et al.[17] for the immobilization of the eye. The original plan consisted of two isocenters with a 1 cm cone and a 1.25 cm cone. For the new plan, one isocenter with a 2 cm partially blocked cone was applied (Fig. 2.8). The conformity for the new plan was increased; the PITV could be reduced from 2.09 to 1.43. Furthermore the dose to the ciliary body was reduced; in the new plan the volume of the ciliary body receiving the dose limit was reduced by 30%. Therefore the probability of neo-vascular glaucoma is reduced.

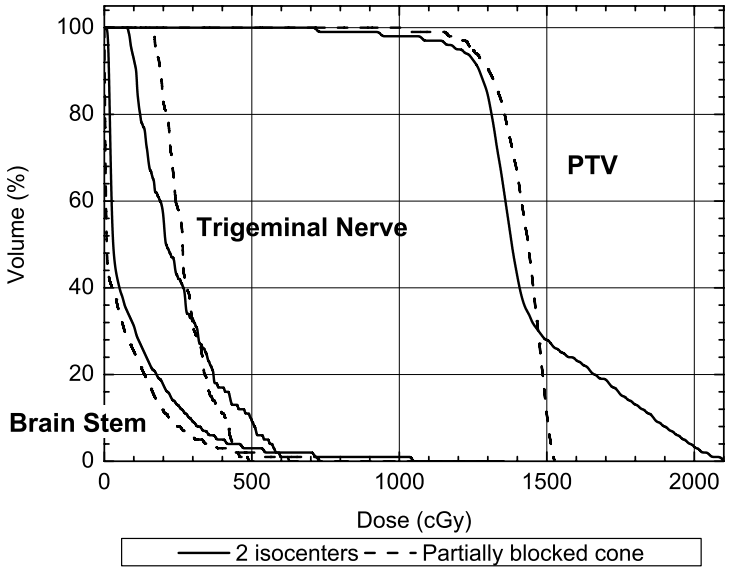

Figure 2.7: Dose volume histograms of two different plans for a vestibular schwannoma: the original plan with two isocenters (solid lines), and the improved plan with one isocenter using a partially blocked cone (dashed lines).

The increase in conformity is also illustrated by Fig. 2.9, which shows the dose distribution in three perpendicular slices through the isocenter. For the partially blocked cone plan, the PTV is encompassed more tightly by the prescribed isodose (10 Gy). Moreover, the low dose volume (e.g. 2 Gy) is reduced considerably.

Recently, other improved treatment techniques for uveal melanoma have been investigated and described. George et al.[7] compared conventional arc treatment with static MMLC fields, intensity modulated MMLC fields, and dynamic arcs. In the latter situation, the MMLC leaves move in a continuous fashion, conforming the BEV projection of the target at every angle along the path of the arc. Using dynamic arc treatments, the high dose homogeneity and conformity to the target of the static MMLC fields are combined with the low dose to all healthy tissue of the arc treatment. The MMLC-based techniques result in an increase in dose conformity. Compared with the static MMLC technique, the conventional arc and the dynamic arc technique have the advantage of dose distributions with a steeper dose gradient. Compared with the described techniques[7], partially blocked cones will result in comparable improved conformity. The dose distributions will have steeper dose gradients compared to static MMLC fields. The technique is less complicated and verification is less time-consuming than dynamic arc or IMRT techniques.

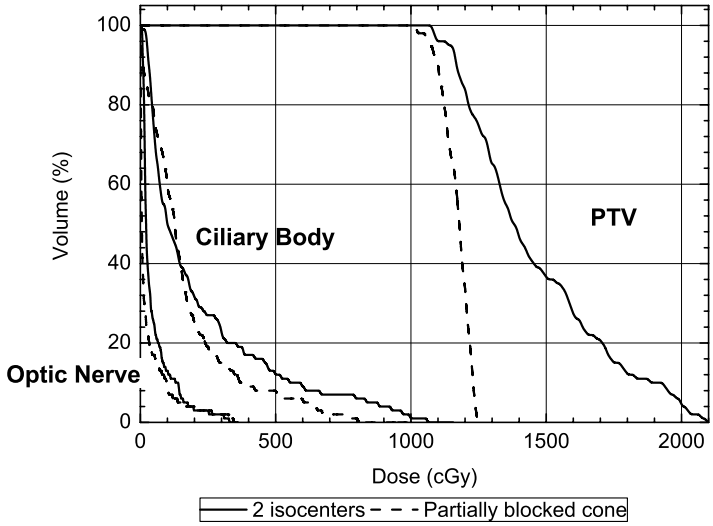

Figure 2.8: Dose volume histograms of two different plans for a uveal melanoma: the original plan with two isocenters (solid lines), and the improved plan with one isocenter using a partially blocked cone (dashed lines).

2.4 Conclusion

Partial blocking of cones with diameters as small as 1.0 cm is an effective way of improving the dose homogeneity and target conformity for small (elongated) intra-cranial lesions. The reproducibility of both the jaw positioning (< 0.3 mm, 1 SD) and the dose delivery ($< 0.8\%$, 1 SD for fields with at least one side equal to 6 mm and $< 0.4\%$, 1 SD for larger fields) is sufficient for clinical use. The dose calculation accuracy of the simple algorithm[8,9] applied in the XKnife software is sufficient for small partially blocked fields with a minimum distance between the jaws and the central beam axis of 0.3 cm. Essential in the dose calculation accuracy are (1) a correct phantom scatter fit, using a correction for increasing electron disequilibrium for field sides smaller than 2.0 cm, and (2) a penumbra fit deconvolved for the spatial extent of the detector used.

The absolute dose calculation on the central beam axis for the partially blocked cones showed an accuracy of -1.0% $\pm$ 1.4% (1 SD) for a large set of fields. The relative dose calculation showed dose off-axis deviations with a maximum of 5%, and a maximum geometrical deviation of 1.5 mm. In most cases, the agreement is within 2% or 1 mm. These accuracies are sufficient to use this algorithm clinically for partially blocked cones with a minimum jaw setting of 0.3 cm, once the mechanical properties of the user's treatment machine are verified.

Clinical treatment plans for small elongated lesions, such as vestibular schwannoma and uveal melanoma can be improved considerably by partially cone blocking. Single isocenter

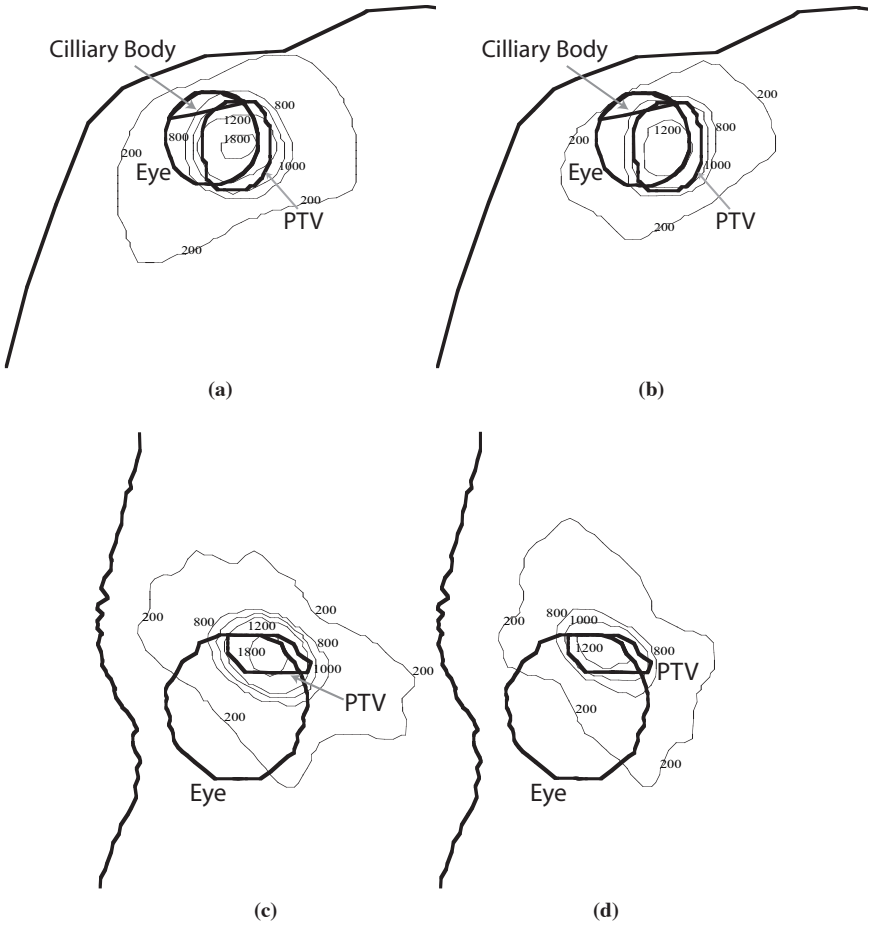

Figure 2.9: Cont'd

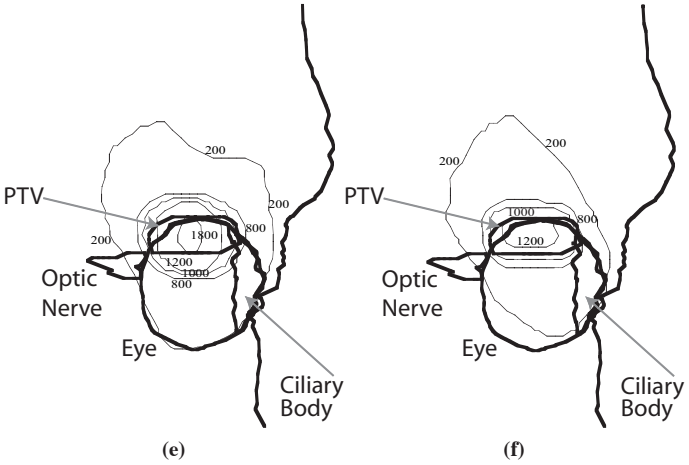

Figure 2.9: Isodose lines for the non-blocked (a, c and e) and the partially blocked plan (b, d and f) for the uveal melanoma case in the axial (a,b), coronal (c,d) and sagittal planes (e,f) through the isocenter.

treatments can be used resulting in a large improvement in dose homogeneity and conformity, and in a reduction of the delivered dose to the critical structures. The reduction in minimal distance between a jaw and the beam axis from 1.0 cm to 0.3 cm only requires a dedicated handling of the input data for the treatment planning system. There is no need for additional routine quality assurance procedures or workload. The technique can be applied in the clinic for a large number of patients.

Bibliography

[1] Bellerive MR, Kooy HM, Loeffler JS. LinAc radiosurgery at the joint centre for radiotherapy *Med Dosim*. 1998;23:187–199.

[2] Shiu AS, Kooy HM, Ewton JR, et al. Comparison of Miniature Multileaf Collimation (MMLC)with Circular collimation for Stereotactic Treatment *Int J Radiat Oncol Biol Phys*. 1997;37:679–688.

[3] Hacker FL, Kooy HM, Bellerive MR, et al. Beam shaping for conformal fractionated stereotactic radiotherapy: a modelling study *Int J Radiat Oncol Biol Phys*. 1997;38:1113–1121.

[4] Nedzi LA, Kooy HM, E.III Alexander, et al. Dynamic field shaping for stereotactic radiosurgery: A modeling Study *Int J Radiat Oncol Biol Phys*. 1993;25:859–869.

[5] Kulik C, Caudrelier J, Vermandel M, et al. Conformal Radiotherapy optimization with micro-multileaf collimators: comparison with radiosurgery techniques *Int J Radiat Oncol Biol Phys*. 2002;53:1038–1050.

[6] Xia P, Geis P, Xing L, et al. Physical characteristics of a miniature multileaf collimator *Med Phys*. 1999;26:65–70.

[7] Georg D, Dieckmann K, Bogner J, et al. Impact of a micromultileaf collimator on stereotactic radiotherapy of uveal melanoma *Int J Radiat Oncol Biol Phys*. 2003;55:881–891.

[8] Kooy HM, Nedzi LA, Loeffler JS, et al. Treatment planning for stereotactic radiosurgery of intracranial lesions *Int J Radiat Oncol Biol Phys*. 1991;21:683–693.

[9] Chui CS, Mohan R. Off-center ratios for three-dimensional dose calculations *Med Phys*. 1986;13:409–412.

[10] Higgins PD, Sibata CH, Siskind L, et al. Deconvolution of detector size effect for small field measurement *Med Phys*. 1995;22:1663–1666.

[11] Garcia-Vicente F, Delgado JM, Peraza C. Experimental determination of the convolution kernel for the study of the spatial response of a detector *Med Phys*. 1997;25:202–207.

[12] 't Veld AA, Luijk P, Praamstra F, et al. Detector line spread functions determined analytically by transport of Compton recoil electrons *Med Phys*. 2001;28:738–751.

[13] Bjarngard BE, Siddon RL. A note on equivalent circles, squares, and rectangles *Med Phys*. 1982;9:258–260.

[14] Bjarngard BE, Tsai JS, Rice RK. Doses on the central axes of narrow 6-MV x-ray beams *Med Phys*. 1990;17:794–799.

[15] Vieira SC, Dirkx ML, Pasma KL, et al. Fast and accurate leaf verification for dynamic multileaf collimation using an electronic portal imaging device *Med Phys*. 2002;29:2034–2040.

[16] Muller K, Nowak PJ, Luyten GP, et al. A modified relocatable stereotactic frame for irradiation of eye melanoma: Design and evaluation of treatment accuracy. *Int J Radiat Oncol Biol Phys*. 2004;58:285–291.

[17] Dieckman K, Bogner J, Georg J, et al. A linac-based stereotactic irradiation technique of uveal melanoma *Radiother Oncol*. 2001;61:49–56.

Chapter 3

Computer optimization of non-coplanar beam set-ups improves stereotactic treatment of liver tumors

JA de Pooter, A Méndez Romero, WPA Jansen, PRM Storchi, E Woudstra, PC Levendag, BJM Heijmen, *Int J Radiat Oncol Biol and Phys*. 2006;**66**:913 - 26

Abstract

Purpose:
To investigate whether computer optimized fully non-coplanar beam set-ups may improve treatment plans for the stereotactic treatment of liver tumors.
Methods:
An algorithm for automated beam orientation and weight selection (Cycle) was extended for non-coplanar stereotactic treatments. For 8 liver patients previously treated in our clinic using a prescription isodose of 65%, Cycle was used to generate non-coplanar and coplanar plans with the highest achievable minimum PTV dose for the clinically delivered isocenter and mean liver doses, while not violating the clinically applied hard planning constraints. The clinical, and the optimized coplanar and non-coplanar plans were compared, with respect to $D_{PTV,\,99\%}$, the dose received by 99% of the PTV, the PTV generalized equivalent uniform dose (gEUD) and the compliance with the clinical constraints.
Results:
For each patient the ratio between $D_{PTV,\,99\%}$ and D_{isoc}, and the $gEUD_{-5}$ and $gEUD_{-20}$ values of the optimized non-coplanar plan were higher than for the clinical plan with an average increase of respectively 18.8% (range 7.8 – 24.0%), 6.4 Gy (range 3.4 – 11.8 Gy) and 10.3 Gy (range 6.7 – 12.5). $D_{PTV,\,99\%}$ / D_{isoc}, $gEUD_{-5}$ and $gEUD_{-20}$ of the optimized non-coplanar plan was always higher than for the optimized coplanar plan with an average increase of respectively 4.5% (range 0.2 – 9.7%), 2.7 Gy (range 0.6 – 9.7 Gy) and 3.4 Gy (range 0.6 – 9.9 Gy). All plans were within the imposed hard constraints. On average, the organs at risk were better spared with the optimized non-coplanar plan than with the optimized coplanar plan and the clinical plan.
Conclusions:
The use of automatically generated, fully non-coplanar beam set-ups results in plans that are favorable compared to coplanar techniques. Due to the automation, we found that the planning workload can be decreased from 1-2 days to 1-2 hours.

3.1 Introduction

The number of patients with metastatic or primary liver tumors treated with external beam radiotherapy is increasing. Often the patients treated with this modality can not be operated or treated with another local modality such as radio frequency ablation (RFA), or percutaneous ethanol injection therapy (PEI).

In some institutes, hypo-fractionated stereotactic radiotherapy is used[1–6], applying a stereotactic body frame (SBF) with abdominal compression for reduction of respiratory tumor motion. In 2002, using the Elekta SBF (Elekta AB, Stockholm, Sweden), this type of treatment has been started in our clinic, for metastatic and hepatocellular carcinoma lesions. Patients accepted for treatment can not be treated with surgery or other local treatments such as RFA or PEI. The maximum allowed diameter of the lesion is 6 cm. With the patient positioned in the SBF, arterial and venous contrast computed tomography (CT) scans are made for tumor definition as well as a planning CT scan for contouring of the organs at risk (OAR). Delineated tumors in the arterial and venous CT-scans are summed to construct the definitive clinical target volume (CTV). To determine the required CTV-to-planning target volume (PTV) margin, the residual respiratory tumor motion, is assessed with fluoroscopy at a conventional simulator using implanted fiducials. The patients are treated mostly with three fractions of 10-12.5 Gy (depending on disease type and tumor size), prescribed at the 65% isodose, that closely surrounds the PTV. This inhomogeneous dose concept is based on the work of Lax et al.[7]. They showed that for a constant dose at the periphery of the PTV, a 50% increase in the target center dose can be obtained, compared to a homogeneous dose concept, without a substantial increase of dose to the normal tissue.

To irradiate liver tumors, most clinics use three-dimensional conformal radiotherapy (3D-CRT) with a set of manually selected beam directions and forward treatment planning. Generally, coplanar beam directions are used, while in some cases non-coplanar set-ups have been applied[8,9]. Thomas et al.[10] investigated for a group of patients whether manually chosen non-coplanar beam set-ups (i.e., with non-coplanar and coplanar directions) are more favorable for intensity modulated radiation therapy treatment of liver tumors. They concluded that for the group of patients with a tumor close to an OAR, the non-coplanar set-up improved the treatment plan. For the other patients, the plans with a non-coplanar beam set-up were as good as those with a 7 beam equidistant coplanar set-up or as those using the beam set-up of the clinical plan.

In this paper, we have investigated the benefit of non-coplanar beam set-ups for hypofractionated, stereotactic treatment of liver tumors, using automated beam direction selection from a large set of coplanar and non-coplanar input directions. For this purpose, our in-house developed beam direction selection algorithm[11], Cycle, was extended for handling of stereotactic (inhomogeneous) PTV dose distributions including an option for beam shape optimization. For 8 liver patients previously treated in our clinic using a prescription isodose of 65%, Cycle was used to generate non-coplanar and coplanar plans with the highest achievable minimum PTV dose for the clinically delivered isocenter and mean liver dose. The clinically applied hard planning constraints were also used for the automated plan gener-

Structure	Constraint	Constraint parameter
PTV	$D_{PTV,\,rel} < D^{tol}_{PTV,\,rel}(n)$	NA
Normal liver	$D_{mean} < D_{mean,\,clinical}$	NA
Normal liver	$D_{50\%} < 15$ Gy	$D_{50\%}$ / 15
Normal liver	$D_{33\%} < 21$ Gy	$D_{33\%}$ / 21
Spinal cord	$D_{max} < 15$ Gy	D_{max} / 15
Bowel, duodenum, Stomach, esophagus, Heart, aorta	$D_{5\,CC} < 21$ Gy	$D_{5\,CC}$ / 21
Kidney's	$D_{33\%} < 15$ Gy	$D_{33\%}$ / 15
R_1	D_{max}	NA
R_2	$D_{max} < 20$ Gy	NA

Table 3.1: Applied constraints in the iterative optimization of the minimum PTV dose. $D^{tol}_{PTV,\,rel}(n)$ is the applied constraint level in iteration n on the relative PTV dose inhomogeneity. In the iterative procedure, $D_{PTV,\,rel}$ is minimized by repeated runs of Cycle with decreasing values of $D^{tol}_{PTV,\,rel}$ (see text). $D_{a\%}$ indicates that a% of the volume receives a dose of at least $D_{a\%}$ and $D_{a\,CC}$ indicates that a CC receives a dose of at least $D_{a\,CC}$. Structures R_1 and R_2 and the maximum tolerated dose in R_1 are defined in the text. The constraint parameters, C_j, for OAR constraints, j, are required for calculation of the DIP (Eq. 3.2). NA = not applicable.

ation. The clinical, and the optimized coplanar and non-coplanar plans were compared, with respect to $D_{PTV,\,99\%}$, the dose received by 99% of the PTV, the PTV generalized equivalent uniform dose (gEUD), and the distance from the applied constraint levels.

3.2 Methods

3.2.1 Description of liver plans

In clinical practice, the liver treatment plans were designed by a dosimetrist using forward trial-and-error planning. Both coplanar and non-coplanar beams (open or wedged) could be selected. For practical reasons not more than 10 different directions were allowed in a plan. The dose (3×10 Gy or 3×12.5 Gy) was prescribed to the 65% isodose level. The clinical treatment plans for the 8 patients in this study consisted of five to nine coplanar beams. In addition, in Case 8, three non-coplanar beams were used. The workload of the manual treatment plan generation was 1-2 days. The delineated OAR with their clinical constraints are summarized in Table 3.1. Because the tumor location was heterogeneous among the patient group, not all OARs were always relevant for all patients.

3.2.2 Short description of Cycle algorithm

The general principles of the Cycle algorithm for automated beam orientation and weight selection have been described in detail by Woudstra et al.[11–14]. Here, a summary is given with the focus on some extensions. The algorithm aims at generating a treatment plan with

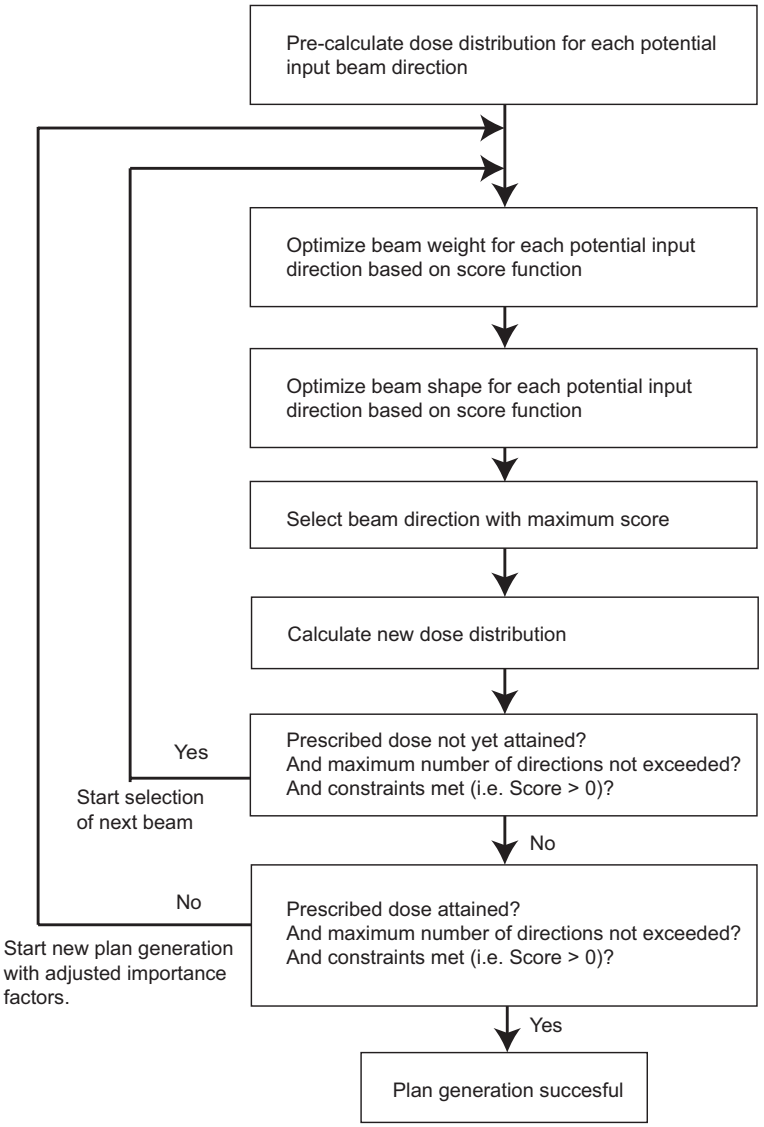

Figure 3.1: Schematic diagram of the Cycle algorithm.

the prescribed tumor dose (isocenter), while not exceeding the imposed hard constraints. The algorithm starts with an empty plan. Sequentially (Fig. 3.1), new beams are added to the plan by selection from a large set of potential input directions based on a score function (see section 3.A).

The selection of beams stops, if the selected beams result in a plan that can be scaled

to the prescribed PTV dose without violation of any constraint level (the plan generation is successful), or if no more beams can be added without violation of one of the constraints, or if the number of allowed directions is reached. In the last two cases a new plan generation is started with automatically adjusted penalty factors in the score function[11,12].

Strictly speaking, by itself Cycle is not an optimization algorithm; its aim is generation of an acceptable plan (i.e., attaining the prescribed dose without exceeding the constraints). The score function is used to build such an acceptable plan, and not to define and generate the "best" plan. However, in an iterative loop, the algorithm may indeed be used to optimize a plan parameter[14]. In this study, such a procedure was used to maximize the minimum PTV dose (see section 3.2.5).

3.2.3 Beam shape optimization

Usually beam direction optimization for three-dimensional conformal radiotherapy is performed with a fixed field/segment shape for each of the beam directions in the initial set[11–15]. Often the beams' eye view (BEV) projection of the target and an additional margin for the penumbra is used for the determination of the field shape[11,16].

In this paper, we study stereotactic treatments with highly inhomogeneous PTV dose distributions that are very sensitive to the selected beam sizes. Because each selected beam passes through the liver, each beam contributes to the mean liver dose. The contribution of an individual beam is approximately proportional to the liver volume incorporated by that beam, which is proportional to the area of the field of that beam. On average, the fields have a diameter in the order of about 5 cm. An addition or subtraction of a margin of 0.5 cm from the field shape, may therefore increase/reduce the field area by about 30%.

Therefore an extension was made to the Cycle algorithm, to enable optimization of the field-shape for each input direction. First an initial field shape is made, based on the BEV projection of the target (without penumbra margin). With this shape the beam weight is optimized (see section 3.A). After that, the algorithm tries to further increase the score by expanding or reducing the margin in small steps (2 mm), in four independent perpendicular directions ($+x$, $-x$, $+y$, $-y$). Each step requires a recalculation of the off-axis dose distribution of the beam. A beam direction can be selected multiple times. In general, each time it will be selected with a different shape and weight; therefore a plan can have multiple segments per beam direction.

3.2.4 Input beam directions

For the coplanar plans, Cycle used 72 input beam directions evenly distributed in the axial plane. For the non-coplanar plans, the input beam directions were distributed in separate sets of 36 or 72 beam directions. The beam directions in each set have the same angle with the axial plane, α, and they are evenly distributed with an equal separation in θ (see Fig. 3.2). For $\alpha = 0$ (i.e., the axial plane), the same 72 input beam directions were used as for the coplanar plans. For sets with other α-values (i.e., for the non-coplanar input beams), 36 input beam directions were used.

Increments in α of 10^{o} were used. The upper and lower α were determined manually, using the BEV (see Table 3.2). The set of non-coplanar beam directions with the α_{up} or α_{low}

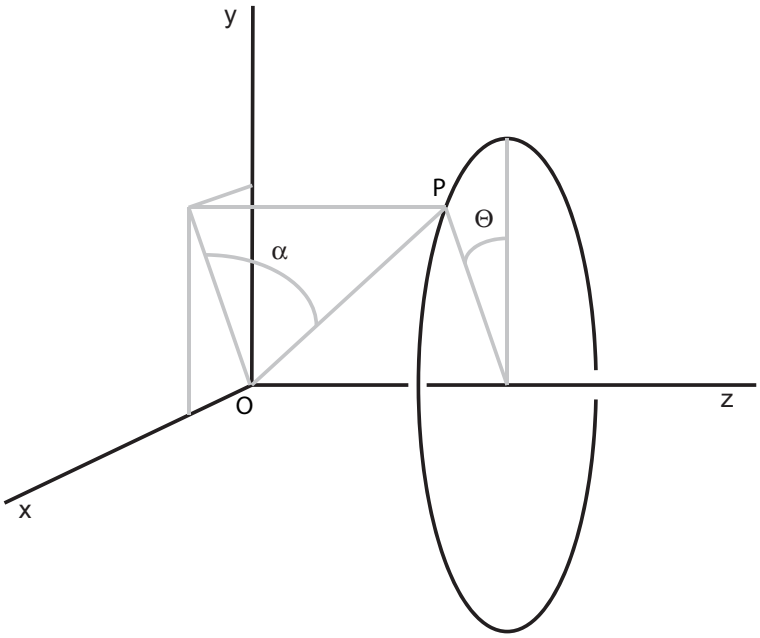

Figure 3.2: Patient coordinate system and angles α, θ, for definition of the input non-coplanar beam directions. O is the isocenter and, *z* is the cranial-caudal direction of the patient. OP is an example of a beam direction. α is the angle of the *xy*-plane (axial plane) with OP.

is the set with the highest $|\alpha|$ for which none of the beams enters through the upper (cranial) or lower (caudal) CT slice, i.e., α_{up} and α_{low} were determined by the cranial-caudal extent of the CT scan. If the separation between α_{up} or α_{low} and the nearest set of input directions was $\geq 5^{o}$, an extra set of input beam directions was defined for α_{up} or α_{low}.

3.2.5 Maximizing the minimum PTV dose

In the procedure to maximize the minimum PTV dose, the isocenter dose in the clinical plan was used as the prescribed dose for the PTV, D^{pre}_{PTV}. The minimum PTV dose was then optimized in an iterative procedure, by minimizing the relative PTV dose inhomogeneity, $D_{PTV,\,rel}=(D_{isoc}-D_{PTV,min})\,/\,D_{isoc}$ (see Table 3.1). In first instance, for the constraint on the relative PTV dose inhomogeneity, $D^{tol}_{PTV,\,rel}$, the level of the clinical plan was used (35%). If Cycle succeeded in generating a plan, the $D^{tol}_{PTV,rel}$ level was decreased with a step of 1%. This was repeated until plan generation was no longer successful, (i.e., D^{pre}_{PTV} could not be attained without a constraint violation). As mentioned above, the allowed maximum number of beam directions in the clinical plans was 10. In order to generate clinically acceptable plans, and for a straightforward comparison with the manually created clinical plans, the allowed number of beam orientations in the Cycle plans was also limited to 10. Apart from the $D^{tol}_{PTV,rel}$ constraint, generation of plans was always subject to the constraints in Table 3.1.

Case	V_{PTV}(CC)	V_{liver}(CC)	Prescription dose (Gy)	α_{low}	α_{up}	No. of input beams
1	74.5	1271.0	3×12.5	-30	5	216
2	113.4	1228.0	3×12.5	-30	19	252
3	121.4	786.3	3×12.5	-30	10	216
4	105.9	1869.0	3×12.5	-30	5	216
5	211.8	1601.0	3×10.0	-20	10	180
6	46.9	1011.0	3×10.0	-30	20	252
7	111.2	985.9	5×5.0	-9	9	144
8	264.7	1632.0	3×12.5	-28	10	216

Table 3.2: Patient characteristics, the prescribed dose for the clinical plans (65 % isodose), the α_{low} and α_{up} defining the sets of input beam directions and, the number of input beam directions for the non-coplanar plan.

To end up with a probability on liver complication for the optimized plans equal to or lower than the clinical plan, the mean dose constraint on the normal liver volume (i.e., the entire liver minus the CTV) was set to the clinically achieved mean normal liver dose value[17]. For cases 5-7, the clinical plan had a relatively low prescribed dose (Table 3.2). For these patients, in a second step, an attempt was made to escalate the absolute isocenter PTV dose. This was again done in an iterative way, by increasing the prescribed isocenter dose while keeping the relative PTV dose inhomogeneity constraint, $D^{tol}_{PTV,rel}$, constant. For $D^{tol}_{PTV,rel}$, the value used in the last iteration of the optimization procedure for the minimum PTV dose (see previous) was used. The iterative procedure was stopped if further isocenter dose increase was prevented by a constraint violation.

3.2.6 Non-organ specific regions in normal tissue

Apart from organ based constraints (e.g., for the kidney's) for automated plan generation, two other regions were defined in the normal tissue by expansions of the PTV (expansion 1 is the PTV plus a 2.0 cm margin, expansion 2 is the PTV plus a 5.0 cm margin). Region, R_1, was all tissue outside expansion 1 and inside expansion 2. Region, R_2, was all tissue outside expansion 2. For each region a maximum dose constraint was imposed (Table 3.1). The constraint on R_1 aims at conformality of the dose distribution to the target volume, while the constraint on R_2 avoids hot spots far away from the target volume. The value for the constraint on R_1 was chosen as 5-10 Gy lower than the minimum PTV dose level. The exact value of this constraint was chosen in such a way, that it was not a limiting constraint for maximizing the minimum PTV dose. If during the optimization process, a plan generation failed because of violating this constraint, the constraint level was relaxed. For R_2, a maximum dose constraint of 20 Gy was used for each patient (Table 3.1).

Case	Clinical	Coplanar	Non-coplanar
1	61.0%	82.3%	85.0%
2	63.2%	76.6%	83.8%
3	70.4%	84.1%	88.4%
4	67.7%	80.0%	87.2%
5	69.1%	87.4%	87.6%
6	83.1%	87.9%	90.9%
7	61.6%	74.6%	84.3%
8	70.5%	88.6%	90.1%
Mean	68.3%	82.7%	87.2%

Table 3.3: $D_{PTV,99\%}$ / D_{isoc} for the clinical and the optimized coplanar and non-coplanar plans.

3.2.7 Plan comparison

As described above, the main goal of the iterative use of Cycle was to maximize the minimum dose in the PTV, while not exceeding the clinically delivered mean liver dose and without violation of the other clinical constraints. In this study, the ratio between $D_{PTV,99\%}$, the minimum dose received by 99% of the PTV, and D_{isoc}, the isocenter dose, was used for evaluation of the plans. Also the gEUD of the PTV was evaluated using the following formula[18],

$$\mathrm{gEUD}_a = \left(\frac{1}{N} \sum_{i=1}^{N} D_i^a \right)^{1/a} \tag{3.1}$$

With N the number of dose points, D_i. The a parameter ($a < 0$) represents the aggressiveness of the tumor, with an increased aggressiveness for more negative a values. In this study the gEUD was calculated with a-values of -5 and -20[10]. Potentially, an improved $D_{PTV,99\%}$ value for a constant mean normal liver dose could be accomplished at the cost of a closer approach of other constraint levels. To evaluate this, the distance from ideal plan (DIP), as defined by Woudstra et al.[12], was calculated for each plan.

$$\mathrm{DIP} = \sqrt{\sum_{j=1}^{M} \frac{C_j^2}{M}} \tag{3.2}$$

In which C_j are the OAR constraint parameters as mentioned in Table 3.1. M is the number of OAR constraints. For the optimized plans the maximum doses delivered to regions R_1 and R_2 in the normal tissue were also evaluated. For plan evaluation, the maximum dose in R_1 was subtracted from $D_{PTV,99\%}$. This value represents the minimum dose gradient between the PTV and region R_1.

3.3 Results

3.3.1 PTV: Optimized non-coplanar plan vs. clinical plan

The results for the PTV of the clinical, the coplanar and the non-coplanar plans are summarized in Tables 3.3 and 3.4. For each case, $D_{PTV,99\%}/D_{isoc}$ and the $gEUD_{-5}$ and $gEUD_{-20}$ values were substantially higher for the optimized non-coplanar plan than for the clinical plan. For $D_{PTV,\,99\%}$ / D_{isoc} the average increase was 18.8% (range 7.8 – 24.0%). The average increase for $gEUD_{-5}$ and $gEUD_{-20}$ was respectively 6.4 Gy (range 3.4 – 11.8 Gy) and 10.3 Gy (range 6.7 – 12.5 Gy) (Table 3.4). In Fig. 3.3, the dose volume histograms (DVH) of the normal liver volume and the PTV are plotted for Case 2. The increase in PTV dose is clearly visible. The high dose volume in the normal liver is slightly higher for the optimized plans, because of the increase in minimum PTV dose. This increase is however compensated by a smaller normal liver volume receiving a low dose, to end up with the same mean liver dose.

3.3.2 PTV: Coplanar vs. non-coplanar plan

In each case, the optimized non-coplanar plan was better than the optimized coplanar plan (Tables 3.3 and 3.4). The increase in the ratio $D_{PTV,\,99\%}$ / D_{isoc} was on average 4.5% (range 0.2 – 9.7%). The average increase in $gEUD_{-5}$ and $gEUD_{-20}$ was respectively 2.7 Gy (range 0.6 – 9.7 Gy) and 3.4 Gy (range 0.6 – 9.9 Gy) (Table 3.4). The total number of selected beam directions was 10 for all of the optimized plans except for one case which had 9 directions for the non-coplanar plan. The average ratio between the number of segments and the number of beam directions in a plan was 2.0 (range 1.4 – 3.1) for the non-coplanar plans, and 2.7 (range 1.8 – 3.9) for the coplanar plans.

Resulting dose distributions of Case 2 are shown in Fig. 3.4. Because of the close proximity of the heart, the aorta and the esophagus to the target and the eccentric position of the target in the liver, this case was rather complicated. In the slice 2 cm cranial from the

	a=-5			*a*=-20		
Case	A	B	C	A	B	C
1	48.2	51.9	53.1	43.7	50.4	52.1
2	46.5	50.6	53.1	40.5	48.1	52.0
3	49.1	54.3	55.7	43.7	53.2	55.2
4	48.9	52.4	54.4	43.5	50.9	53.9
5	39.9	46.9	47.5	35.8	46.3	46.9
6	44.4	46.6	56.2	43.4	46.0	55.9
7	31.1	32.9	34.5	27.0	31.0	33.7
8	49.4	51.5	54.3	43.5	50.2	53.5
Mean	44.7	48.4	51.1	40.1	47.0	50.4

Table 3.4: $gEUD_{-5}$ and $gEUD_{-20}$ values for the clinical (A) and the optimized coplanar (B) and non-coplanar plans (C).

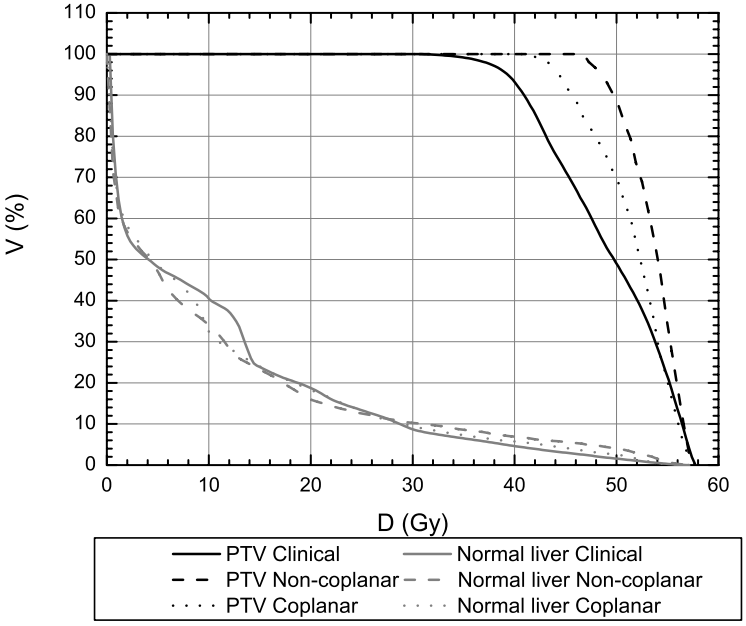

Figure 3.3: DVHs of the dose distributions in the PTV and the normal liver for the clinical plan and the optimized non-coplanar and coplanar plans of Case 2.

isocenter slice, the increased dose homogeneity for the non-coplanar plan can be seen from the 45 Gy isodose, which is at the edge of the PTV for the non-coplanar plan (Fig. 3.4(b)) and inside the PTV for the coplanar plan (Fig. 3.4(d)).

3.3.3 PTV: dose escalation

For Cases 5-7, it was tried to escalate the isocenter dose with a constant PTV inhomogeneity as described above. Escalation succeeded for the Cases 5 and 6. The increase in D_{isoc} with respect to the clinical plan was 3.5 Gy and 2.9 Gy for respectively the non-coplanar plan and the coplanar plan of Case 5 and 11.0 Gy and 1.5 Gy for respectively the non-coplanar plan and the coplanar plan of Case 6. For the non-coplanar plan of Case 6, the iteration procedure for minimization of the relative PTV dose inhomogeneity (first step, see section 3.2.5) was stopped after the 90% PTV dose homogeneity level was reached, which was not the highest achievable homogeneity level. This explains the large increase in D_{isoc}. The liver volume in Case 7 was relatively small (Table 3.2), and the PTV was situated in the center of the liver. For Cases 5 and 6, the PTV was located at the edge of the liver. In the latter cases, beams could be selected that involved a rather small volume of normal liver, whereas in Case 7 this was not possible.

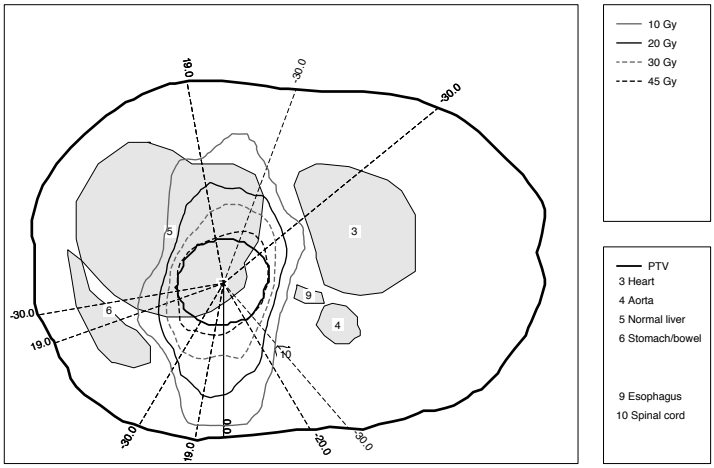
10 Gy
20 Gy
30 Gy
45 Gy
PTV
3 Heart
4 Aorta
5 Normal liver
6 Stomach/bowel
9 Esophagus
10 Spinal cord
19.0
-30.0
-30.0
-30.0
19.0
-30.0
0.0
-20.0
-30.0
-30.0
19.0
5
3
9
4
6
10

(a)

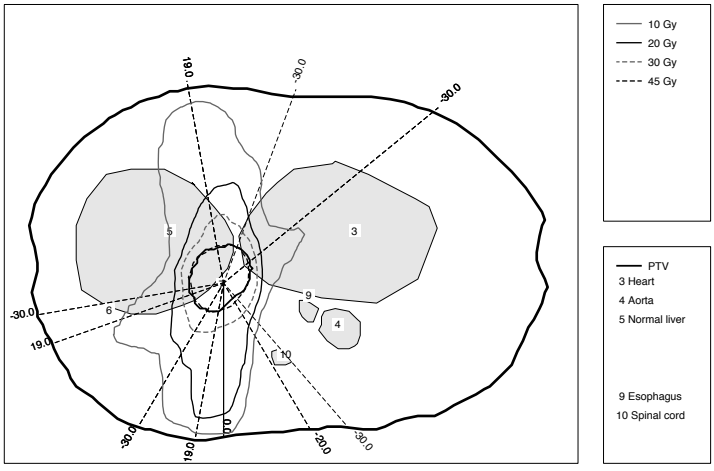
10 Gy
20 Gy
30 Gy
45 Gy
PTV
3 Heart
4 Aorta
5 Normal liver
9 Esophagus
10 Spinal cord
19.0
-30.0
-30.0
-30.0
19.0
-30.0
0.0
-20.0
-30.0
-30.0
19.0
5
3
9
4
6
10

(b)

Figure 3.4

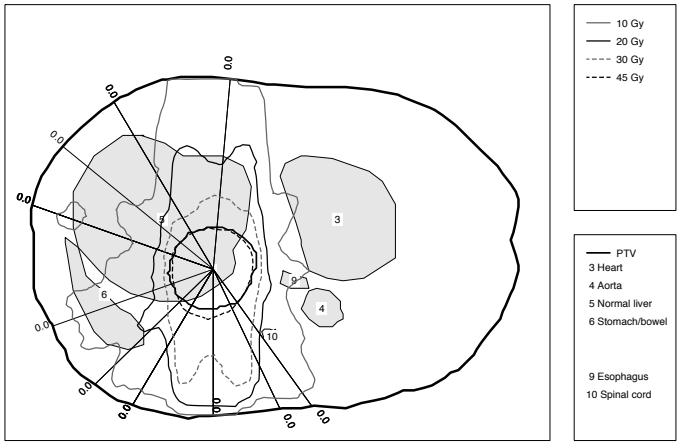

(c)

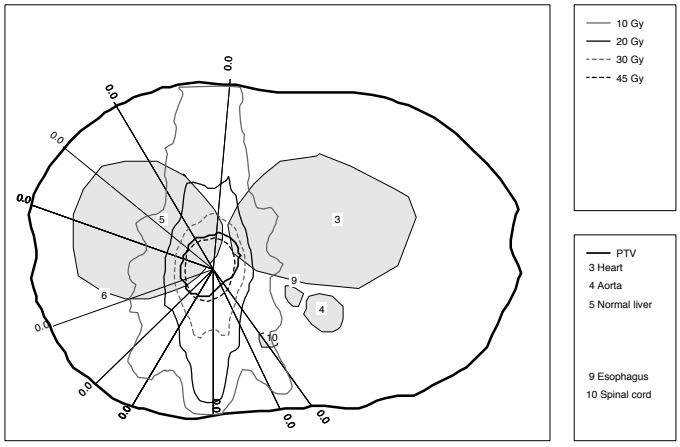

(d)

Figure 3.4: Dose distributions for case 2 for the non-coplanar plan (a and b) and the coplanar plan (c and d) for the isocenter slice (a and c) and a slice 2 cm cranial from the isocenter (b and d). The dashed lines are the projections of the beam axis of the non-coplanar beam directions in the axial slices, the solid lines are the beam axis of the coplanar beam directions. The labels indicate the angle, α between the beam axis and the axial slices.

	$D_{PTV,\,99\%}$-$D_{R_1,\,max}$			$D_{R_2,\,max}$		
Case	A	B	C	A	B	C
1	8.2	6.3	14.7	19.6	19.2	17.9
2	3.4	4.5	11.8	22.1	20.0	15.6
3	1.1	21.1	22.3	21.3	18.8	17.3
4	5.3	20.3	18.1	26.3	17.8	19.1
5	3.3	7.6	8.6	12.2	19.8	19.2
6	8.5	12.5	16.4	21.4	19.2	19.0
7	6.0	5.3	7.7	13.1	13.3	14.3
8	-0.1	1.5	8.0	24.7	19.9	18.7

Table 3.5: Comparison between the clinical (A), the coplanar(B), and the non-coplanar (C) plans with respect to the maximum dose delivered to the normal tissue regions R_1 and R_2.

3.3.4 Normal tissues

As aimed for, all optimized plans delivered the clinically prescribed isocenter dose with the same mean liver dose as for the clinical plan, without violation of the normal tissue constraints. The mean liver dose constraint was the limiting constraint for further increase of the minimum PTV dose in each case. In Table 3.5, the clinical plan and the optimized coplanar and non-coplanar plans are compared with respect to the maximum doses in the regions R_1 and R_2. In 6 of the 8 cases, the optimized coplanar plans have a higher difference between $D_{PTV,99\%}$ and the maximum dose in R_1, than the clinical plans. In 7 of the 8 cases, the optimized non-coplanar plans have a higher $D_{PTV,\,99\%}$-$D_{R_1,\,max}$, than the optimized coplanar plans. In 6 of the 8 cases the maximum dose in R_2 is lower for the optimized coplanar plan than for the clinical plan. In 6 of the 8 cases the maximum dose in R_2 is lower for the non-coplanar plan than for the coplanar plan.

The DIP was calculated for each case as explained in section 3.2.7. The average DIP of the optimized non-coplanar plans was both lower than the DIP for the clinical plans, and lower than the DIP for the optimized coplanar plans (Table 3.6). Tables 3.3-3.6 illustrate that non-coplanar beam set-ups allow the highest minimum PTV doses, and $gEUD_{-5}$ and $gEUD_{-20}$ values, while avoiding most approaching OAR constraint levels.

3.4 Discussion

Automatically optimized beam selection for stereotactic treatment of liver tumors results in increased $D_{PTV,\,99\%}$ values compared to the clinical plan, for the same isocenter and mean normal liver doses, without violation of the clinical constraints, and even avoiding best approaching these constraints. For non-coplanar beam set-ups the improvement in $D_{PTV,\,99\%}$ is higher than for coplanar beam set-ups. Automatically selected non-coplanar beam set-ups also have a higher dose gradient between the PTV and the normal tissue region R_1 than the automatically selected coplanar beam set-ups, and on average a lower DIP than the coplanar

Case	Non-coplanar	Coplanar	Clinical
1	0.025	0.115	0.094
2	0.224	0.264	0.254
3	0.257	0.292	0.293
4	0.223	0.255	0.205
5	0.169	0.160	0.161
6	0.159	0.213	0.246
7	0.175	0.137	0.155
8	0.240	0.243	0.231
Mean	0.184	0.210	0.205

Table 3.6: Distance from ideal plan for the optimized coplanar and non-coplanar plans and the clinical plan.

plans. A plan produced by Cycle has an optimal number of beams, in the sense that Cycle stops adding beams when the prescribed dose is attained. In this study, the number of selected beam directions was dependent on how strict the relative PTV dose inhomogeneity constraint, $D^{tol}_{PTV,\,rel}$, was set. In the first steps of the iterative optimization procedure, when $D^{tol}_{PTV,rel}$ was not very strict (see section 3.2.5), the number of selected beam directions was usually lower than 10. With the $D^{tol}_{PTV,rel}$ constraint becoming more strict, the number of selected directions increased, until the maximum number of allowed beams per plan (i.e., 10) was reached. Unlike the number of beam directions, the number of segments was not limited in the plan optimization. It was demonstrated that in a coplanar plan the average number of beam segments per beam orientation was substantially higher than for the non-coplanar plan (2.7 vs. 2.0).

Except for one case, the number of beam directions for the plans generated by Cycle was 10. With regard to the required treatment time, this might be a high number, especially for non-coplanar cases because of the need for couch rotation. However, the treatment is given in only three fractions. So the relative effect of the high number of beams on the treatment time is much less than for a treatment with a conventional fractionation scheme. For most cases all selected directions are non-coplanar directions. Cases 5 and 8 had respectively 6 and 7 non-coplanar directions in the beam set-up of the non-coplanar plan. These two cases had the lowest improvement in $D_{PTV,\,99\%}$, see Table 3.3.

Thomas et al.[10] also investigated the use of non-coplanar beam set-ups for treatment of liver tumors, comparing three IMRT plans, each with a different beam set-up. One set-up contained non-coplanar directions, one set-up used the directions applied in the clinical plan and one set-up used 7 equidistant coplanar directions. They saw that the non-coplanar beam set-up was only favorable in cases where the PTV incorporated another OAR besides the liver. In our study we see a clear advantage of applying non-coplanar directions in the beam set-up for each case. A reason for these different observations might be that in our study the

non-coplanar beam directions are computer optimized for each individual patient, which is not the case in the study by Thomas et al. Moreover in our study relatively small tumors are considered with small CTV-PTV margins, resulting from the abdominal compression, treated with stereotactic (inhomogeneous) PTV dose distributions.

The maximum calculation time for a plan with Cycle (allowing 10 restarts with adjusted penalty factors, see above) on a workstation with an Intel Xeon 3.2 GHz processor was 2 hours for a non-coplanar plan. For coplanar planning this calculation time was reduced by a factor of three.

In this study, we have assumed that the probability of liver complications is correlated with the mean normal liver dose, as found by Dawson et al.[17]. Recently, Cheng et al.[19] showed for the treatment of primary tumors, that for HBV carriers and/or Child Pugh grade B, this probability might be more correlated with the high dose delivered to the normal liver. Separate analysis would be required to assess the advantage of non-coplanar beam set-ups for these cases.

For all patients, the tumor was located in the upper part of the set of CT-slices. Therefore, for 6/8 patients, α_{up} was not larger than 10^o (Table 3.2), so only one set of non-coplanar directions entering the patient from the cranial direction could be defined. Despite the small angles between these non-coplanar directions and the axial plane, the non-coplanar plans are better than the coplanar plans for these six patients. A larger improvement may be expected if a larger part of the patient in the cranial direction is scanned.

Here, we have investigated the use of computer optimized non-coplanar beam set-ups to improve the PTV dose distribution for liver tumors treated with stereotactic radiotherapy. It was decided to aim at an increase in the minimum PTV dose in order to better approach the homogeneous PTV dose distribution in conventional radiotherapy. Cycle would also have allowed escalation of the isocenter dose while keeping the dose inhomogeneity constant, or escalation of the PTV gEUD. The choice to focus on elevation of the minimum PTV dose is in line with recent findings of Wulf et al.[20] who found that in stereotactic treatment of lung tumors the dose at the PTV margin was the only significant variable for local control. Currently, integration of Cycle in the commercial treatment planning system XIO (CMS, Inc., St. Louis, MO) is being investigated.

3.5 Conclusions

The use of automatically optimized non-coplanar beam set-ups for stereotactic treatment of liver tumors results in treatment plans with improved PTV coverage and reduced dose delivery to healthy tissues. Compared to manual forward planning, the planning workload can be reduced from 1-2 days to 2 h at maximum.

3.A Appendix: Beam selection and score function

For the selection of a beam, each input beam direction is temporarily added to the plan and its weight and shape are optimized based on a score function. The beam direction with the highest score is selected. The score function in Cycle is based on a trade-off between

increasing the PTV dose and approaching the constraint levels for the PTV and the normal tissues. Touching or exceeding a hard constraint results in a zero score. The hard constraints used in this study are given in Table 3.1.

The score function, S_k, for the selection of beam k is given by,

$$S_k(\psi,\phi,w) = S^1_{PTV,k} \cdot S^2_{PTV,k} \cdot \prod_j S_{j,k} \cdot S_{liver,mean,k} \tag{3.3}$$

with,

$$S^1_{PTV,k} = \frac{\Delta D_{PTV}(\psi,\phi,w,k)}{\Delta D^{pre}_{PTV}(k)} \tag{3.4}$$

$$S^2_{PTV,k} = \left[1 - \frac{D_{PTV,rel}(\psi,\phi,w,k)}{D^{tol}_{PTV,rel}} \cdot f^b\right]^p \tag{3.5}$$

$$S_{j,k} = \left[1 - \frac{\Delta P_j(\psi,\phi,w,k)}{\Delta P^{tol}_j(k)}\right]^{p_j} \tag{3.6}$$

$$S_{liver,mean,k} = \left[1 - \frac{\Delta P_j(\psi,\phi,w,k)}{\Delta P^{tol}_j(k)} \cdot \left(\frac{\Delta D^{pre}_{PTV}(k)}{\Delta D_{PTV}(\psi,\phi,w,k)}\right)^a\right]^p \tag{3.7}$$

and:

- $\Delta\, D_{PTV}\ (\psi,\phi,w,k)$ the increase in the delivered PTV dose (isocenter), because of the addition of a beam k with gantry angle ψ, couch angle ϕ, and weight w to the previously selected $k-1$ beams.
- $\Delta\, D^{pre}_{PTV}\ (k)$, the prescribed PTV dose minus the PTV dose (isocenter) delivered by the first $k-1$ beams.
- $D_{PTV,\,rel}\ (\psi,\phi,w,k)$, the relative PTV dose inhomogeneity (= ($D_{isoc,\,k}$ -$D_{PTV,\,min,\,k}$) / $D_{isoc,\,k}$) after the addition of a beam k, with ψ, ϕ, and w.
- $D^{tol}_{PTV,\,rel}$, the tolerated relative PTV dose inhomogeneity (D^{pre}_{PTV} - $D^{tol}_{PTV,\,min}$)/D^{pre}_{PTV}.
- f=($D_{isoc,\,k}$ / D^{pre}_{PTV}), the ratio between the isocenter dose after the addition of beam k and the prescribed dose.
- $\Delta\, P_j\ (\psi,\phi,w,k)$, the increase in the dose distribution parameter P_j (e.g., the maximum dose delivered in an OAR), because of the addition of a beam k, with ψ, ϕ, and w.
- $\Delta\, P^{tol}_j(k)$, the tolerance value for parameter P_j (e.g. the maximum dose allowed in an OAR) minus the parameter value resulting from the previously selected $k-1$ beams.
- p_j, penalty factor that determines the penalty for approaching constraint j.

$S^1_{PTV,k}$ in Eq. 3.4 ensures that the score increases with increasing isocenter dose. The extent of the increase depends on the penalty terms $S^2_{PTV,k}$, $S_{j,k}$ and $S_{liver,mean,k}$, which decrease if w goes up because of a closer approach to the constraints. $S^2_{PTV,k}$ (Eq. 3.5) and $S_{liver,mean,k}$ (Eq. 3.7) prevent violation of the relative PTV dose inhomogeneity constraint and the mean liver dose constraint, respectively. The terms $S_{j,k}$ (Eq. 3.6) impose a penalty for approaching the other hard constraints.

The dose distribution after the first selected beam will generally have a rather high relative PTV dose inhomogeneity, because the attenuation of this beam is not yet compensated by beams from other directions. The term f^b in $S^2_{PTV,k}$ ($b = 0.5$ in this study) allows for exceeding of the tolerated relative PTV dose inhomogeneity, $D^{tol}_{PTV,rel}$, for selection of the first beams. If the isocenter dose approaches the prescribed dose, f^b goes to 1 and the relative dose inhomogeneity, $D_{PTV,rel}(\psi,\phi,w,k)$, is forced to become smaller than the tolerated inhomogeneity. If the value of the dose distribution parameter P_j is much smaller than the tolerated value (which is the case in the first selected beams) the penalty term $S_{j,k}$ (Eq. 3.6) is less sensitive to an increase in P_j than when P_j is close to the tolerated dose. This may result in selection of beam directions that pass through OARs. For most OARs this is not a problem, because in a further stage of the plan generation, beam directions will be selected that avoid this OAR. As the PTV is located inside the liver, this OAR can not be avoided by any beam direction. In addition, the mean liver dose constraint is the most limiting constraint. Therefore it is important that also for the selection of the first beams the score is sensitive to the mean liver dose parameter. This has been solved by a generalization of the term $S_{j,k}$ (Eq. 3.6), yielding $S_{liver,mean,k}$ (Eq. 3.7), with $P_j = D_{liver,mean}$. If a equals 0, $S_{liver,mean,k}$ is the same as $S_{j,k}$. In this study, a value of 0.5 has been used.

Bibliography

[1] Hadinger U, Thiele W, Wulf J. Extracranial stereotactic radiotherapy: evaluation of PTV coverage and dose conformity *Z Med Phys*. 2002;12:221–229.

[2] Wulf J, Hadinger U, Oppitz U, et al. Stereotactic radiotherapy for primary lung cancer and pulmonary metastases: a noninvasive treatment approach in medically inoperable patients *Int J Radiat Oncol Biol Phys*. 2004;60:186–196.

[3] Wulf J, Hadinger U, Oppitz U, et al. Impact of target reproducibility on tumor dose in stereotactic radiotherapy of targets in the lung and liver *Radiother Oncol*. 2003;66:141–150.

[4] Wulf J, Hadinger U, Oppitz U, et al. Stereotactic radiotherapy of targets in the lung and liver *Strahlenther Onkol*. 2001;177:645–655.

[5] Schefter TE, Kavanagh BD, Timmerman RD, et al. A phase I trial of stereotactic body radiation therapy (SBRT) for liver metastases *Int J Radiat Oncol Biol Phys*. 2005;62:1371–1378.

[6] Timmerman RD, Kavanagh BD. Stereotactic body radiation therapy *Curr Probl Cancer.* 2005;29:120–157.

[7] Lax I. Target dose versus extratarget dose in stereotactic radiosurgery *Acta Oncol*. 1993;32:453–457.

[8] Park W, Lim DH, Paik SW, et al. Local radiotherapy for patients with unresectable hepatocellular carcinoma *Int J Radiat Oncol Biol Phys*. 2005;61:1143–1150.

[9] Ten Haken RK, Balter JM, Marsh LH, et al. Potential benefits of eliminating planning target volume expansions for patient breathing in the treatment of liver tumors *Int J Radiat Oncol Biol Phys*. 1997;38:613–617.

[10] Thomas E, Chapet O, Kessler ML, et al. Benefit of using biologic parameters (EUD and NTCP) in IMRT optimization for treatment of intrahepatic tumors *Int J Radiat Oncol Biol Phys*. 2005;62:571–578.

[11] Woudstra E, Storchi PR. Constrained treatment planning using sequential beam selection *Phys Med Biol*. 2000;45:2133–2149.

[12] Woudstra E, Heijmen BJM. Automated beam angle and weight selection in radiotherapy treatment planning applied to pancreas tumors *Int J Radiat Oncol Biol Phys*. 2003;56:878–888.

[13] Woudstra E, Heijmen BJM, Storchi PR. A comparison of an algorithm for automated sequential beam orientations selection with exhaustive search and simulated annealing *Med Phys*. 2005.

[14] Woudstra E, Heijmen BJ, Storchi PR. Automated selection of beam orientations and segmented intensity-modulated radiotherapy (IMRT) for treatment of oesophagus tumors *Radiother Oncol*. 2005;77:254–261.

[15] Beaulieu F, Beaulieu L, Tremblay D, et al. Simultaneous optimization of beam orientations, wedge filters and field weights for inverse planning with anatomy-based MLC fields *Med Phys*. 2004;31:1546–1557.

[16] Beaulieu F, Beaulieu L, Tremblay D, et al. Automatic generation of anatomy-based MLC fields in aperture-based IMRT *Med Phys*. 2004;31:1539–1545.

[17] Dawson LA, Normolle D, Balter JM, et al. Analysis of radiation-induced liver disease using the Lyman NTCP model *Int J Radiat Oncol Biol Phys*. 2002;53:810–821.

[18] Niemierko A. A generalized concept of equivalent uniform dose (EUD) *Med Phys*. 1999;26:1100.

[19] Cheng JC, Wu JK, Lee PC, et al. Biologic susceptibility of hepatocellular carcinoma patients treated with radiotherapy to radiation-induced liver disease *Int J Radiat Oncol Biol Phys*. 2004;60:1502–1509.

[20] Wulf J, Baier K, Muller G, et al. Dose-response in stereotactic irradiation of lung tumors *Radiother Oncol*. 2005;77:83–87.

Chapter 4

PTV dose prescription strategies for SBRT of metastatic liver tumors

JA de Pooter, W Wunderink, A Méndez Romero, PRM Storchi, BJM Heijmen, *Radiother Oncol*. 2007;**85**(2):260-6

Abstract

Purpose:
Recently we have demonstrated that our in-house developed algorithm for automated plan generation for fully non-coplanar SBRT of liver patients (designated Cycle) yields plans that are superior to conventionally generated plans of experienced dosimetrists. Here we use Cycle in the comparison of plans with prescription isodoses of 65% or 80% of the isocenter dose.
Methods:
Plans were generated using CT-data of 15 previously treated patients. For each patient, both for the 65%- and the 80% strategy, Cycle was used to generate a plan with the maximum isocenter dose, D_{isoc}, while strictly obeying a set of hard constraints for the organs at risk (OAR). Plans for the two strategies were compared using D_{isoc}, $D_{PTV,\,99\%}$ (the minimum dose delivered to 99% of the PTV), and the generalized equivalent uniform dose, $gEUD_{PTV}(a)$, for several values of the parameter a. Moreover, for the OARs, the distance to the constraint values was analysed.
Results:
The 65% strategy resulted in treatment plans with a higher D_{isoc} (average 17.6%, range 7.6% – 31.1%) than the 80% strategy, at the cost of a somewhat lower $D_{PTV,99\%}$ (average -2.0%, range -9.6% – 9.3%). On average, voxels with a dose in the 65% strategy, lower than the minimum PTV dose in the 80% strategy, were within 0.2 cm from the PTV surface. For $a \geq$ -10, the 65% strategy yielded on average a significantly ($P<0.01$) higher $gEUD_{PTV}(a)$ than the 80% strategy, whereas for highly negative a-values the 80% approach was slightly better, although not significantly. Large variations between patients were observed. Generally, for the OAR the approach to the constraint levels was similar for the two strategies.
Conclusion:
On average, PTV dose delivery is superior with the 65% strategy. However, apart from the isocenter dose, for each applied PTV dose parameter at least one patient would have been better off with the 80% dose prescription strategy.

4.1 Introduction

In treatment plan design for stereotactic body radiation therapy (SBRT) of liver metastases, different dose prescription strategies are applied. Some institutes prescribe the dose to the 65%[1–4] isodose, other institutes[5,6] prescribe to the 80% isodose, resulting in treatment plans with an inhomogeneous and a more homogeneous PTV dose distribution respectively. In both strategies, the prescription isodose closely surrounds the PTV. The 65% dose prescription strategy is based on the work of Lax[7], who investigated the trade-off between target dose and normal tissue dose for stereotactic radiosurgery. He found that an inhomogeneous PTV dose distribution (D_{min} / D_{max} = 60%) yields an increased mean PTV dose compared to a more homogeneous PTV dose distribution (D_{min} / D_{max} = 85%), for the same dose at the periphery of the PTV, and for almost the same dose to the normal tissue. He used a 4π-beam distribution with 201 equally weighted cone shaped beams to simulate an intra-cranial treatment performed with a gamma-knife.

SBRT for liver metastases differs from the radiosurgery treatment simulated by Lax on the following aspects. SBRT is performed with a linear accelerator using a relatively small number of MLC shaped coplanar and non-coplanar beams (in our case 10 beams at maximum). The angle of the non-coplanar directions with the axial plane is limited due to forbidden couch-gantry angle combinations. The purpose of this paper is to compare the 65% and 80% strategy for SBRT of liver metastases.

4.2 Methods

4.2.1 Automatic plan generation with Cycle

In this study, plans are automatically generated using an in-house developed algorithm, designated Cycle. The algorithm has been described in detail[8–10], here a short summary is given. Cycle aims at generating a treatment plan with the prescribed PTV isocenter dose, while strictly obeying the imposed constraint levels on the PTV dose inhomogeneity, OARs and other normal tissues. Cycle starts plan generation with an empty plan. Sequentially new beam directions are selected and added to the plan from a large set of input directions containing coplanar and non-coplanar beams. Dose distributions for input directions are precalculated, with a pencil beam algorithm.

To select a new beam, k, each beam in the set of input directions is temporarily added to the plan (consisting of the previously selected k-1 beams). For each temporarily added input beam direction, the weight and beam shape are optimised, based on a score function. The score function represents a trade-off between increasing the PTV dose and approaching the imposed constraint levels. The score function takes into account the dose distribution of the previously selected k-1 beams. The optimized score, s_{max}, for all beam directions in the input set are compared and the beam direction with the highest score is selected and added to the plan. The score function can be made more sensitive for a certain constraint by increasing the corresponding importance factor. Further selection of beams stops if one of the following is true:

- Maximum number of allowed beam directions per plan is reached
- A constraint is violated
- The prescribed dose has been attained, i.e., plan generation was successful

In the first two situations a new plan generation is started with automatically adjusted importance factors for the score function to better avoid approaching critical constraints. In this study, for each patient and each strategy, Cycle was used repeatedly for increased doses to generate the plan with the highest prescribed isocenter dose, while not violating any of the constraints.

4.2.2 Input beam directions

In a previous paper we showed the advantage of automatically generated fully non-coplanar beam set-ups[8]. Therefore in this study, the set of input beam directions consisted of 72 coplanar beams and a number of sets of 36 non-coplanar beams. Each set of non-coplanar beams had a constant angle, α, with the axial plane. The separation in α between two sets was 10^o. The maximum α for which none of the input beam directions enters the CT patient volume through the upper or lower CT slice was determined for each patient individually. The maximum α determines the number of sets of non-coplanar input beam directions. In this study the number of beams in the input set ranged from 216 to 252 (including the 72 coplanar beams).

4.2.3 Planning constraints

The clinical planning constraints used in this study are summarized in Table 4.1. For the OARs, the constraints of the clinical protocol are used. Due to a history of surgical resection, some patients have a rather small liver volume. For these patients applying only the dose volume histogram (DVH) liver constraints, defined as a fixed percentage (33% and 50%) of the total liver volume may result in a small absolute liver volume that receives a low dose. To avoid this, the DVH constraint proposed by Schefter et al.[6] was applied, which states that at least 700 CC of the normal liver volume should receive a dose lower than 15 Gy.

Maximum dose constraints were applied to two non-organ-based regions in the normal tissue. Region R_2 is defined as all tissue outside a PTV expansion of 5.0 cm. Region R_1 is defined as all tissue outside a PTV expansion of 2.0 cm, excluding region R_2.

4.2.4 Plan optimisation

For CT-data of 15 patients previously treated at our institute[2] Cycle was used to generate plans for the two strategies. For both strategies, the isocenter dose was maximised, while keeping the ratio between the minimum PTV dose and the prescribed isocenter dose, constant at either 65% or 80%. The constraints mentioned in Table 4.1 were hard constraints, so no constraint violations were allowed. The maximum number of beams allowed per plan was set to 10. The spherically shaped PTV and CTV have average volumes of respectively 146 CC (49 – 405 CC) and 56 CC (12 – 200 CC).

For isocenter dose maximisation Cycle was used in an iterative procedure. In each iteration, Cycle tried to generate a plan with the prescribed isocenter dose, while strictly obeying

Structure	Constraint	C_j
PTV	$D_{PTV,\ min}$ = 0.65 or 0.80 × D_{isoc}	NA
Liver	$D_{33\%} < 21$ Gy	$D_{33\%}$ / 21
Liver	$D_{50\%}$ or $D_{700\ CC} < 15$ Gy	$D_{50\%}$ / 15
Spinal Cord	$D_{max} < 15$ Gy	D_{max} / 15
Bowel, duodenum, stomach, esophagus	$D_{5\ CC} < 21$ Gy	$D_{5\ CC}$ / 21
Heart	$D_{5\,CC} < 21$ Gy	$D_{5\,CC}$ / 21
Kidney's	$D_{33\%} < 15$ Gy	$D_{33\%}$ / 15
R_1	$D_{max} < D_{PTV,\ min}$ - 5 Gy	NA
R_2	$D_{max} < 20$ Gy	D_{max} / 20

Table 4.1: Applied constraints for the plan optimisation and their corresponding constraint parameters, C_j, for the calculation of the DIP (Eq. 4.2).

the imposed constraints. If the plan generation was successful, the prescribed isocenter dose was slightly increased. This was repeated until further increase of the prescribed isocenter dose did no longer result in a plan without constraint violation even after repeated adjustments of the importance factors in the score function (see above). For plan generation, the relative PTV dose inhomogeneity constraint $D^{tol}_{PTV,\ rel} = (D^{pre}_{PTV} - D^{tol}_{PTV,\ min}) / D^{pre}_{PTV}$ was set to 0.35 and 0.2 for the 65% and the 80% strategy respectively[8], where D^{pre}_{PTV} is the prescribed isocenter dose and $D^{tol}_{PTV,\ min}$ the tolerated minimum PTV dose.

4.2.5 Comparison of strategies

For the PTV, optimal plans for the two strategies were compared with respect to the generalised equivalent uniform dose, gEUD, mean dose, isocenter dose and $D_{PTV,\ 99\%}$ (the minimum dose delivered to 99% of the PTV). The gEUD(a) is given by the following formula.

$$\mathrm{gEUD}(a) = \left(\frac{1}{N} \sum_{i=1}^{N} D_i^a \right)^{1/a} \tag{4.1}$$

Here a is a tissue specific parameter which is negative for tumors[11]. The summation is over N voxels with index i. Since the exact value of a for liver metastases is unknown, the comparison was done for the following levels of a: -100, -50, -20, -10, -5, -1. Statistical significance was tested with a paired two-tailed t-test.

As expected it turned out, that the inhomogeneous 65% planning strategy led to the highest isocenter dose. However, some patients had voxels close to the PTV surface with a dose lower than the minimum dose in the 80% strategy. To evaluate the importance of this PTV volume receiving a low dose with the 65% strategy, $\mathrm{gEUD}_{PTV\text{-}0.25}(a)$ and $D_{PTV\text{-}0.25,\ 99\%}$ values were calculated for the PTV minus a margin of 0.25 cm. Moreover, the fraction of the PTV voxels for which the 65% strategy receives a lower dose than the minimum PTV dose of the 80% strategy, $F(D_j^{65\%} < D^{80\%}_{PTV,min})$, and the maximum distance, d_{max}, of these voxels

to the PTV surface was calculated. To calculate d_{max}, a triangulation of the PTV surface was made based on the available PTV contour points. Then, for each PTV voxel that received for the 65% strategy a dose lower than the minimum PTV dose of the 80% strategy, the distances between the voxel and all the PTV surface triangles were calculated. The minimum of these distances was the distance of the voxel from the PTV surface.

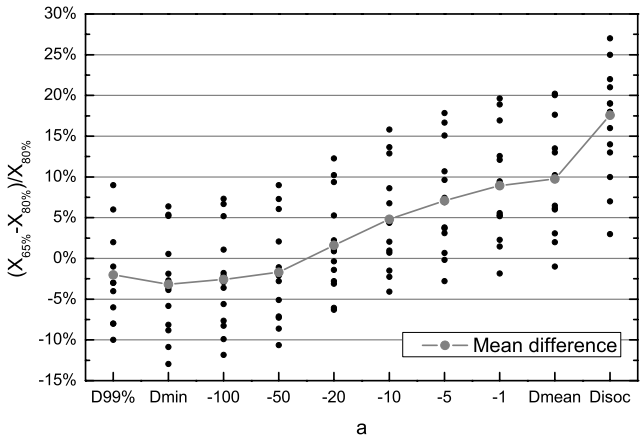

Figure 4.1: Relative differences between the 65% and 80% strategies in the parameters (indicated by X on the left axis) $D_{PTV,\,99\%}$, $D_{PTV,\,mean}$, D_{isoc}, and $gEUD_{PTV}(a)$ for a–values ranging from -100 to -1. The dots represent comparisons for individual patients. The line connects patient mean values.

To evaluate the dose delivered to the OARs, the distance from ideal plan[8,10], DIP, and the conformality index, CI, were calculated for each plan. The DIP measures how far an optimised plan stays away from the applied constraint levels. The DIP is given by the following formula,

$$\mathrm{DIP} = \sqrt{\sum_{j=1}^{M} \frac{C_j^2}{M}} \tag{4.2}$$

M is the number of OAR constraints. C_j, the constraint parameter for the j-th constraint, is the ratio between its actual level and the applied constraint level, see Table 4.1. CI is defined in this study as the ratio between the volume of the $D_{PTV,\,99\%}$ isodose and the total PTV volume. Per plan and per strategy, the limiting structures were evaluated. The limiting structure is that structure, where constraints prevent further increase of the isocenter dose (section 4.2.4).

4.3 Results

4.3.1 PTV evaluation

Results for the isocenter dose, PTV mean dose, $D_{PTV,\,99\%}$ and $gEUD_{PTV}(a)$ comparisons are shown in Fig. 4.1. For $a \geq$ -20 the gEUD(a) for the 65% strategy plans is on average higher than for the 80% strategy, with a considerable variation between individual patients. For a = -20 and a = -10 the increase for the 65% strategy is on average 1.4% (range -6.3% – 12.3%) and 4.8% (range -4.1% – 15.8%) respectively. The increase is significant for $a \geq$ -10 ($P < 0.01$), for $a \leq$ -20 and for the $D_{PTV,\,99\%}$ both strategies are not statistically different. The isocenter dose and the mean PTV dose are on average higher for the 65% strategy, 17.6% (range 2.9% – 31.1%), and 9.8% (range -1.4% – 20.2%), respectively.

Results for the PTV minus a margin of 0.25 cm are shown in Fig. 4.2. For each strategy and each a parameter the $gEUD_{PTV\text{-}0.25}(a)$ of a plan is higher than the $gEUD_{PTV}(a)$. This increase in $gEUD_{PTV\text{-}0.25}(a)$ is higher for the 65% strategy than for the 80% strategy, resulting in larger mean relative differences between the strategies. The average of $gEUD_{PTV\text{-}0.25}(a)$ for the 65% strategy is higher than for the 80% strategy for each value of the a-parameter. The differences are significant for $a \geq$ -20 ($P < 0.01$), for lower a-values both strategies are not statistically different. For a = -20 and a = -10 the gEUD for the 65% strategy is on average 6.4% (range -2.6% – 18.2%) and 8.8% (range -1.4% – 20.4%) higher, respectively. $D_{PTV\text{-}0.25,\,99\%}$ is on average 2.8% higher for the 65% strategy, however the increase is not

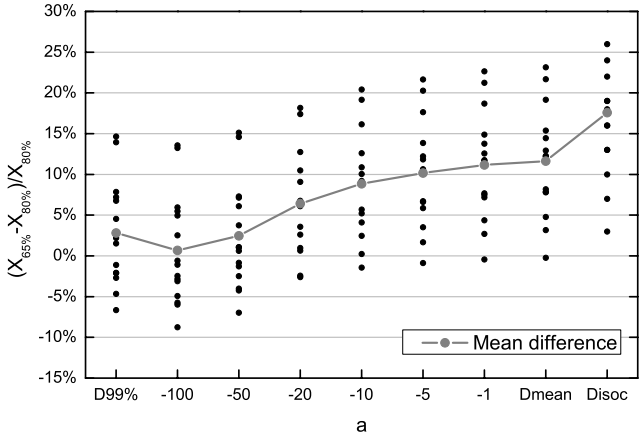

Figure 4.2: Relative differences between the 65% and 80% strategies in the parameters (indicated by X on the left axis) $D_{PTV\text{-}0.25,\,99\%}$, $D_{PTV\text{-}0.25,\,mean}$, D_{isoc} and $gEUD_{PTV\text{-}0.25}(a)$ for a–values ranging from -100 to -1. The dots represents comparisons for individual patients. The line connects patient mean values.

statistically significant (P = 0.132).

The results for $F(D_j^{65\%} < D_{PTV,min}^{80\%})$ are shown in Table 4.2. On average 3% (range 0% – 9%) of the PTV voxels receive for the 65% strategy plan a dose lower than the minimum PTV dose of the 80% strategy plan. The maximum distance, $d_{max,}$ of these voxels to the PTV surface has for the whole patient group an average value of 0.16 cm with a maximum of 0.48 cm (Table 4.2, last column). The voxels of the PTV for which the 65% strategy is lower than the minimum PTV dose of the 80% strategy are categorised according to their difference between the dose received for the 65% strategy and the minimum PTV dose of the 80% strategy. For the voxels in each category the maximum distance, d_{max}, to the PTV surface was calculated (see column 3-6 of Table 4.2). It can be seen that d_{max}, increases with a decreasing dose difference. For voxels receiving in the 65% strategy a dose more than 5% lower than the minimum PTV dose of the 80% strategy the highest d_{max} in the patient group is 0.31 cm.

Fig. 4.3 shows for case 4 dose distributions in the isocenter plane for the 65% strategy (Fig. 4.3(a)) and the 80% strategy (Fig. 4.3(b)), and a crossline dose profile (Fig. 4.3(c)). The dose in the central part of the PTV is considerably higher for the 65% strategy. From the

Case	F	d_{max} (cm)				
		0 - 2%	2 - 5%	5 - 10%	10 - 15%	Overall
1	0.02	0.10	0.11			0.11
2	0.02	0.16	0.13			0.16
3	0.05	0.48	0.45	0.31	0.09	0.48
4	0.06	0.31	0.22	0.22		0.31
5	0.00					0.00
6	0.03	0.06	0.18			0.18
7	0.00					0.00
8	0.01	0.11				0.11
9	0.02		0.21			0.21
10	0.02	0.11	0.03			0.11
11	0.04	0.18	0.26	0.21		0.26
12	0.03	0.19	0.18	0.08		0.19
13	0.09	0.23	0.25	0.18	0.09	0.25
14	0.00					0.00
15	0.00					0.00
Average	**0.03**	**0.19**	**0.20**	**0.20**	**0.09**	**0.16**

Table 4.2: Data on PTV voxels for which the dose in the 65% strategy is lower than the minimum dose of the 80% strategy. F is the fraction of these PTV voxels. d_{max} is the maximum distance of these voxels to the PTV surface. In columns 3-6 the voxels are categorized according to their dose difference with the minimum PTV dose for the 80% strategy. The last column show overall d_{max} values.

crossline profile it can be seen that there is a small volume at the edge of the PTV that receives a dose lower than the minimum dose level of the 80% strategy. This small underdosage at the PTV edge is not observed for each crossline profile. The selected isocenter slice dose distribution is a worst case for the whole patient group.

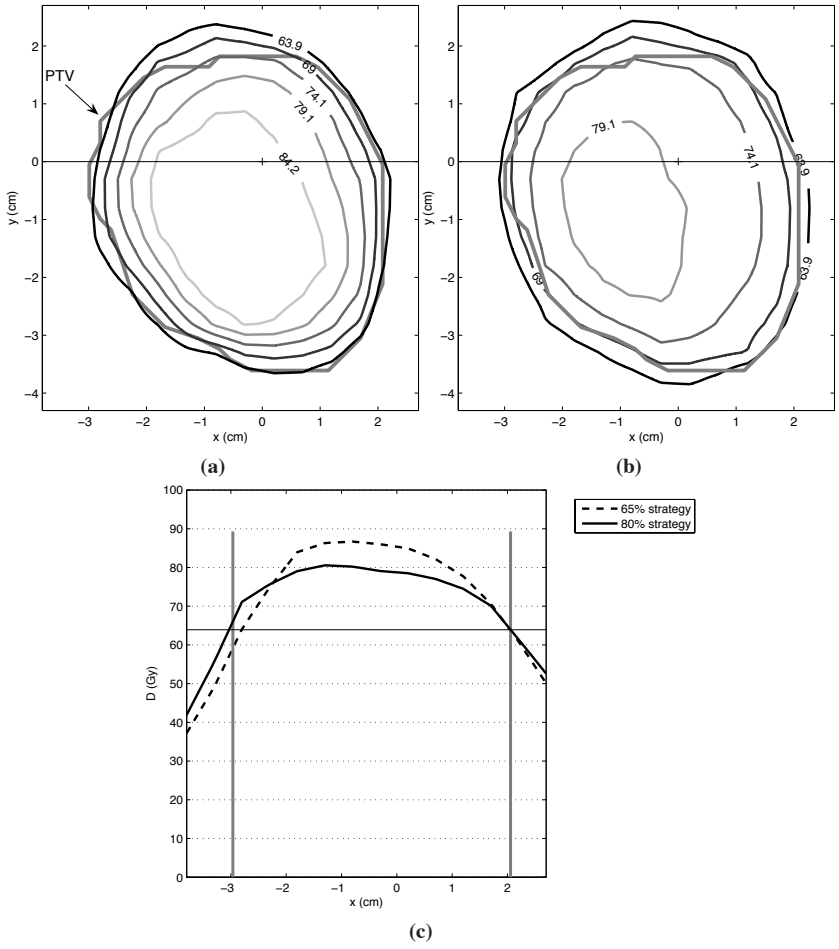

Figure 4.3: PTV contour (thick grey polyline) and dose distributions for case 4 for the 65% (a) and the 80% strategy (b) in the isocenter slice. Only isodoses (in Gy) between the minimum and maximum PTV dose are plotted. (c) crossline profiles of the distributions in a. and b. plotted with the minimum dose level of the 80% strategy (horizontal line) and the edges of the PTV (thick vertical lines).

Case	DIP		Limiting constraints	
	65%	80%	65%	80%
1	0.240	0.237	Liver, NT	Liver, NT
2	0.268	0.258	Myelum, Heart	Myelum, Heart
3	0.299	0.295	Kidney, NT	Kidney, NT
4	0.274	0.260	Esophagus, NT	Myelum, Bowel, NT
5	0.233	0.222	Myelum, NT	NT
6	0.264	0.278	Liver	Liver
7	0.207	0.200	Liver	Liver
8	0.281	0.268	Heart, NT	Heart, NT
9	0.216	0.222	NT	NT
10	0.240	0.256	NT	NT
11	0.286	0.278	NT	NT
12	0.239	0.253	NT	Bowel, NT
13	0.254	0.261	Bowel, NT	Bowel, NT
14	0.233	0.244	Esophagus	Esophagus, NT
15	0.280	0.280	Myelum, Heart	Myelum
	0.254	**0.254**		

Table 4.3: DIP (Eq. 4.2) values calculated for the 65% and the 80% strategy. Structures with limiting constraints for both strategies. NT indicate the normal tissue constraints on R_1 and R_2.

4.3.2 Normal tissue evaluation

The results for the DIP calculations are shown in Table 4.3. The differences in DIP value between the two strategies are rather small. The CI of the generated plans had a mean value of 1.26 (range 1.14 – 1.38) and 1.18 (range 1.09 – 1.31) for the 65% and the 80% strategy, respectively. In Table 4.3, also the limiting structures are summarized per case and per planning strategy. Further increase of PTV was prevented by violation of one or more OAR and/or normal tissue constraints in combination with the minimum PTV dose constraint. For 10/15 patients the complete set of limiting structures is the same in both strategies (Table 4.3). For the other five cases at least one limiting structure is the same in both strategies.

4.4 Discussion

The 65% strategy results in plans that have a considerably higher peak dose in the central part of the PTV (isocenter dose) than for the 80% strategy, at the cost of a somewhat lower dose in voxels close to the boundaries of the PTV. The OAR dose is on average the same for both strategies and within the applied planning constraint levels. The conformality as measured with the CI is somewhat higher for the 65% strategy, and within the limit of 1.4 as proposed by Timmerman et al[12].

The considerable increase in mean PTV dose for the 65% planning strategy is in agreement with the results of Lax[7]. He found an increase of 29% in the mean PTV dose if a dose

concept with a high PTV dose inhomogeneity was applied instead of a concept with a low PTV dose inhomogeneity, while in this study the increase was 9.8% on average. The higher value found by Lax can be partially explained by differences in the planning approach. In our approach the OAR constraints were constant for both strategies, while in the approach of Lax the dose at the periphery of the PTV was constant. Furthermore, the strategies in the study of Lax have different PTV dose inhomogeneities, 60% and 85%, than the ones used in this study, 65% and 80%. Also, the study of Lax was designed to simulate an intra-cranial radiosurgery treatment using a large number of cone shaped beams, while in this study the maximum number of beams per plan was set to 10. In theory, the conclusions in this paper could be biased by selection of tuning parameters of the Cycle algorithm for the 65% and 80% strategies. However, there are only a few tuning parameters, that have been established a long time ago[9]. For both strategies these parameters were used. Moreover, our conclusions are in line with the findings of Lax (above).

Since for inhomogeneous dose distributions the radiobiological effect on the tumour cannot be fully described with only the minimum PTV dose or the mean PTV dose, the gEUD(a)[11] was used to investigate which planning strategy results in the highest PTV dose. The gEUD(a) weights the dose in each voxel of the PTV, the lower the selected a value, the higher the weight of voxels with low dose, i.e. the PTV periphery. The gEUD(a) of the PTV is on average higher for the 65% strategy than for the 80% strategy for a values of -20 and higher. The increase for the 65% strategy is statistically significant for a-values of -10 and higher. For a-values smaller than -20, the differences between the strategies were statistically insignificant.

The exact value of the a-parameter for gEUD calculations of metastatic liver tumors is unknown. Thomas et al.[13] used values of -5 and -20 as representative values for a low-grade and an aggressive tumour respectively, for IMRT treatment plan comparison for metastatic liver patients. By matching the expressions for the surviving fraction in the gEUD model and the linear quadratic (LQ) model, a value for a can be estimated[14] by using the formula $a = -\mathrm{D}(\alpha + 2\mathrm{D}\beta)$. Under the assumption of α=0.5 Gy^{-1}, α/β=10 Gy and a fraction dose, D, of 12.5 Gy, the value for a is -21.9.

The colon is the site of the primary tumour for most of the liver metastases treated with SBRT in our institute[2]. As shown by van Laarhoven et al.[15] liver metastases from colorectal cancer contain hypoxic regions. Hypoxia leads to a decrease of the radio sensitivity parameter α and can be incorporated in the LQ model with the oxygen enhancement ratio (OER), which is defined as the ratio between the α under aerobic conditions and the α under hypoxic conditions. Carlson et al.[16] give values for the OER in a range of 2.3 to 3.3 and conclude that the OER value is nearly independent of cell type. If α decreases with a factor of 2.8, the estimated a parameter increases to a value of -17.9 using the same assumptions as above. Niemierko et al.[11] fitted clinical data for chordoma tumors to the gEUD model and found a value of -13.1 for the a parameter. These considerations indicate that the true value of the a parameter might be -20 or higher.

In clinical practice, we use a stereotactic body frame (SBF) with abdominal compression

for reduction of respiratory tumour motion, generally resulting in a residual tumour top-to-top motion of 0.5 cm or less (amplitude $<$ 0.25 cm). The planning CTV to PTV margin applied for this treatment is determined by the residual tumour motion and the set-up errors, yielding a margin of 1.0 cm and 0.5 cm in the cranial-caudal direction and the axial directions respectively. As shown by Wunderink et al.[17], these margins are sufficient for the applied patient positioning method to ensure that the tumour remains inside the PTV during the whole treatment. This means that in the equilibrium tumour position formed by the midpoint of the respiratory cycle, the tumour is always within the PTV minus 0.25 cm margin, i.e. the PTV-0.25. Only for a maximum set-up error and with the tumour in the maximum position of the breathing excursion, the tumour touches the PTV surface. For 12 of the 15 patients, the maximum distance, d_{max}, of the PTV voxels that receive for the 65% strategy plan a dose lower than the minimum dose of the 80% strategy plan is smaller than 0.25 cm. This means that in the equilibrium position of the tumour's motion range, none of these voxels can be covered by tumour tissue. Further, it has to be considered, that if the tumour moves to the PTV edge (into the low dose region), the other side of the tumour wil move inwards, i.e. towards higher doses. Since for the 65% strategy, the dose in the central part is higher than for the 80% strategy, the effect of the low dose region on one side will be more compensated by the central part for the 65% strategy than for the 80% strategy. N.B. this compensation does not hold for systematic problems, e.g. in finding the isocenter coordinate.

A gEUD calculated for the total PTV volume assumes that the whole PTV is covered with tumour uniformly. Since this is not the case for SBRT of liver metastases, a gEUD calculation that takes into account the true variation of tumour coverage over the PTV volume gives a better representation of the radiobiological effect to the tumour. As an approximation to the true tumour coverage, the outer PTV shell of 0.25 cm thickness was set to zero coverage while the rest of the PTV was set to 1 coverage resulting in the $gEUD_{PTV\text{-}0.25}$. The relative difference between the 65% strategy and the 80% strategy for the $gEUD_{PTV}$ was always lower than for the $gEUD_{PTV\text{-}0.25}$. The $gEUD_{PTV\text{-}0.25}(a)$ was on average higher for the 65% than for the 80% strategy for each a value. The average increase was significant for a-values of -20 and higher.

In a clinical protocol, the whole patient group is generally treated with the same PTV dose inhomogeneity. For $a <$ -20 no statistical differences were found in gEUD(a) between the 65% and the 80% strategy. If the tumour coverage of the PTV is taken into account, the 65% strategy results in plans with a significant higher gEUD(a) for a = -20. For $a \geq$ -10 the increase in gEUD(a) for the 65% strategy is significant, irrespective of taking into account the tumour coverage of the PTV. Since the 65% strategy is on average never worse than the 80% strategy and for the most relevant range of a-parameters better than the 80% strategy, the 65% strategy is more favourable than the 80% strategy if the whole patient group is treated with the same PTV dose inhomogeneity. If the PTV dose inhomogeneity is individualised, some patients may benefit from applying the 80% strategy. Another way to compare the two planning strategies is by scaling plans of both strategies to the same gEUD(a) for a certain value of a. In that case the dose delivered to the OAR as measured with the DIP will be lower

for the 65% strategy than for the 80% strategy. The amount of OAR dose reduction will be dependent on the value of the used *a* parameter for the gEUD(*a*).

4.5 Conclusion

PTV dose maximisation for SBRT of liver metastases with an inhomogeneous PTV dose prescription strategy (65%) compared to a more homogeneous dose prescription strategy (80%) leads to plans with a higher peak dose and mean dose in the PTV at the cost of small parts with a somewhat lower dose close to the edges of the PTV. The dose in the OARs is the same for both strategies. On average, PTV dose delivery is superior with the 65% strategy. However, apart from the isocenter dose, for each applied PTV dose parameter at least one patient would have been better off with the 80% dose prescription strategy.

Bibliography

[1] Blomgren H, Lax I, Naslund I, et al. Stereotactic high dose fraction radiation therapy of extracranial tumors using an accelerator. Clinical experience of the first thirty-one patients *Acta Oncol*. 1995;34:861–870.

[2] Méndez Romero A, Wunderink W, Hussain SM, et al. Stereotactic body radiation therapy for primary and metastatic liver tumors: A single institution phase I-II study *Acta Oncol*. 2006;45:831–837.

[3] Wulf J, Hadinger U, Oppitz U, et al. Stereotactic radiotherapy of targets in the lung and liver *Strahlenther Onkol*. 2001;177:645–655.

[4] Wulf J, Hadinger U, Oppitz U, et al. Stereotactic radiotherapy for primary lung cancer and pulmonary metastases: a noninvasive treatment approach in medically inoperable patients *Int J Radiat Oncol Biol Phys*. 2004;60:186–196.

[5] Herfarth KK, Debus J, Lohr F, et al. Stereotactic single-dose radiation therapy of liver tumors: results of a phase I/II trial *J Clin Oncol*. 2001;19:164–170.

[6] Schefter TE, Kavanagh BD, Timmerman RD, et al. A phase I trial of stereotactic body radiation therapy (SBRT) for liver metastases *Int J Radiat Oncol Biol Phys*. 2005;62:1371–1378.

[7] Lax I. Target dose versus extratarget dose in stereotactic radiosurgery *Acta Oncol*. 1993;32:453–457.

[8] de Pooter JA, Méndez Romero A, Jansen WP, et al. Computer optimization of noncoplanar beam setups improves stereotactic treatment of liver tumors *Int J Radiat Oncol Biol Phys*. 2006;66:913–922.

[9] Woudstra E, Storchi PR. Constrained treatment planning using sequential beam selection *Phys Med Biol*. 2000;45:2133–2149.

[10] Woudstra E, Heijmen BJM. Automated beam angle and weight selection in radiotherapy treatment planning applied to pancreas tumors *Int J Radiat Oncol Biol Phys*. 2003;56:878–888.

[11] Niemierko A. A generalized concept of equivalent uniform dose (EUD) *Med Phys*. 1999;26:1100.

[12] Timmerman RD, Kavanagh BD. Stereotactic body radiation therapy *Curr Probl Cancer.* 2005;29:120–157.

[13] Thomas E, Chapet O, Kessler ML, et al. Benefit of using biologic parameters (EUD and NTCP) in IMRT optimization for treatment of intrahepatic tumors *Int J Radiat Oncol Biol Phys*. 2005;62:571–578.

[14] Zhou SM, Das S, Wang Z, et al. Relationship between the generalized equivalent uniform dose formulation and the Poisson statistics-based tumor control probability model *Med Phys*. 2004;31:2606–2609.

[15] Laarhoven HW, Kaanders JH, Lok J, et al. Hypoxia in relation to vasculature and proliferation in liver metastases in patients with colorectal cancer *Int J Radiat Oncol Biol Phys*. 2006;64:473–482.

[16] Carlson DJ, Stewart RD, Semenenko VA. Effects of oxygen on intrinsic radiation sensitivity: A test of the relationship between aerobic and hypoxic linear-quadratic model parameters *Med Phys*. 2006;33:3105–15.

[17] Wunderink W, Méndez Romero A, Vasquez Osorio EM, et al. Target coverage in image-guided stereotactic body radiotherapy of liver tumors *Int J Radiat Oncol Biol Phys*. 2007;68:282–290.

Chapter 5

Computer generation of fully non-coplanar treatment plans for SBRT of liver tumours based on gEUD optimisation

BJM Heijmen, JA de Pooter, A Méndez Romero, W Wunderink, E Woudstra, PR Storchi, PC Levendag, *Proceedings of the 15th International conference on the use of computers in radiation therapy, Toronto, Canada*. 2007:333-337

5.1 Introduction

In stereotactic body radiation therapy (SBRT) of liver tumors, the dose is generally prescribed to the 65%[1–4], or 80% isodose[5,6], closely surrounding the PTV. Treatment plans are normally generated by a dosimetrist, applying a lengthy, trial-and-error planning procedure. Currently, most patients at Erasmus MC are treated with 3×12.5 Gy, prescribed to the 65% isodose. The maximum tumour diameter is 6 cm. Treatment results are promising[2,7].

We have developed an algorithm, designated Cycle, for automated treatment plan design. Beam directions are automatically selected from a large input set of coplanar and non-coplanar orientations ($>$ 250), and beam shapes, sizes and weights are optimized. Generated plans do strictly adhere to imposed hard constraints for organs at risk[8–11]. In a recent study[9], we have demonstrated that on average dose prescription to the 65% isodose is superior to prescription to 80%. However, some patients are better off with the latter.

Here, Cycle has been extended to maximize $\mathrm{gEUD}_{\mathrm{PTV}}(a)$, the generalized Equivalent Uniform Dose for the PTV for a selected parameter a (Eq. 5.2), while not exceeding OAR hard constraints. There are no restrictions on the minimum PTV dose. For a = -20, treatment plans are compared to plans with optimized isocenter doses ($\mathrm{D_{iso}}$) with a surrounding 65% or 80% isodose, and also strictly obeying the OAR constraints. In the remainder, these three planning approaches are referred to as gEUD(-20), 65%, and 80% strategy. Other terminology used is biological (gEUD(-20)), and conventional (65% and 80%). The hypothesis was that, not fixing the minimum PTV dose in the $\mathrm{gEUD}(-20)$ strategy to a constant percentage would generate freedom for Cycle to enhance dose delivery to the PTV, within the same imposed OAR hard constraints (possibly, but not necessarily approaching more closely some of the constraint levels).

5.2 Materials and methods

5.2.1 Patients

Plan comparisons have been based on the planning CT datasets of the 15 patients also studied in chapter 4. The imposed (clinical) OAR hard constraints were also the same (Tab. 5.1).

Structure	Constraint	Constraint parameter
Liver	$\mathrm{D_{33\%}} < 21$ Gy	$\mathrm{D_{33\%}}$ / 15
Liver	$\mathrm{D_{50\%}}$ or $\mathrm{D_{700\,CC}} < 15$ Gy	$\mathrm{D_{50\%\,/\,700\,CC}}$ / 15
Spinal Cord	$\mathrm{D_{max}} < 15$ Gy	$\mathrm{D_{max}}$ / 15
Bowel, duodenum, stomach, esophagus	$\mathrm{D_{5\,CC}} < 21$ Gy	$\mathrm{D_{5\,CC}}$ / 21
Heart	$\mathrm{D_{5\,CC}} < 21$ Gy	$\mathrm{D_{5\,CC}}$ / 21
Kidney's	$\mathrm{D_{33\%}} < 15$ Gy	$\mathrm{D_{33\%}}$ / 15

Table 5.1: Applied OAR hard constraints for plan optimizations.

5.2.2 Automatic plan generation with Cycle

Cycle has been described in detail in [8–11]. In this study, the version of [8] has been used for plan generations with the 65% and 80% strategies (in fact the plans for the 65% and 80% strategies are identical to those generated in chapter 4). To maximize $gEUD_{PTV}$(-20) instead, an option has been built in to replace the score function $S_k(\psi,\phi,w)$, used for selection of beam k (Eq. 3.3), by

$$S_k(a=-20,\psi,\phi,w) = \frac{\Delta(\mathrm{gEUD}_{\mathrm{PTV}}(a=-20,\psi,\phi,w,k))}{\Delta(\mathrm{gEUD}^{\mathrm{ref}}_{\mathrm{PTV}}(a=-20,k))} \times \prod_j S_{j,k} \tag{5.1}$$

The definitions are the same as in 3.A. The first term ensures that the score goes up when $gEUD_{PTV}$(-20) increases. The terms $S_{j,k}$ cause the score to decrease when OAR constraint parameters j approach their imposed constraint levels. $S_k(a=-20,\psi,\phi,w)$ is zero when a constraint level is hit.

For each patient, the set of input beam orientations (ψ,ϕ) was the same as in chapter 4. The allowed maximum number of selected beams was also 10. Similar to maximization of D_{iso}, Cycle was used in an iterative procedure with stepwise increases of the prescribed $gEUD_{PTV}$(-20), to obtain the plan with the highest possible $gEUD_{PTV}$(-20), while just not exceeding hard constraints.

5.2.3 Plan comparison

For the PTV, optimized plans were mainly compared using $D_{PTV,\,min}$, the minimum PTV dose, $D_{99\%}$, the minimum dose delivered to 99% of the PTV, and $gEUD_{PTV}(a)$, defined by

$$\mathrm{gEUD}(a) = \left(\frac{1}{N}\sum_{i=1}^{N} D_i^a\right)^{1/a} \tag{5.2}$$

The summation is over all N PTV voxels i with dose D_i [12]. For tumors, the parameter a is negative, but its value is uncertain. Therefore, comparisons were done for a range of a: -100, -50, -20, -10, -5, -1. So while a=-20 was used to define the score function in the gEUD(-20) strategy (Eq. 5.1), a range of a-values is used for comparison of the resulting plans with the 65% and 80% strategies.

To evaluate dose delivered to OARs, the distance from the ideal plan, DIP [8,10], the DIP taking into account only dose delivery to healthy liver, DIP_{liver}, and the conformality index, CI, were calculated for each plan. An ideal plan has zero dose delivery to the organs at risk. The DIP measures how close a plan is to this situation, and is defined by,

$$\mathrm{DIP} = \sqrt{\sum_{j=1}^{M} \frac{C_j^2}{M}} \tag{5.3}$$

M is the number of OAR constraints in the optimization. C_j is the ratio between the actual dose/volume parameter of constraint j in the plan (e.g. the actual maximum spinal cord dose), and its constraint level (e.g. 50 Gy). DIP_{liver} is defined as Eq. 5.3, but contains

only the two healthy liver parameters involved in the plan optimizations (Table 5.1). CI is here defined as the ratio between the volume of the $D_{PTV,\,99\%}$ isodose and the total PTV volume.

5.3 Results and Discussion

5.3.1 PTV dose evaluation

Figs. 5.1 and 5.2 show for the PTV, comparisons of gEUD(a), D_{min}, $D_{99\%}$, D_{mean}, and D_{iso} between the gEUD(-20) approach and the 65% and 80% strategies, respectively. With the gEUD(-20) optimisation strategy, the obtained gEUD(-20) for the PTV is up to 16.5% higher than for the two conventional strategies. On average, the gain in gEUD(-20) is 4.5% range [-2.0, 14.1] and 6.0%, range [-2.0, 16.5], compared to the 65% and the 80% strategy, respectively.

For $a \in$[-100, -5], obtained gEUD(a) values are on average highest for the gEUD(-20) strategy. For a=-100, and a=-50 this is most pronounced when compared to the 65% strategy. For the other a-values the mean gain in gEUD(a) is highest when compared to the 80% strategy. The ratio D_{min}/D_{iso} is 75%, range [68, 84], 66%, range [65, 68], and 80% range [80, 81], for the biological approach and the two conventional approaches, respectively. For all patients, the gEUD(-20) approach yielded a higher $D_{99\%}$ than the 65% strategy; the same holds for most plans of the 80% strategy (Fig. 5.2). It is important to note that large inter-patient variations are observed, especially in Fig. 5.2.

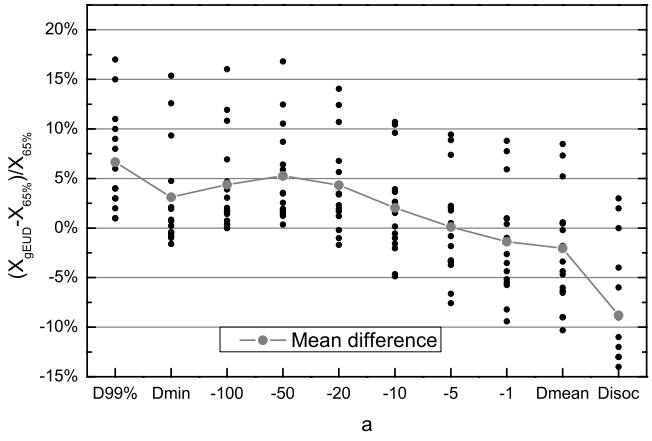

Figure 5.1: Relative differences between the gEUD(-20) and 65% strategies in the parameters (indicated by X on the left axis) $D_{PTV,\,99\%}$, $D_{PTV,\,mean}$, D_{isoc} and $gEUD_{PTV}(a)$ for a values ranging from -100 to -1. The dots represents comparisons for individual patients. The line connects patient mean values.

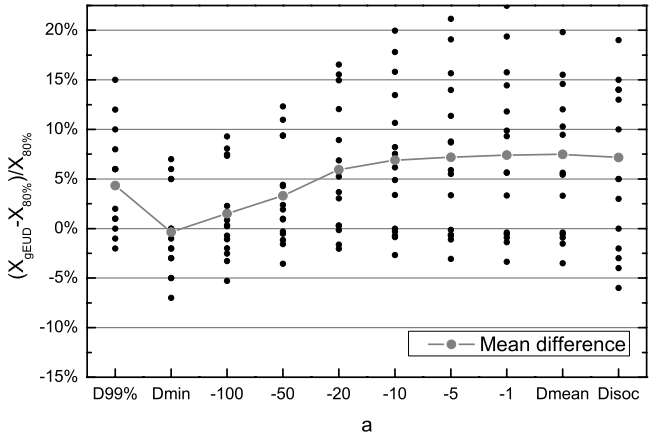

Figure 5.2: Relative differences between the gEUD(-20) and 80% strategies in the parameters (indicated by X on the left axis) $D_{PTV,\,99\%}$, $D_{PTV,\,mean}$, D_{isoc} and $gEUD_{PTV}(a)$ for a values ranging from -100 to -1. The dots represents comparisons for individual patients. The line connects patient mean values.

5.3.2 Normal tissue evaluation

For the biological approach, the patient mean DIP-value is 0.263 ($\pm$ 0.024). Differences with the 65% and 80% strategies are 0.009 ($\pm$ 0.015) and 0.009 ($\pm$ 0.012), respectively. The mean DIP_{liver} for the gEUD(-20) optimized plans is 0.80 ($\pm$ 0.15). Compared to the 65% and 80% strategies, increases in DIP_{liver} are 0.04 ($\pm$ 0.06), and 0.02 ($\pm$ 0.03), respectively. Observed CI are 1.30 ($\pm$ 0.09), 1.26 ($\pm$ 0.08), and 1.18 ($\pm$ 0.07) for the biological approach, the 65% strategy, and the 80% strategy, respectively.

There is a tendency that dose delivery to normal tissues is somewhat increased for the gEUD(-20) strategy, compared to both other strategies. However, since all plans do strictly adhere to all OAR constraints (which makes them clinically acceptable), and PTV dose delivery is generally superior for the gEUD(-20) approach, there is an overall advantage for the use of this strategy, rather than the 65% or 80% strategies. However, individual patients may be better off with one of the latter two approaches.

5.4 Conclusion

An algorithm has been developed for automated treatment plan generation for liver tumors. Beam directions are automatically selected from a large input set of coplanar and non-coplanar orientations (> 250), and beam shapes, sizes and weights are optimized. Generated plans do strictly adhere to imposed hard constraints for organs at risk (OAR). Using this algorithm it has been demonstrated that on average, biological optimization is superior to conventional strategies with a 65% or 80% isodose that closely surrounds the PTV. However, individual

patients may benefit most from one of the latter approaches.

Bibliography

[1] Blomgren H, Lax I, Naslund I, et al. Stereotactic high dose fraction radiation therapy of extracranial tumors using an accelerator. Clinical experience of the first thirty-one patients *Acta Oncol*. 1995;34:861–870.

[2] Méndez Romero A, Wunderink W, Hussain SM, et al. Stereotactic body radiation therapy for primary and metastatic liver tumors: A single institution phase I-II study *Acta Oncol*. 2006;45:831–837.

[3] Wulf J, Hadinger U, Oppitz U, et al. Stereotactic radiotherapy of targets in the lung and liver *Strahlenther Onkol*. 2001;177:645–655.

[4] Wulf J, Hadinger U, Oppitz U, et al. Stereotactic radiotherapy for primary lung cancer and pulmonary metastases: a noninvasive treatment approach in medically inoperable patients *Int J Radiat Oncol Biol Phys*. 2004;60:186–196.

[5] Herfarth KK, Debus J, Lohr F, et al. Stereotactic single-dose radiation therapy of liver tumors: results of a phase I/II trial *J Clin Oncol*. 2001;19:164–170.

[6] Schefter TE, Kavanagh BD, Timmerman RD, et al. A phase I trial of stereotactic body radiation therapy (SBRT) for liver metastases *Int J Radiat Oncol Biol Phys*. 2005;62:1371–1378.

[7] Wunderink W, Méndez Romero A, Vasquez Osorio EM, et al. Target coverage in image-guided stereotactic body radiotherapy of liver tumors *Int J Radiat Oncol Biol Phys*. 2007;68:282–290.

[8] de Pooter JA, Méndez Romero A, Jansen WP, et al. Computer optimization of noncoplanar beam setups improves stereotactic treatment of liver tumors *Int J Radiat Oncol Biol Phys*. 2006;66:913–922.

[9] de Pooter JA, Wunderink W, Méndez Romero A, et al. PTV dose prescription strategies for SBRT of metastatic liver tumours *Radiother Oncol*. 2007;85:260–266.

[10] Woudstra E, Heijmen BJM. Automated beam angle and weight selection in radiotherapy treatment planning applied to pancreas tumors *Int J Radiat Oncol Biol Phys*. 2003;56:878–888.

[11] Woudstra E, Storchi PR. Constrained treatment planning using sequential beam selection *Phys Med Biol*. 2000;45:2133–2149.

[12] Niemierko A. A generalized concept of equivalent uniform dose (EUD) *Med Phys*. 1999;26:1100.

Chapter 6

Automated non-coplanar beam direction optimization improves IMRT in SBRT of liver metastasis

JA de Pooter, A Méndez Romero, W Wunderink, PRM Storchi, BJM Heijmen, *Radiother Oncol., Accepted for publication*

Abstract

Purpose:
To investigate whether automatically optimized coplanar, or non-coplanar beam setups improve IMRT treatment plans for SBRT of liver tumors, compared to an equi-angular IMRT plan (the reference).
Methods:
For a group of 13 liver patients, an in-house developed beam selection algorithm (Cycle) was used for generation of 3D-CRT plans with either optimized coplanar, or non-coplanar beam setups. These 10 field, coplanar and non-coplanar setups, and an 11 field, equi-angular coplanar reference setup were then used as input for generation of IMRT plans. For all plans, the PTV dose was maximized in an iterative procedure by increasing the prescribed PTV dose in small steps until further increase was prevented by constraint violation(s).
Results:
For optimized non-coplanar setups, $D_{PTV,\,max}$ increased by on average 30% (range 8 – 64 %) compared to the corresponding reference IMRT plan. Similar increases were observed for $D_{PTV,\,99\%}$ and gEUD(a). For optimized coplanar setups, mean PTV dose increases were only $\sim$4%. After re-scaling all plans to the clinically applied dose, optimized non-coplanar configurations resulted in the best sparing of organs at risk (healthy liver, spinal cord, bowel).
Conclusion:
Compared to an equi-angular beam setup, computer optimized non-coplanar setups do result in substantial improvements in IMRT plans for SBRT of liver tumors.

6.1 Introduction

Stereotactic body radiation therapy (SBRT) is a promising technique for treatment of small liver tumors with a high local control and low toxicity[1–7]. In Rotterdam, patients are treated in a Stereotactic Body Frame (Elekta Oncology Systems, Stockholm, Sweden), using abdominal compression to reduce respiratory tumor motion (generally below 5 mm, top-top[8]).

In SBRT for liver tumors, patients are mostly treated with a 3D conformal radiotherapy (3D-CRT) technique. Generally, treatment plans consist of a large number of beams with coplanar and non-coplanar directions, selected by a dosimetrist, and shaped with a multi-leaf collimator[4,9–11]. Some institutes apply coplanar arcs in combination with circular collimators[11]. Thomas et al.[12] showed for radiotherapy of liver tumors with conventional fractionation schemes, that IMRT improves 3D-CRT treatment plans. They also found that a standard non-coplanar beam setup improves IMRT plans, compared to a standard coplanar setup. Tumor sizes in the latter study were much larger than the sizes normally allowed for hypo-fractionated radiation therapy of liver tumors.

Since the tumor location inside the liver, the total liver volume, and the distance of the tumor to other organs at risk (OAR) are rather heterogeneous among liver patients, application of a standard setup may lead to sub-optimal solutions, compared to individualized beam configurations. Beam selection is generally a trial-and-error procedure performed by the dosimetrist. Liu et al.[13,14] reported on the application of an algorithm for automatic generation of geometrically optimized beam setups to determine the optimal number of beams for SBRT of lung and liver lesions, when using a 3D-CRT dose delivery technique. Recently, we have developed an algorithm for dosimetrical optimization of beam setups, designated Cycle[15]. In a previous study we have demonstrated that in 3D-CRT, automatic beam angle optimization with Cycle may significantly improve treatment plans for SBRT of liver tumors, especially for non-coplanar setups[16]. Recently, Cycle was used to investigate differences between prescribing dose to the 65% or the 80% isodose[17].

The purpose of this study was to investigate whether for SBRT of liver tumors, computer optimized coplanar and non-coplanar beam setups result in better IMRT treatment plans than an 11 equi-angular coplanar beam setup.

6.2 Methods

6.2.1 Plan generation

For 13 single metastasis patients, previously treated in our institute with SBRT, three IMRT plans were generated, one with an optimized coplanar beam setup, one with an optimized non-coplanar configuration, and one reference plan with 11 equi-angular coplanar beams. IMRT plan generation with optimized beam setups was performed in two steps. First, for each patient, the in-house developed algorithm, Cycle, was used for generation of both a coplanar and a non-coplanar 3D-CRT plan with optimized beam directions, beam weights and beam shapes. Second, using the beam setups of the Cycle plans, IMRT plans were generated with the commercial XIO (CMS, Inc.) treatment planning software. Except for the constraint on the conformality index, CI, planning constraints and objectives used in Cycle and XIO were

identical (Table 6.1). The reference IMRT plans were also generated with XIO, again using the same constraints and objectives.

6.2.2 Cycle for generation of a feasible beam setup

In this study, beam setups were optimized by iterative use of Cycle (next section). By itself, Cycle only aims at generation of a feasible setup, i.e. a treatment plan with the prescribed PTV isocenter dose, while strictly obeying all imposed constraints on PTV dose inhomogeneity, OARs, and other normal tissues. No explicit attempt is made to find the 'best' treatment plan. Generation of feasible setups has been described in detail in[15,16,18]. Here a short summary is given. Cycle starts plan generation with an empty plan. Sequentially, new beam directions are selected from a large set of input directions, and added to the plan.

To select a new beam, k, each beam in the set of input directions is temporarily added to the plan (consisting of the previously selected k-1 beams). For each temporarily added input beam direction the weight and beam shape are optimized, based on a score function. The score function represents a trade-off between increasing the PTV dose and approaching the imposed constraint levels, while accounting for the dose distribution resulting from the previously selected k-1 beams. The beam direction with the highest score is added as beam k to the plan. Further selection of beams stops if one of the following is true:

- Maximum number of allowed beam directions per plan is reached
- A constraint is violated
- The prescribed dose has been attained, i.e., plan generation was successful

In the first two situations Cycle starts a new plan generation with automatically adjusted importance factors for the score function to better avoid approaching critical constraints.

6.2.3 Iterative use of Cycle for beam direction, shape and weight optimization

In this study, Cycle was used in an iterative procedure to automatically generate beam setups with the highest possible PTV dose within all imposed constraints. Starting with the clinical dose prescription of 3×12.5 Gy at 65% of the isocenter dose, feasible plans were generated with stepwise increased prescribed doses, until further dose increase was prohibited by unavoidable constraint violations. For the coplanar and non-coplanar plans, beams were selected from input sets consisting of 72 or 252 orientations, respectively. The 252 input beams for generation of non-coplanar plans included the 72 orientations, also used for coplanar optimization. The maximum angle of the non-coplanar beams with the axial plane was 30^{o}. The maximum allowed number of beam directions per plan was 10 (N.B. a single beam direction could be selected multiple times with different weights and beams eye view field shapes/ penumbra margins).

6.2.4 IMRT optimization

For each of the three beam configurations per patient, XIO was used in an iterative procedure to generate the IMRT plan with the highest possible PTV dose without violating the applied planning constraints. As for beam setup optimization with Cycle (previous section), the

maximum allowed PTV dose was established by stepwise increasing the prescribed dose, while keeping the constraint levels for OAR and normal tissue constant.

In case of a constraint violation, the XIO optimization was restarted with the same set of constraint levels, but with an increased importance factor (ranging from 2.0 to 5.0, increases in steps of 0.5) for the violated constraint. For the maximum dose constraints, and for the minimum PTV dose constraint a deviation of 1% volume from the constraint level was allowed. If one of the constraints was violated while its' importance factor had the maximum value of 5.0, the iterative procedure was stopped, and the plan with the highest PTV dose within the applied constraints was selected as the optimal plan. Optimal plans were segmented using a minimum segment size of 1×1 cm^2, and 5 discrete fluence levels.

Structure	Constraint
PTV	$D_{PTV,\,min} = 0.65 \times D_{isoc}$
Liver	$V_{D\,>\,21\,Gy} < 33\%$
Liver	$V_{D\,>\,15\,Gy} < 50\%$ or $V_{D\,<\,15\,Gy} > 700$ ml
Myelum	$D_{max} < 15$ Gy
Bowel	$D_{max} < 21$ Gy
Heart	$D_{max} < 21$ Gy
Kidney	$V_{D\,>\,15\,Gy} < 33\%$
R_0	See text
R_1	$D_{max} < D_{PTV,\,min}$ - 5 Gy
R_2	$D_{max} < 20$ Gy

Table 6.1: Applied planning constraints for the PTV, the OAR and the non-organ-based regions R_0, R_1, R_2.

6.2.5 Planning constraints

Applied planning constraints are summarized in Table 6.1. For the liver DVH constraint with a dose level of 15 Gy, one of the two volume levels is used. For patients with a normal liver volume smaller than 1400 CC, at least 700 CC should receive a dose lower than 15 Gy [4]. For patients with a larger normal liver volume, 50% of the volume should receive a dose lower than 15 Gy.

R_0, R_1 and R_2 are three non-organ based regions. R_0 is all normal tissue in a 2.0 cm margin around the PTV. R_1 is all normal tissue outside R_0, but inside a PTV expansion of 5.0 cm. R_2 is all tissue outside the PTV expansion of 5.0 cm. The constraint on R_2 was used to avoid hot spots far away from the PTV. The constraint on R_1 enforces a dose gradient between normal tissue and the target volume. For generation of IMRT plans, a DVH constraint was imposed on region R_0 to keep the conformality index (defined as the ratio between the volume of the prescription isodose and the PTV) lower than 1.4. The dose level of this DVH constraint was set equal to the allowed minimum PTV dose ($= 0.65 \times D_{isoc}$), and the volume level to $(0.4 \times V_{PTV})$, implying that at maximum $0.4 \times V_{PTV}$ of the R_0 volume is allowed to receive a dose higher than the imposed PTV dose.

6.2.6 Plan evaluation

For comparison of PTV dose distributions of optimized plans the following parameters were used: the minimum dose received by at least 99% of the PTV volume, $D_{PTV,\,99\%}$, the maximum PTV dose, $D_{PTV,\,max}$, and the generalized equivalent uniform doses, gEUD(-5) and gEUD(-20)[19], calculated using

$$\mathrm{gEUD}(a) = \left(\frac{1}{N} \sum_{i=1}^{N} D_i^a \right)^{1/a} \tag{6.1}$$

For comparison of OAR dose delivery, all plans with maximized isocenter doses were first scaled back to the clinical prescription of 3×12.5 Gy at the 65% isodose. The dose to the liver was evaluated using the mean liver dose, $D_{liver,\,mean}$, and the liver volumes that receive doses higher than 15 Gy and 21 Gy, $V_{liver,\,D>15\,Gy}$ and $V_{liver,\,D>21\,Gy}$ respectively. For the spinal cord, bowel, and heart, the dose received by at least 1% of the volume, $D_{1\%}$, was evaluated, and for the kidney's the $V_{kidney,\,D>15\,Gy}$ (Table 6.1). The conformality index was evaluated as the ratio between the volume of the $D_{PTV,\,99\%}$ isodose and the PTV volume.

6.3 Results

6.3.1 PTV

For each patient, PTV dose parameters for the three maximized IMRT plans are plotted in Fig. 6.1. The patient group means, and corresponding standard deviations are depicted in Fig. 6.2. For the optimized non-coplanar beam configurations, mean increases in $D_{PTV,\,max}$, $D_{PTV,\,99\%}$, gEUD(-5), and gEUD(-20) relative to the corresponding 11 field equi-angular reference setup were 30.4% (range: 8.2% – 64.0%), 28.2% (range: 4.8% – 56.1%), 29.9% (range: 6.9% – 57.6%), 29.3% (range: 3.9% – 55.6%). Relative to the optimized coplanar setups, increases for the optimized non-coplanar plans were 26.4% (range: -4.6% – 46.8%), 23.2% (range: -5.4% – 40.7%), 25.4% (range: -5.7% – 44.1%), 24.1% (range: 3.6% – 41.8%). Mean increases for optimized coplanar plans relative to reference plans were small, i.e. ∼4%. Apart from patient 12, all four evaluated PTV dose parameters were definitely highest for the optimized non-coplanar setup. For patient 12, the PTV was located directly next to the bowel, which might explain the almost equal PTV doses for the three plans. N.B. the close proximity of the bowel to the PTV in this patient prevented for all setups delivery of the prescribed dose (3×12.5 Gy).

6.3.2 Normal tissues

OAR results after plan re-normalization to 3×12.5 Gy are presented in Fig 6.3. For the optimized non-coplanar IMRT plans, the average decreases in $V_{liver,\,D>15\,Gy}$ and $V_{liver,\,D>21\,Gy}$ relative to the corresponding reference plans were considerably larger than for the optimized coplanar plans, with values of 14.7% and 9.4%, respectively, compared to 3.3% and 2.9%. A decrease in these parameters was observed for each patient, except for patient 12. For the mean liver dose, improvements relative to the reference plan were similar for the coplanar (-3.7%), and the non-coplanar (-5.4%) setups. For the optimized coplanar and non-coplanar

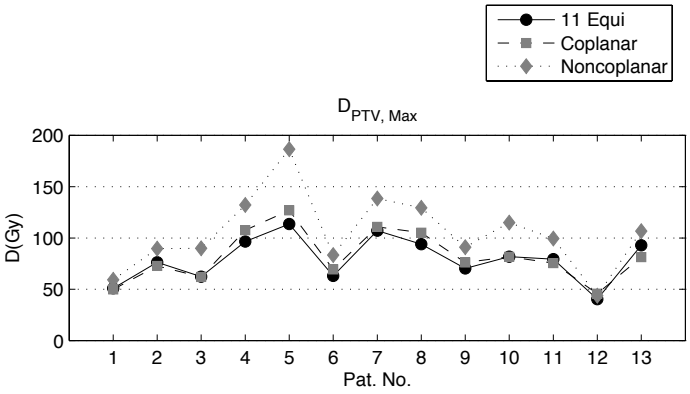

(a)

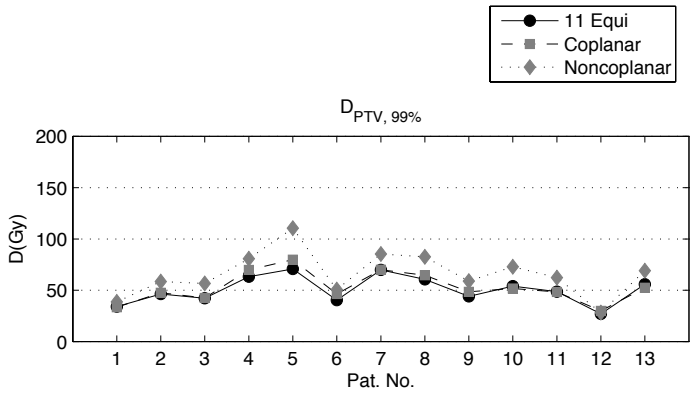

(b)

Figure 6.1: Cont'd

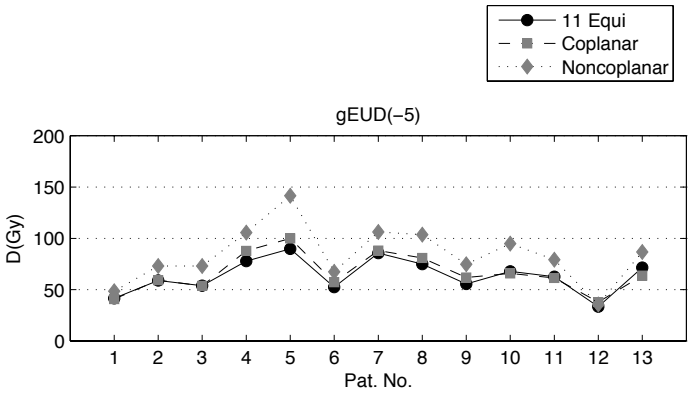

(c)

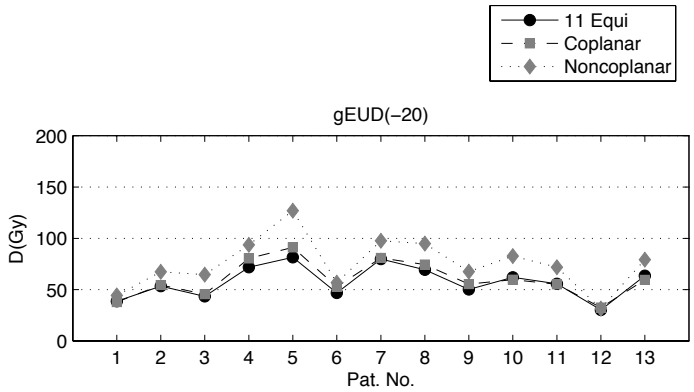

(d)

Figure 6.1: For each patient, PTV dose parameters, $D_{PTV,\,max}$ (a), $D_{PTV,\,99\%}$ (b), gEUD(-5) (c), and gEUD(-20) (d).

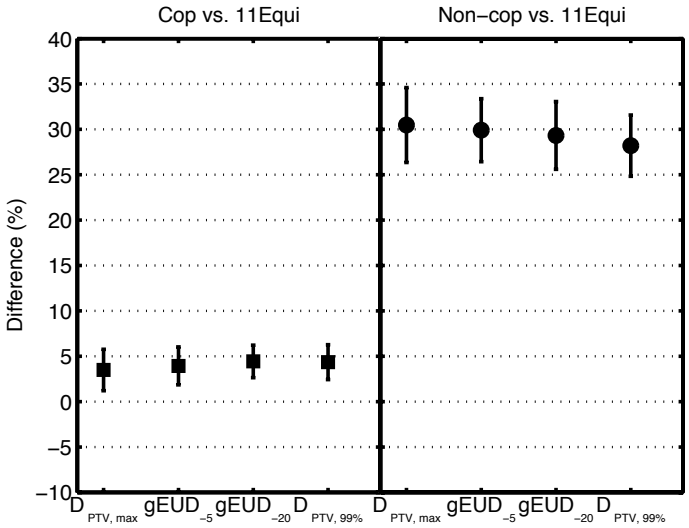

Figure 6.2: Patient group mean differences for the PTV dose parameters, $D_{PTV,\,max}$, $gEUD_{PTV}(-5)$, $gEUD_{PTV}(-20)$ and $D_{PTV,\,99\%}$ between IMRT plans with an optimized coplanar (■) or non-coplanar (●) beam setup, and the reference plan with an 11 equi-angular beam setup. The error bars represent ± 1 standard deviation variation around the population means.

setups, 11/13 and 13/13 patients showed a decrease in $D_{spinal\ cord,\,1\%}$, with population mean decreases of 12.3% and 46.7%, respectively.

For seven patients the bowel was contoured and included in the optimizations. Despite the average decrease of 7.3% for the coplanar plans, only 4 of the 7 patients had a lower $D_{bowel,\,1\%}$ in the optimized coplanar plan compared to the reference plan. For the non-coplanar optimization, 6 of the 7 patients presented a lower $D_{bowel,\,1\%}$, with an average decrease of 21.7%. Except for patient 12, all plans had a $D_{bowel,\,1\%}$ lower than the constraint level of 21 Gy. For patient 12 this value is higher since for this patient the dose had to be scaled upwards to achieve the regular clinical dose prescription level for the PTV (above). For 12/13 patients, the $V_{kidney,\,D>15\ Gy}$ was far below the constraint level of 33% with a maximum value of 17.7%. For patient 3 the $V_{kidney,\,D\,>\,15\ Gy}$ values were 26.4%, 28.6% and 18.2% for the IMRT plans with respectively the reference, the optimized coplanar and the optimized non-coplanar beam setup.

For 4 patients the heart was contoured. Compared to corresponding reference plans, mean decreases in heart doses of 10.7% and 20.0% were observed for optimized coplanar and non-coplanar setups, respectively. Observed population mean CI were 1.28 ± 0.09, 1.27 ± 0.10, and 1.32 ± 0.08 for the reference, the optimized coplanar, and the optimized non-coplanar beam setups, respectively.

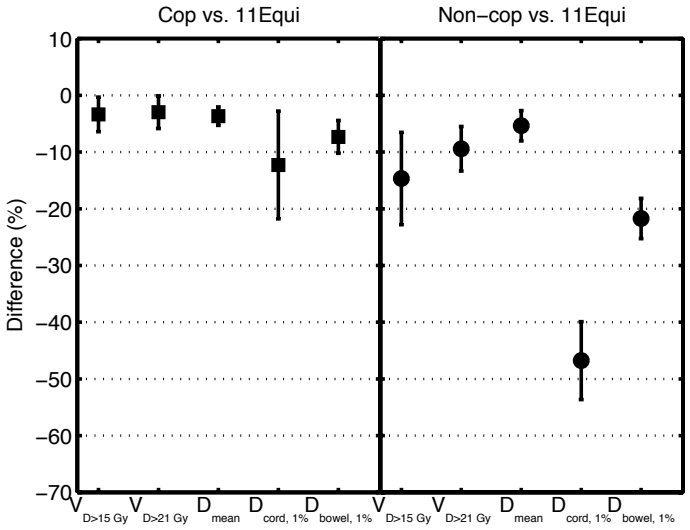

Figure 6.3: Patient group mean differences for the OAR dose parameters, $D_{liver,\,mean}$, $V_{liver,\,D>15\,Gy}$, liver, $V_{liver,\,D>21\,Gy}$, $D_{bowel,\,1\%}$ and $D_{spinal\,cord,\,1\%}$ between IMRT plans with an optimized coplanar (■) or non-coplanar (●) beam setup, and the reference plan with an 11 beam equi-angular setup. The error bars represent ± 1 standard deviation variation around the population means.

6.4 Discussion

Optimized non-coplanar beam setups resulted in IMRT plans with 30% higher PTV doses than plans for an 11 field equi-angular set-up, and 26% higher doses than for plans based on optimized coplanar setups. The results of the present study are in agreement with the study by Thomas et al.[12], who also observed an improvement by non-coplanar beam setups in IMRT treatment planning for liver tumors. The target volumes in their study were considerable larger than in this study. Therefore, the results of the two studies are complementary, supporting the conclusion that IMRT planning of liver tumors may be improved by applying non-coplanar beam setups.

All Cycle generated plans included 10 different beam orientations (the maximum allowed number in this study). For equi-angular beam setups in IMRT, generally an odd number is chosen to avoid opposing beams. In this study, 11 orientations were used for the equi-angular reference setup, one more than for the optimized beam setups. Even with one orientation less, the optimized setups performed better than the reference setup. Liu et al.[14] investigated the optimal number of beams for SBRT of liver tumors by applying beam direction optimization. They concluded that for lesions >2 cm no significant improvement is observed if the number of beams is 9 or higher.

In this study, plans were optimized by sequential optimization of beam orientations (3D-CRT with Cycle), and beam intensity profiles (XIO). Especially in combination with non-coplanar optimization in Cycle, this resulted in IMRT plans that were clearly superior to plans generated for the reference setup. However, for 5 of the 13 patients, the plan based on the optimized coplanar beam setup had a (slightly) lower PTV dose than the 11 field equi-angular IMRT plan, showing that sequential optimization of angles and profiles may also result in suboptimal IMRT plans. This emphasizes the need for integration of beam angle and intensity profile optimization for SBRT of liver tumors. Several algorithms have been developed for combined optimization of profiles and angles[20,21]. Since the search space increases dramatically, approximations and simplifications are needed for staying within reasonable calculation times. Currently, a research project is running in our institute, investigating integration of beam angle and beam intensity profile optimization for SBRT.

In this paper, the maximum allowed number of optimized beam directions was set to 10. Baisden et al.[22] presented a theoretical study on the relation between the maximum tolerable dose (MTD), which can be prescribed to the 95% of the PTV (i.e. the $D_{PTV,\,95\%}$) without violation of the constraints on the OARs, and the PTV and liver volume. The treatment plans for their patients were generated for a helical TomoTherapy unit, and can be considered as an IMRT plan with a very high number of coplanar beams. For the patient group average volumes of the liver and the PTV in the present study, 1566 CC and 152 CC respectively, they reported a $D_{PTV,\,95\%}$ of 60 Gy which is higher than for the plans in the present study with an optimized coplanar beam setup ($D_{PTV,\,95\%}$ = 57 Gy), and lower than for those with an optimized non-coplanar beam setups ($D_{PTV,\,95\%}$ = 71 Gy). Part of the increase in MTD for their plans, compared to the IMRT plans with an optimized beam setup in this study, is caused by the application of less strict planning constraints. In on-going studies we compare the optimized non-coplanar 10 field setups with multi-field plans designed for treatment with helical TomoTherapy and with the robotic CyberKnife.

6.5 Conclusion

IMRT treatment plans for SBRT of liver tumors may be considerably improved if optimized non-coplanar beam orientations are used instead of an 11 field equi-angular setup, or an optimized coplanar setup. IMRT cannot make up for sub-optimal beam selection.

Bibliography

[1] Hoyer M., Roed H., Traberg Hansen A., et al. Phase II study on stereotactic body radiotherapy of colorectal metastases *Acta Oncol.*. 2006;45:823–830.

[2] Kavanagh B. D., Schefter T. E., Cardenes H. R., et al. Interim analysis of a prospective phase I/II trial of SBRT for liver metastases *Acta Oncol.*. 2006;45:848–855.

[3] Méndez Romero A, Wunderink W, Hussain SM, et al. Stereotactic body radiation therapy for primary and metastatic liver tumors: A single institution phase I-II study *Acta Oncol*. 2006;45:831–837.

[4] Schefter TE, Kavanagh BD, Timmerman RD, et al. A phase I trial of stereotactic body radiation therapy (SBRT) for liver metastases *Int J Radiat Oncol Biol Phys*. 2005;62:1371–1378.

[5] Wulf J, Hadinger U, Oppitz U, et al. Stereotactic radiotherapy of targets in the lung and liver *Strahlenther Onkol*. 2001;177:645–655.

[6] Herfarth KK, Debus J, Lohr F, et al. Stereotactic single-dose radiation therapy of liver tumors: results of a phase I/II trial *J Clin Oncol*. 2001;19:164–170.

[7] Blomgren H, Lax I, Naslund I, et al. Stereotactic high dose fraction radiation therapy of extracranial tumors using an accelerator. Clinical experience of the first thirty-one patients *Acta Oncol*. 1995;34:861–870.

[8] Wunderink W, Méndez Romero A, Vasquez Osorio EM, et al. Target coverage in image-guided stereotactic body radiotherapy of liver tumors *Int J Radiat Oncol Biol Phys*. 2007;68:282–290.

[9] Wulf J, Hadinger U, Oppitz U, et al. Stereotactic radiotherapy for primary lung cancer and pulmonary metastases: a noninvasive treatment approach in medically inoperable patients *Int J Radiat Oncol Biol Phys*. 2004;60:186–196.

[10] Wulf J, Hadinger U, Oppitz U, et al. Impact of target reproducibility on tumor dose in stereotactic radiotherapy of targets in the lung and liver *Radiother Oncol*. 2003;66:141–150.

[11] Meeks S. L., Buatti J. M., Bouchet L. G., et al. Ultrasound-guided extracranial radiosurgery: technique and application *Int J Radiat Oncol Biol Phys*. 2003;55:1092–1101.

[12] Thomas E, Chapet O, Kessler ML, et al. Benefit of using biologic parameters (EUD and NTCP) in IMRT optimization for treatment of intrahepatic tumors *Int J Radiat Oncol Biol Phys*. 2005;62:571–578.

[13] Liu R., Wagner T. H., Buatti J. M., et al. Geometrically based optimization for extracranial radiosurgery *Phys Med Biol*. 2004;49:987–996.

[14] Liu R., Buatti J. M., Howes T. L., et al. Optimal number of beams for stereotactic body radiotherapy of lung and liver lesions *Int J Radiat Oncol Biol Phys*. 2006;66:906–912.

[15] Woudstra E, Storchi PR. Constrained treatment planning using sequential beam selection *Phys Med Biol*. 2000;45:2133–2149.

[16] de Pooter JA, Méndez Romero A, Jansen WP, et al. Computer optimization of noncoplanar beam setups improves stereotactic treatment of liver tumors *Int J Radiat Oncol Biol Phys*. 2006;66:913–922.

[17] de Pooter JA, Wunderink W, Méndez Romero A, et al. PTV dose prescription strategies for SBRT of metastatic liver tumours *Radiother Oncol*. 2007;85:260–266.

[18] Woudstra E, Heijmen BJM. Automated beam angle and weight selection in radiotherapy treatment planning applied to pancreas tumors *Int J Radiat Oncol Biol Phys*. 2003;56:878–888.

[19] Niemierko A. A generalized concept of equivalent uniform dose (EUD) *Med Phys*. 1999;26:1100.

[20] Lee E. K., Fox T., Crocker I.. Simultaneous beam geometry and intensity map optimization in intensity-modulated radiation therapy *Int J Radiat Oncol Biol Phys*. 2006;64:301–320.

[21] Pugachev A, Xing L. Incorporating prior knowledge into beam orientation optimization in IMRT *Int J Radiat Oncol Biol Phys*. 2002;54:1565–1574.

[22] Baisden J. M., Reish A. G., Sheng K., et al. Dose as a function of liver volume and planning target volume in helical tomotherapy, intensity-modulated radiation therapy-based stereotactic body radiation therapy for hepatic metastasis *Int J Radiat Oncol Biol Phys*. 2006;66:620–625.

Chapter 7

Simultaneous tumour dose escalation and liver sparing in Stereotactic Body Radiation Therapy (SBRT) for liver tumours due to CTV-to-PTV margin reduction

S Molinelli, JA de Pooter, A Méndez Romero, W Wunderink, MG Cattaneo, R Calandrino, BJM Heijmen, *Radiother Oncol*. 2008;**87**:432 - 8

Abstract

Purpose:
To quantify potential benefits of CTV-to-PTV margin reduction for SBRT of liver tumours, as allowed by enhanced treatment precision.
Methods and Materials:
For 14 patients plans were generated for the clinical margin and for 3 tighter margins. An in-house developed algorithm was used to optimise beam directions, shapes and weights for generation of the plan with the highest isocenter dose (D_{isoc}), while keeping the minimum PTV dose at least $65\% \times D_{isoc}$ and strictly adhering to all imposed hard OAR constraints. Each plan contains 10 optimal beam directions, automatically selected from up to 252 co-planar and non-coplanar input directions.
Results:
Apart from the expected tumour dose escalation in D_{isoc}, EUD_{PTV}, and $gEUD_{PTV}$) with decreasing margin, a simultaneous improved sparing of the normal liver ($D_{33\%}$, $D_{50\%}$, D_{mean}) was also observed. The smaller the margin was, the bigger both effects. For renormalized plans with D_{isoc} equal to the clinical value (3×19.2 Gy), and a margin reduction of 50% (2.5 mm laterally, 5 mm longitudinally), normal liver $D_{33\%}$ and $D_{50\%}$ reduced on average by 22% (maximum 38%), and 26% (maximum 47%), respectively.
Conclusions:
Using an algorithm for beam direction, shape and weight optimization, large increases in the therapeutic ratio of liver plans could be obtained for reduced margins.

7.1 Introduction

Stereotactic Body Radiation Therapy has been documented to provide a non-invasive treatment alternative for malignant liver lesions when established curative treatment modalities cannot be applied[1,2]. Current experience supports the perceived curative potential of this new modality for ablative treatment of lesions in the liver with diameters ideally not exceeding 5 to 6 cm[1,3–6]. A dose response relationship exists in treatment of primary and metastatic intra-hepatic tumours, with an association between delivery of a higher dose and improved clinical outcome[7–10]. By using stereotactic patient immobilization and set up, advanced lesion targeting techniques, high degrees of dose conformality, and steep dose gradients, the overall amount of normal liver tissue (liver - GTV) exposed to potentially harmful radiation doses can be substantially reduced[1,2,11], allowing delivery of very high biologically equivalent tumour doses.

At the Erasmus MC, stereotactic treatment of liver tumours is currently performed using a stereotactic body frame (SBF, Elekta Oncology Systems, Stockholm, Sweden) for tumour set-up, immobilization and abdominal compression, and a single slice spiral CT-scanner for daily image guidance, achieving excellent local control rates and low toxicity[5,12]. This treatment approach yields a substantial reduction in tumour motion related uncertainties, both intra and inter fraction[12,13]. In a single-slice spiral CT-scanner, (residual) respiratory motion may result in imaging artefacts, causing uncertainties in the mean position, size, and shape of the tumour that have to be accounted for in the CTV-to-PTV margin[14,15]. Further improvements in the in-room imaging system are currently under examination to optimise the therapeutic ratio of SBRT for liver tumours. A substantial increase in treatment precision will allow the reduction of CTV-to-PTV margin[11,12,16], yielding a potential for dose escalation and/or better protection of the surrounding healthy liver tissue. To evaluate the magnitude of feasible target dose escalation, the impact of CTV-to-PTV margin reduction on treatment plan quality has been investigated systematically using the planning CT-data of 14 patients, previously treated for liver malignancies. For each patient, treatment plans were automatically generated for several margin reduction protocols, with an in-house developed algorithm for simultaneous optimisation of beam angles, weights and shapes, designated Cycle. Cycle was used in an iterative procedure to maximally escalate the dose in the tumour centre, while keeping the minimum PTV dose at least equal to the 65% isodose level, and strictly obeying all normal tissue constraints. The obtained plans have an optimal balance between dose delivery to the tumour and sparing of normal tissues, i.e. a theoretically optimum therapeutic ratio for each of the selected margin protocols.

7.2 Materials and Methods

7.2.1 Patients

Most of the 14 patients included in this study were previously treated with 3×12.5 Gy, always prescribed at the 65% isodose level that closely surrounded the PTV. Patients accepted for treatment were not eligible for surgery or RFA. The maximum lesion size was 6 cm[5].

7.2.2 CTV-to-PTV margins

For tumour definition and treatment planning all patients had arterial and venous contrast CT-scans, and a planning CT-scan, acquired without contrast and fully including all relevant critical organs. Delineated tumours in the arterial and venous contrast CT-scans were summed to construct the definitive CTV. The tumour delineations were assisted by MRI scans, and reviewed by an experienced radiologist. Both on the day of treatment preparation and on treatment days, the patients were positioned in the Elekta SBF with maximum tolerable abdominal compression to reduce respiratory tumour motion. Implanted gold fiducials and fluoroscopy are used to assess residual tumour motion in all directions. For most of the patients, the clinically applied CTV-PTV margins were 10 mm in cranio-caudal direction, and 5 mm in antero-posterior and latero-lateral directions.

To investigate the potential benefits of margin reduction, for each patient four PTVs were generated on the Cadplan Treatment Planning System (Varian Oncology System, Palo Alto, CA) applying different margin protocols:

1. Protocol 0_0: 0 mm expansion in all directions, (PTV $\equiv$ clinical CTV);
2. Protocol 0_5: 0 mm expansion in the radial (antero-posterior and latero-lateral) directions, 5 mm in the cranio-caudal direction;
3. Protocol 5_5: 5 mm expansion in all directions;
4. Protocol 5_10: 5 mm expansion in the radial directions, 10 mm in the cranio-caudal direction (the clinically applied margin for most patients, see above).

In the remainder of this work, the protocols 1-3 are referred to as experimental protocols, and protocol 4 as the reference protocol. The 0_0 and 0_5 protocols are not clinically feasible as the PTV margins cannot be zero, e.g. because of set-up errors and residual uncertainty in tumour motion and delineation. However, inclusion of these protocols does demonstrate what is maximally possible. Moreover, using interpolation, 0_0 and 0_5 data may be used for estimation of the impact of margins in the range 0 to 5 mm.

7.2.3 Plan generation and optimisation

For each PTV, an optimal treatment plan was generated with Cycle, an advanced, in-house developed algorithm for computer generation of stereotactic treatment plans. The general principles of beam orientation selection and weight optimization with Cycle, based on precalculated dose distributions for a large set of coplanar and non-coplanar input beam directions (up to 252 in this study), have been described in detail by Woudstra et al.[17,18]. De Pooter et al. have recently extended Cycle for SBRT, including field shape optimization[19]. They have demonstrated that the use of computer optimized non-coplanar beam set-ups can significantly improve dose distributions for liver patients treated with SBRT. The latter version of Cycle has been used in this study.

By itself Cycle is not an optimisation algorithm, as it (only) aims for generation of a treatment plan with the prescribed tumour dose, while efficiently minimizing the approach

of, and never exceeding, the imposed constraint levels. However, in an iterative loop, the algorithm may indeed be used to optimize a plan parameter[18,19]. In this study, for each patient-PTV combination, a non-coplanar treatment plan was generated with the highest achievable PTV isocenter dose, while not violating the applied hard planning constraints, as described below. In the procedure to maximize D_{isoc}, the isocenter dose of the clinical plan was used as a starting point. The PTV dose was then maximized in an iterative way by repeated runs of Cycle with successive small increases in the prescribed D_{isoc} and keeping the D_{min} constraint at 65% of D_{isoc}. The normal tissue planning constraints were kept constant (see next section). The maximum number of selected beam directions per plan was set to 10. The iterative procedure was stopped if further isocenter dose increase was obstructed by constraint violation, i.e. the next prescribed D_{isoc} could not be obtained without a constraint violation.

7.2.4 Planning constraints

The following organ at risk (OAR) constraints were used in clinical treatment planning: for normal liver, $D_{33\%} < 21$ Gy, $D_{50\%} < 15$ Gy; for bowel, duodenum, stomach, heart, aorta and oesophagus $D_{5\,cc} < 21$ Gy; for spinal cord $D_{max} < 15$ Gy; and for kidney $D_{33\%} < 15$ Gy[5]. $D_{a\%}$ indicates that a% of the volume receives a dose of at least $D_{a\%}$. According to Schefter et al.[6], at least 700 ml of normal liver should receive a total dose < 15 Gy. In this study, when 700 ml was less than 50% of the liver, the above mentioned $D_{50\%}$ dose constraint was replaced by $D_{700\,ml} > 15$ Gy (see sections 4.2.3 and 6.2.5). From now on this constraint will be referred to as $D_{50\%\,/\,700\,ml}$, where data for $D_{50\%}$ and $D_{700\,ml}$ have been merged together in the patients sample. All other OAR constraints are the same as the clinical constraints.

For the automatic plan generations in this study, apart from the OAR constraints, two additional regions were defined in the normal tissue by expansions of the PTV (expansion 1 is the PTV plus a 2.0 cm margin, expansion 2 the PTV plus a 5.0 cm margin). Region R_1 includes all tissue outside expansion 1 and inside expansion 2. Region R_2 is all tissue outside expansion 2. For each region a maximum dose constraint was imposed. The constraint on R_1 aims at conformality of the dose distribution to the target volume, while the constraint on R_2 avoids hot spots and limits dose delivery far away from the target volume. The value for the constraint on R_1 was always chosen 5 Gy lower than the desired minimum PTV dose (D_{min}) level. For R_2, a maximum dose constraint of 20 Gy was used for each patient. In each plan generation process the constraints were considered hard constraints, i.e. for no reason constraint violations were allowed (see previous section).

7.2.5 Plan evaluation

The impact of the three experimental margin protocols on treatment plan quality was first investigated by comparing the achieved escalated tumour doses with the maximised dose for the reference protocol, as a primary endpoint, and dose delivery to the adjacent healthy liver (within constraints) as a secondary endpoint. The optimised 3D dose distributions were then rescaled to the same prescription dose (3×12.5 Gy at the 65% isodose level), in order to evaluate the potential gain in liver sparing as a primary end point.

For evaluation of PTV dose distributions, D_{isoc}, the Equivalent Uniform Dose (EUD), and the generalized EUD (gEUD) were applied[9,20]. EUD was calculated according to the

expression which takes into account the fractionation effect, with SF_2 (Surviving Fraction after 2 Gy irradiation) equal to 0.5[21]. The gEUD was calculated according to Niemierko et al.[22], with a = -20.[19,23]

The $D_{33\%}$ and $D_{50\% / 700\ ml}$ values for healthy liver were used for the automatic plan generations in this study. Apart from these DVH parameters, the effective dose (D_{eff})[24–26] and the fraction damaged (f_{dam})[27,28] were used for liver exposure evaluations. A wide range of values for the volume parameter n has been reported in the literature[29–32] for hepatic D_{eff} calculation, according to the Lyman Kutcher Burman NTCP model. The values 0.26, 0.52, 0.97, and 1 ($D_{eff}(n = 1) = D_{mean}$) were used in the analysis presented as follow. For what concerns f_{dam} evaluation, the critical volume NTCP model has been applied with k = 1.95 and $D_{1/2}$ = 41.2 Gy, as estimated by Jackson et al.[33]. For the calculations of $D_{eff}(n)$ and f_{dam}, the physical 3D dose distributions were first converted into Normalized Total Dose (NTD) distributions, using the linear quadratic model with an α/β ratio of 2 Gy[34].

7.3 Results

7.3.1 Dose escalation

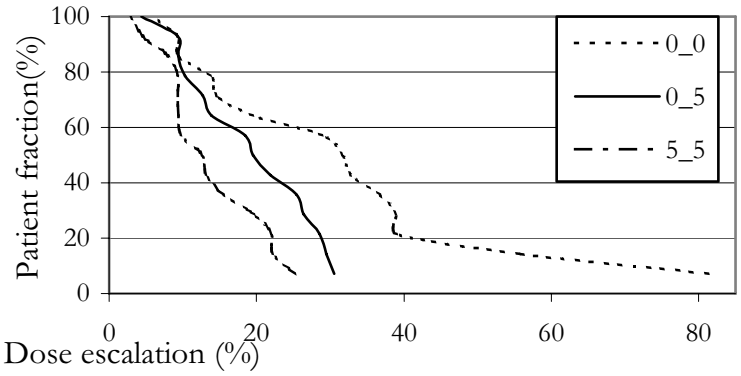

Figure 7.1: Dose Escalation Histogram: fraction of patients that experienced a dose escalation equal or higher than the respective x value. The experimental 0_0, 0_5, 5_5 protocols are compared with the reference 5_10 protocol.

Per definition, a PTV includes normal tissue regions to account for tumour motion and set-up uncertainties. The smaller the margins, the less normal tissue is included in the high dose region. For a correctly implemented optimisation algorithm, the isocenter dose should therefore always increase, as a function of margin decrease. This result was confirmed, as shown by the cumulative distributions of dose escalation, for the 0_0, 0_5 and 5_5 protocols, plotted in Fig. 7.1. For each experimental margin, 100% of the patients (14), had a positive dose escalation. Escalated PTV dose increases with decreasing CTV-to-PTV margin. Fig. 7.1 shows that 50% of the patients experienced a dose escalation higher than 31%, 19% and 12%

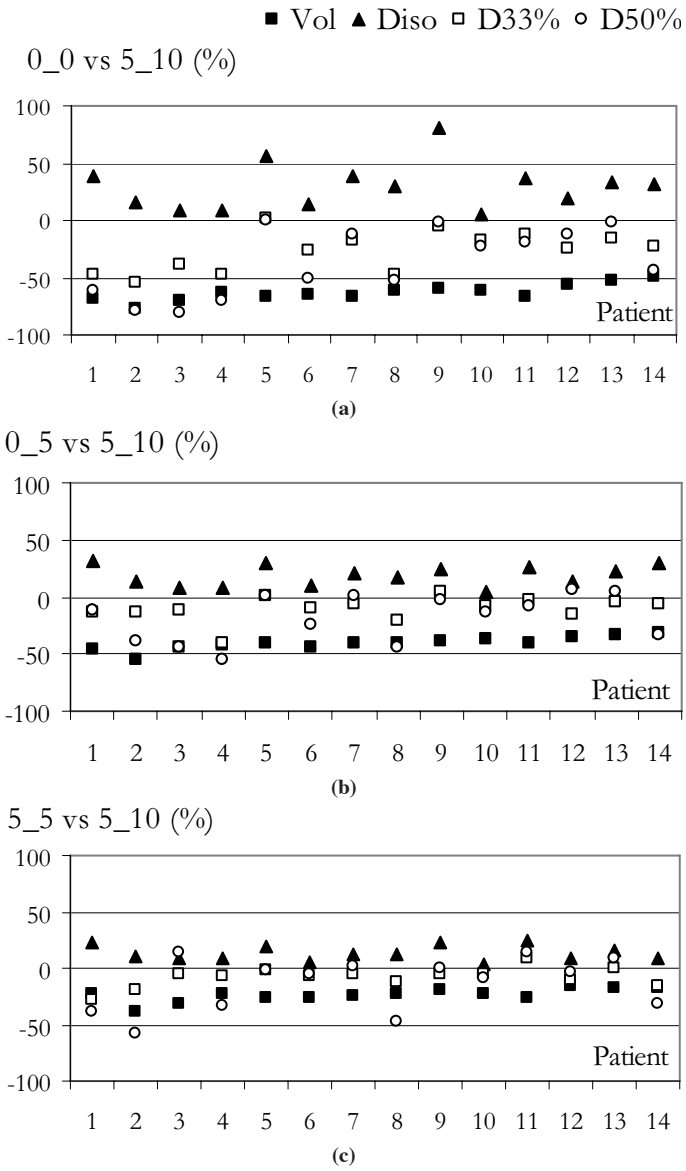

Figure 7.2: Relative changes in PTV volume (Vol), PTV isocenter dose (D_{isoc}), normal liver $D_{33\%}$ and $D_{50\% / 700\ ml}$, for the 0_0 (a), 0_5 (b), 5_5 (c) protocols compared to the reference 5_10 protocol, for 14 patients.

for the 0_0, 0_5 and 5_5 protocols, respectively. For each patient and margin, the reduction in PTV volume, the escalated D_{isoc}, and the corresponding changes in the $D_{33\%}$ and $D_{50\% / 700\ ml}$ liver values are plotted in Fig. 7.2. The EUD and gEUD dose escalations, as shown in Fig. 7.3, were not statistically different from the increases in D_{isoc}.

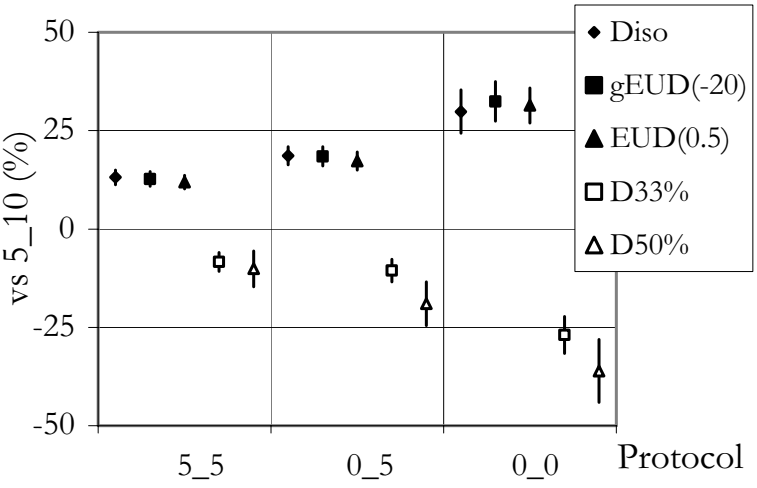

Figure 7.3: Population mean differences (%) for the escalated PTV isocenter dose (D_{isoc}), and corresponding changes in PTV EUD and gEUD, and normal liver $D_{33\%}$ and $D_{50\% / 700\ ml}$ values, as a function of the applied margin protocol, and compared to the reference 5_10 protocol. The error bars represent $\pm$ 1 SD for the mean values. All the reported differences are statistically significant, according to the applied t-test ($p < 0.03$).

As mentioned above, the increase in D_{isoc} for each patient was expected. On the other hand, it is interesting to note that for most patients, the PTV dose escalation was accompanied with a simultaneous decrease in the liver $D_{33\%}$ and $D_{50\% / 700\ ml}$ values (Fig. 7.2). Also mean relative differences in both parameters are significantly below zero (Fig. 7.3). After all, the aim of the optimisation was to maximally increase the PTV dose while just not violating any of the normal tissue constraints, with no effort in actually reducing the dose to the OARs.

Fig. 7.4 summarizes the impact of the dose escalations on all normal liver parameters used in this study (section 7.2.5). In a relative comparison with the reference margin protocol, all experimental protocols have a statistically significant lower f_{dam}, consistent with the findings for $D_{33\%}$ and $D_{50\% / 700\ ml}$. Also, each of these three parameters shows a gain in liver sparing with decreasing margin. The balance between the counter-acting effects of increasing liver doses, and reducing the amount of normal liver tissue inside the PTV (high dose region), is well expressed by the behaviour of $D_{eff}(n)$. For all values of n, an overall increasing gain with margin reduction is still evident. However, depending on the applied margin and volume parameter, n, the reduction in D_{eff} may become small, and statistically insignificant, making dose escalation with a concurrent sparing of the liver not always possible.

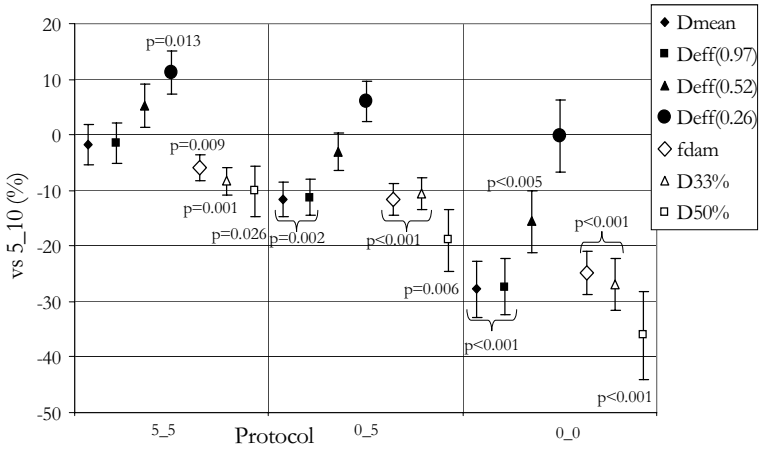

Figure 7.4: Population mean differences (%) of normal liver D_{mean}, $D_{eff}(0.26, 0.52, 0.97)$, f_{dam} and $D_{33\%}$, $D_{50\% \,/\, 700\,ml}$, between the experimental protocols and the 5_10 reference protocol. The error bars represent $\pm$ 1 SD for the mean values, the numbers are p-values, calculated with a t-test, for statistically significant ($p < 0.05$) differences.

7.3.2 Normal liver sparing

With the applied dose escalation procedure, the dose delivered to OARs is iteratively redistributed such that the highest possible D_{isoc} is obtained without exceeding any of the constraints. In this way, plans are generated with an optimal therapeutic ratio. The impact of reduced PTV margins on the dose delivery to OARs was studied systematically by renormalising all optimised dose escalated plans to 3×12.5 Gy at the 65% isodose. Being the liver the major cause of complications in SBRT for intra-hepatic malignancies, the attention was again focused on normal liver sparing. The data obtained for $D_{33\%}$, $D_{50\% \,/\, 700\,ml}$ and D_{mean} are presented in Fig 7.5. All three dose parameters show a large decrease, proportional to the reduction in margins.

7.4 Discussion

As far as we know, this is the first systematic study on the dosimetric impact of selected PTV margins in SBRT of liver tumours. Using commonly applied indicators for the risk of normal tissue damage, it has been demonstrated that reduction of CTV-to-PTV margins allows substantial target dose escalation for all studied patients. For each patient, the allowed target dose increase depends on the extent of the margin reduction. The observed potential for dose escalation is in agreement with previous investigations conducted on the effects of breathing margin reduction in conformal radiotherapy of liver and lung tumours [35–37]. Moreover, in our work, for all plan generations with reduced margins, the beam set-ups were optimised independently from the geometry of the clinical treatment beams, using an in-

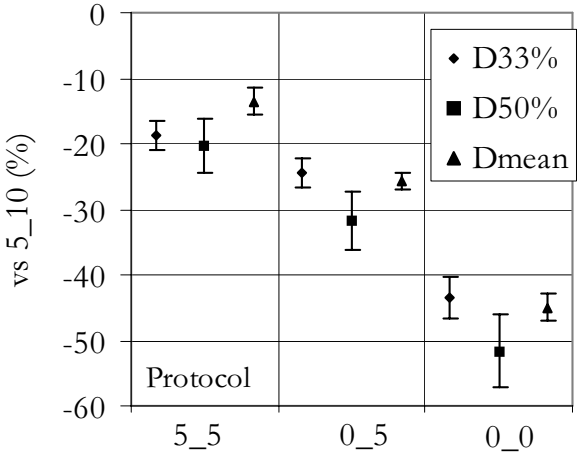

Figure 7.5: Population mean differences (%) in normal liver $D_{33\%}$, $D_{50\% / 700\ ml}$, and D_{mean} as a function of the applied margin protocol, compared to the reference 5_10 protocol. The involved optimized plans were all normalized at 3×12.5Gy @65%. The error bars represent ± 1 SD for the mean values. All the reported differences are statistically significant, according to the applied t-test ($p < 0.001$).

house developed plan optimisation algorithm. This approach gives more degrees of freedom to optimally take advantage of the reduction in target volume, without limitations in the beam configuration, except for the maximum allowed number of beam directions (10 in this case). The importance of beam angle optimization for SBRT of liver tumours has recently been demonstrated by de Pooter et al.[19].

For each patient in the study, an escalation in D_{isoc} was possible in each of the three experimental margin protocols. The larger the margin reduction, the higher was the allowed increase in D_{isoc}. Percentage increases in the single point parameter D_{isoc} translated in almost equal increases in PTV EUD and gEUD, the latter two taking into account the full 3D dose distribution of the PTV. This is probably due to the minimum PTV dose constraint applied in the optimisation process ($D_{min} \geq 65\% \times D_{isoc}$), resulting in a high similarity in the obtained PTV dose distributions. Mean PTV dose increases were 30%, 19%, and 13%, respectively, for the 0_0, 0_5, and 5_5 protocols. Interpolation in Figure 7.3 shows that for a 50% margin reduction in all directions (2.5_5 protocol), the obtained mean dose escalation is 16% (maximum increase 27%). While increases in D_{isoc}, and PTV EUD and gEUD as a function of margin reduction were to be expected, the concurrent statistically significant average decreases in the normal liver parameters $D_{33\%}$, $D_{50\% / 700\ ml}$, for all protocols, were not foreseen. In fact, the optimisation process was carried out with the hard condition of not exceeding the clinically applied constraints, without any attempt to reduce dose to normal tissues. Obviously, for these parameters, the positive effect of decreasing the amount of normal liver tissue

inside the high dose region surrounding the CTV, by reducing the CTV-to-PTV margin, was higher than the negative effect of liver dose increase caused by PTV dose escalation.

Due to the present lack of statistics and follow up time, there's still no validated radiobiological model to predict normal tissue complication for hypofractionated stereotactic treatment of lesions in the liver. One of the main issues to be addressed is the influence of the fractionation schedule (very high doses-few fractions) on the underlying damage (and repair) mechanisms and the related biological endpoints. D_{eff} and f_{dam} represent the core quantities of the NTCP models most frequently used to predict healthy liver complication probability for conventional radiotherapy. The role of these parameters, as applied here, is intended as an estimation of the trend of relative variation, in comparison with the dosimetric DVH quantities $D_{33\%}$ and $D_{50\% / 700\ ml}$.

For the three applied margin protocols, no evidence was found of a correlation between tumour and liver size and the magnitude of PTV dose escalation and normal liver sparing. The analysis was carried out, for each patient individually, as a relative comparison between different protocols; whereas, to evaluate the role of target (and liver) volume in the whole population, patients heterogeneity, in particular for what concerns tumour position relative to the OARs, should be considered.

Specific attention was paid to possibilities for dose escalation with the 5_5 protocol after clinical implementation of a new multi-slice CT-scanner, involving a significant reduction in image artefacts due to target motion, both in the planning CT and in the treatment CT-scans, and a consequent decrease in target position and dimension uncertainties[12,14,16]. As mentioned above, this protocol resulted in a mean dose escalation of 13% (maximum increase 25%). The results also showed that 100% (14), 57% (8) and 43% (6) of the patients were suitable for a 3×15, 3×17.5 and 3×20 Gy (65% isodose) fractionation protocol, respectively, without violation of any of the clinical constraints. Only in three of fourteen cases, the liver constraints limited an escalation to 17.5 and 20 Gy. Depending on the severity of the violation and the importance of the related OAR complication, a single patient risk-benefit evaluation should be made between the potential improvement in tumour control and the higher risk for normal tissues[38].

With abdominal compression in a SBF, respiratory tumour motion can generally be limited to 0.5 cm (cranio-caudal direction, top-top amplitude). Recently, we have demonstrated that when using a single-slice spiral CT-scanner, motion artefacts in the 3D planning CT-scan and the daily 3D treatment CT-scans, caused by the residual motion, give rise to substantial target volume increases, together with the amount of uninvolved tissue irradiated[12,16]. It is well known that also 4D CT scans may exhibit artefacts. Future clinical studies on motion artefacts in 4D CT scans of patients treated with abdominal compression in a SBF are needed to assess the allowed margin reduction with daily 4D CT guidance.

In this study plans were generated with an optimal therapeutic ratio; the gain in this ratio might be used for dose escalation (above), or to maximally spare the OARs. The magnitude of the potential for OARs sparing (in particular the liver) was studied by renormalizing all maximally escalated plans to the clinical prescription, i.e. 3×12.5 Gy at the 65% isodose

surrounding the PTV. Even with the small margin reduction of the 5_5 protocol, decreases in mean $D_{33\%}$ and $D_{50\% / 700\ ml}$ as high as (19±2)%, and (20±4)%, respectively, were obtained. Interpolation in Figure 7.5 shows that for the 2.5_5 protocol $D_{33\%}$ and $D_{50\%}$ go down by on average 22% (maximum 38%), and 26% (maximum 47%), respectively.

7.5 Conclusions

Implications of margin reduction for tumour dose escalation and OAR sparing have been systematically investigated with an in-house developed algorithm (Cycle) for generation of stereotactic plans, with optimised coplanar and non-coplanar beam orientations, weights and shapes. Apart from the expected tumour dose escalation, margin reduction also allowed a (concurrent) substantially improved sparing of healthy liver tissue, as evidenced by dosimetric quantities variations in agreement with common predictors of liver toxicity occurrence.

Bibliography

[1] Fuss M, Thomas Jr. CR. Stereotactic body radiation therapy: an ablative treatment option for primary and secondary liver tumors *Ann Surg Oncol*. 2004;11:130–138.

[2] Kavanagh BD, Timmerman RD, eds. Stereotactic Body Radiation Therapy, Lippincott, Williams, and Wilkins, Baltimore, MD 2005.

[3] Dawson LA, Hawkins M, Eccles C, et al. Phase I study of stereotactic radiotherapy for unresectable primary and metastatic liver cancer *Radiother Oncol*. 2006;80:S19–S20.

[4] Herfarth KK, Debus J, Lohr F, et al. Stereotactic single-dose radiation therapy of liver tumors: results of a phase I/II trial *J Clin Oncol*. 2001;19:164–170.

[5] Méndez Romero A, Wunderink W, Hussain SM, et al. Stereotactic body radiation therapy for primary and metastatic liver tumors: A single institution phase I-II study *Acta Oncol*. 2006;45:831–837.

[6] Schefter TE, Kavanagh BD, Timmerman RD, et al. A phase I trial of stereotactic body radiation therapy (SBRT) for liver metastases *Int J Radiat Oncol Biol Phys*. 2005;62:1371–1378.

[7] Dawson LA, McGinn CJ, Normolle D, et al. Escalated focal liver radiation and concurrent hepatic artery fluorodeoxyuridine for unresectable intrahepatic malignancies. *J Clin Oncol*. 2000;18:2210–2218.

[8] Kavanagh BD, Zaemisch R, Schefter TE, et al. The Influence of Dose and Tumor Volume on Local Control Following Stereotactic Body Radiation Therapy *Int J Radiat Oncol Biol Phys*. 2005;63:S480.

[9] McCammon R, Schefter TE, Zaemisch R, et al. Improved Local Control Associated With Dose-Escalated Stereotactic Body Radiation Therapy (SBRT) Indicates Dose-Response Relationship *Int J Radiat Oncol Biol Phys*. 2007;69:S152:S153.

[10] Park W, Lim DH, Paik SW, et al. Local radiotherapy for patients with unresectable hepatocellular carcinoma *Int J Radiat Oncol Biol Phys*. 2005;61:1143–1150.

[11] Dawson LA. Improving inter- and intra-fraction reproducibility *Radiother Oncol*. 2006;78:S15–S16.

[12] Wunderink W, Méndez Romero A, Vasquez Osorio EM, et al. Target coverage in image-guided stereotactic body radiotherapy of liver tumors *Int J Radiat Oncol Biol Phys*. 2007;68:282–290.

[13] Wulf J, Hadinger U, Oppitz U, et al. Stereotactic radiotherapy of extracranial targets: CT-simulation and accuracy of treatment in the stereotactic body frame. *Radiother Oncol*. 2000;57:225–236.

[14] Balter JM, Ten Haken RK, Lawrence TS, et al. Uncertainties in CT-based radiation therapy treatment planning associated with patient breathing *Int J Radiat Oncol Biol Phys*. 1996;36:167–174.

[15] Chen GT, Kung JH, Beaudette KP. Artifacts in computed tomography scanning of moving objects *Semin Radiat Oncol*.. 2004;14:19–26.

[16] Xi M, Liu MZ, Deng XW, et al. Defining internal target volume (ITV) for hepatocellular carcinoma using four-dimensional CT. *Radiother Oncol*. 2007;84:272–278.

[17] Woudstra E, Storchi PR. Constrained treatment planning using sequential beam selection *Phys Med Biol*. 2000;45:2133–2149.

[18] Woudstra E, Heijmen BJM. Automated beam angle and weight selection in radiotherapy treatment planning applied to pancreas tumors *Int J Radiat Oncol Biol Phys*. 2003;56:878–888.

[19] de Pooter JA, Méndez Romero A, Jansen WP, et al. Computer optimization of noncoplanar beam setups improves stereotactic treatment of liver tumors *Int J Radiat Oncol Biol Phys*. 2006;66:913–922.

[20] Kavanagh BD, Timmerman RD, Benedict SH, et al. How should we describe the radiobiologic effect of extracranial stereotactic radiosurgery: equivalent uniform dose or tumor control probability? *Med Phys*. 2003;30:321–324.

[21] Niemierko A. Reporting and analyzing dose distributions: a concept of equivalent uniform dose *Med Phys*. 1997;24:103–110.

[22] Niemierko A. A generalized concept of equivalent uniform dose (EUD) *Med Phys*. 1999;26:1100.

[23] Thomas E, Chapet O, Kessler ML, et al. Benefit of using biologic parameters (EUD and NTCP) in IMRT optimization for treatment of intrahepatic tumors *Int J Radiat Oncol Biol Phys*. 2005;62:571–578.

[24] Kutcher GJ, Burman C. Calculation of complication probability factors for non-uniform normal tissue irradiation: the effective volume method *Int J Radiat Oncol Biol Phys*. 1989;16:1623–1630.

[25] Lyman JT. Complication probability as assessed from dose-volume histograms *Radiat Res Suppl*. 1985;8:S13–S19.

[26] Lyman JT, Wolbarst AB. Optimization of radiation therapy, III: A method of assessing complication probabilities from dose-volume histograms *Int J Radiat Oncol Biol Phys*. 1987;13:103–109.

[27] Jackson A, Kutcher GJ, Yorke ED. Probability of radiation-induced complications for normal tissues with parallel architecture subject to non-uniform irradiation. *Med Phys*. 1993;20:613–625.

[28] Niemierko A, Goitein M. Modeling of normal tissue response to radiation: the critical volume model. *Int J Radiat Oncol Biol Phys*. 1993;25:135–145.

[29] Cheng JC, Wu JK, Lee PC, et al. Biologic susceptibility of hepatocellular carcinoma patients treated with radiotherapy to radiation-induced liver disease *Int J Radiat Oncol Biol Phys*. 2004;60:1502–1509.

[30] Dawson LA, Normolle D, Balter JM, et al. Analysis of radiation-induced liver disease using the Lyman NTCP model *Int J Radiat Oncol Biol Phys*. 2002;53:810–821.

[31] Dawson LA, Ten Haken RK. Partial volume tolerance of the liver to radiation *Semin Radiat Oncol*. 2005;15:279–283.

[32] Xu ZY, Liang SX, Zhu J, et al. Prediction of radiation-induced liver disease by Lyman normal-tissue complication probability model in three-dimensional conformal radiation therapy for primary liver carcinoma. *Int J Radiat Oncol Biol Phys*. 2006;65:189–195.

[33] Jackson A, Ten Haken RK, Robertson JM, et al. Analysis of clinical complication data for radiation hepatitis using a parallel architecture model. *Int J Radiat Oncol Biol Phys*. 1995;31:883–891.

[34] Trott KR and Herrmann T. Radiation effects on abdominal organs. In: Scherer E, Streffer C, Trott KR, eds. Radiopathology of organs and tissues:329–338, New York: Springer 1991.

[35] Engelsman M, Remeijer P, van Herk M, et al. Field size reduction enables iso-NTCP escalation of tumor control probability forirradiation of lung tumors. *Int J Radiat Oncol Biol Phys*. 2001;51:1290–1298.

[36] Nelson C, Starkschall G, Chang JY. The potential for dose escalation in lung cancer as a result of systematically reducing margins used to generate planning target volume *Int J Radiat Oncol Biol Phys*. 2006;65:573–586.

[37] Ten Haken RK, Balter JM, Marsh LH, et al. Potential benefits of eliminating planning target volume expansions for patient breathing in the treatment of liver tumors *Int J Radiat Oncol Biol Phys*. 1997;38:613–617.

[38] Dawson LA. Individualizing and adapting treatment delivery: the liver model *Radiother Oncol*. 2006;78:S27.

Chapter 8

General discussion

8.1 Introduction

In stereotactic radiotherapy the total dose is delivered in a low number of fractions. This increases the biological effectiveness for eradication of tumors (e.g. 60 Gy in 3 fractions of 20 Gy may be equivalent to 150 Gy delivered in fractions of 2 Gy). Due to the high effective dose, the local control of stereotactic radiotherapy for metastatic liver patients is better than for radiotherapy using conventional fractionation schemes[1,2]. Because of the low number of fractions, the biological damage to surrounding healthy tissues might also increase, potentially leading to more toxicity. To prevent this, improved treatment technology and treatment planning are necessary for better avoidance of dose delivery to involved organs at risk (OAR).

This thesis discusses several techniques for more focused stereotactic irradiation of intra-cranial (chapter 2) and extra-cranial (liver) tumors (chapters 3 to 7). In the remainder of this chapter, issues related to further improvement of treatment planning for stereotactic radiotherapy are discussed. The automated beam direction selection algorithm, Cycle, was successfully applied for treatment planning of SBRT of liver tumors. In section 8.2, possibilities to implement Cycle for automated selection and optimization of stereotactic arc therapy for intra-cranial lesions are discussed. The clinical value of automated beam direction optimization was demonstrated in chapters 3 and 6. Technical issues related to clinical implementation of Cycle, and clinical issues related to improved treatment planning for SBRT are discussed in sections 8.3 and 8.4, respectively. In chapters 3 and 6, the value of non-coplanar treatment planning was proven for respectively 3D-CRT and IMRT. A discrepancy suggested in the quantitative results of both chapters, is further discussed in section 8.5.

8.2 Cycle for treatment plan optimization in stereotactic arc radiotherapy for intra-cranial lesions

Selection of arcs and their weights in stereotactic arc therapy for intra-cranial lesions is largely based on beams eye views (BEV). Arcs having BEV field projections with small overlaps with OARs are generally preferred. Arcs with a uniform angular distribution contribute to the conformality of the prescription isodose to the PTV. In a study by Lu et al.[3], it was shown that automatic optimization of stereotactic arc therapy improvises the treatment planning. Since the search space is large, full dosimetrical optimization becomes very computation intensive. In the study by Lu et al.[3] this was anticipated by first selecting a set of arcs based on BEV images, and in a second step applying a dosimetrical optimization of these arcs. Cycle has shown to be an efficient algorithm in terms of computer power for optimization problems with a large number of degrees of freedom. It might also be possible to extend it for improved treatment planning of stereotactic arc treatments.

A way to do this could be to treat arcs in the same way as beams in the current approach (Fig. 3.1), meaning that Cycle sequentially selects the arcs from a large initial set of precalculated arcs. Each entry in the initial set is characterized by a start and stop gantry angle, and a couch angle. These angles have discrete values with an equal separation between neighboring angles. The structure of the sequential selection loop, and the score function

in the Cycle algorithm stay the same, see Fig. 3.1 and section 3.2.2. This means that for selection of arc *k*, each arc from the initial set is temporarily added to the plan consisting of the previous selected *k*-1 arcs. The weight of each temporarily added arc is optimized based on the score function. The arc with the highest score is selected and added to the plan. The same stop criteria might be used as for selection of beam directions in the current approach (section 3.2.2).

For pre-calculation of a dose distribution of an arc in the initial set, the dose distributions of a discrete set of individual beams, separated equi-angularly between the start and stop gantry angles, have to be summed. An angle separation of 10^{o} between the individual beams results in sufficient accurate calculation of dose distributions[4]. Since a beam direction can be used in multiple arcs, the dose distributions of all the required beams have to be calculated before starting calculation of the dose distributions of the arcs in the initial set.

For 10^{o} separations in both the couch and the gantry (start and stop) angles, the total number of arcs in the initial set can be up to 22000. Due to this large number of arcs in the initial set, the computation time will be high. This might be resolved by parallel computing, see section 8.3.2. Other solutions are to constrain the lengths of arcs with a minimum and maximum limit. For stereotactic arc therapy with cone shaped collimators, beam shape optimization in Cycle treatment planning is not needed, since proper cone diameters have to be selected in advance. For dynamic arc therapy using a multi-leaf collimator to continuously adjust the beam shape according to the PTV BEV projection, automated arc selection has to include beam shape optimization.

8.3 Technical issues related to clinical application of Cycle for liver SBRT

8.3.1 Introduction

This thesis presents investigations on increasing the therapeutic ratio for liver cancer treatment by improved treatment planning techniques. Although the current liver SBRT treatment has an acceptable toxicity and high local control[1], further increase of the therapeutic ratio by clinical introduction of the proposed technical developments is still beneficial;

- Current toxicity is acceptable, but not negligible, especially for HCC patients[1]. Important reductions are still desired.
- Despite the high actuarial two-year local control rates of 86% for metastases and 75% for HCC tumors[1], there remains room for improvement, which probably can be achieved by escalation of the PTV dose. Recently, higher PTV doses were allowed for patients with liver metastases. Because of the observed toxicity in our own HCC patient group[1], and reported toxicities in the literature[5,6], the PTV dose for these patients was not increased, despite the lower control rate.
- The median follow-up of the patient group is short, and a decrease in local control cannot be ruled out. In that case, increase of the therapeutic ratio allows for escalation of the PTV dose for new patients, without or with a small increase in OAR dose. Patients with a relapse might be safely re-treated.

- Currently, only lesions with a diameter smaller than 6 cm are treated. Increase of this limit will unavoidably lead to larger PTVs and, without improved techniques, also to increased volumes of normal tissue and OARs irradiated with a high dose. With improved technology, larger tumors might be treated, while avoiding a higher chance on toxicity.

- In the current treatment protocol, patients with more than 3 lesions are not eligible for treatment. Dose to the normal tissues, and in particular to the liver, will increase with the number of lesions to be treated. By introducing new techniques to better spare healthy tissues, patients with a higher number of lesions might also be treated, while still not increasing toxicity.

The current Cycle algorithm has been mainly used for research purposes. Clinical treatment planning was performed with Cycle for some difficult clinical cases, by manually importing the Cycle selected beam angles and weights into the clinical treatment planning system. For more large-scale clinical use of Cycle, a number of important technical issues are addressed in this section, such as calculation time, dose calculation engine and the feasibility of beam directions in the initial set. In the last two paragraphs, future technical developments are discussed; integration of Cycle with IMRT, and 4D planning with Cycle.

8.3.2 CPU time for plan optimization with Cycle

Computer generation of optimal plans with Cycle is almost fully automated. Only a few steps do still involve operator time, but with a few straightforward software changes, involvement of operators can be fully avoided. For the Cycle planning procedure described in chapter 6 the total calculation time was around 10 hours on an Intel Xeon 3.2 GHz single processor workstation. Optimized plans have the best value of a selected plan parameter (e.g. tumor dose), while strictly adhering to applied constraints. For generation of the plan with the most favorable plan parameter value (highest minimum PTV dose in section 3.2.5, or highest maximum PTV dose in section 6.2.3), the prescription for the involved parameter was gradually changed with fixed, small steps, each time followed by a new plan generation with Cycle. The convergence speed of this procedure can probably be increased substantially by allowing bigger prescription changes if for the previous prescription a plan could easily be attained.

In each iteration step, the plan generation is based on sequential selection of treatment beams, and each selection involves temporary addition of all (250) input beams to the plan for optimization of the corresponding weight and shape, using a score function. The latter process mainly determines the computation time per iteration step. Currently, these temporary additions and optimizations are performed sequentially with a single processor workstation. However, this process can easily be parallelized using a cluster of PCs with a high number of nodes. The input beams are then distributed among the nodes of such a cluster for weight and shape optimizations. In this way, the calculation time will decrease at maximum with a factor equal to the number of nodes. The actual decrease will be somewhat lower due to CPU time required for collection of the optimization results of the satellite nodes on the central node. If

10 or more nodes are used, the total calculation time for a non-coplanar optimized plan can be reduced to one hour or less.

8.3.3 Clinically feasible beam directions

The initial set of non-coplanar beam directions for plan optimization with Cycle used in chapters 3-7 was composed of beams uniformly distributed between the maximum upper and lower angles with the axial plane (Fig. 3.2), α_{up} and α_{low}. The applied α_{up} and α_{low} were constrained by the limitation that none of the beams may intersect the upper or lower CT-slice (see section 3.2.4).

Possibly, there are beams in these sets, which are not feasible to deliver in clinical practice because of collision with treatment couch or other equipment. Therefore, the presented increases in plan quality for treatment planning with non-coplanar beams instead of coplanar beams in chapter 3 and 6, might in some cases be an overestimation of the practically achievable increase.

On the other hand, the scan lengths of the applied planning CT scans were relatively small, as the scans were initially not intended for generation of optimized non-coplanar plans. Consequently, for most patients, the allowed α_{up} and α_{low} (Tab. 3.2), restricted possibilities for generation of optimal non-coplanar plans. Therefore, the presented improvement of treatment planning with non-coplanar beams can be an underestimation of what can be achieved in clinical practice.

Currently, the number of planning CT slices for liver SBRT patients is increased to allow beams with larger α angles. Furthermore, treatment couches are being developed that are controlled with a robotic arm, yielding a larger collision free area, and thereby allowing for a larger set of allowed non-coplanar beams. Both developments have the potential to further enhance advantages of non-coplanar beam set-ups for SBRT of liver patients, compared to coplanar treatments.

8.3.4 Dose calculation engine

Optimization with Cycle is based on pre-calculated dose distributions for all beams in the initial set (section 3.2.4). In the current version of Cycle, a pencil beam algorithm is used for pre-calculation of these dose distributions, which is sufficiently accurate for dose calculation of liver treatment plans. The dose in each voxel is calculated as the product of the off-axis dose and the depth dose. The off-axis dose is calculated with a 2D-convolution of pencil beams. Connecting Cycle with an external dose calculation engine using a more advanced algorithm, such as collapsed cone or even Monte Carlo, for pre-calculating dose distributions can easily be accomplished. For treatment planning of lung tumors these advanced algorithms are necessary to avoid loss of accuracy in dose calculation[7].

For beam shape optimization in Cycle, the off-axis dose has to be re-calculated after each change of the beam shape (see section 3.2.3). In the current Cycle version, these re-calculation steps use half of the total calculation time for generation of a treatment plan. When introducing more advanced dose calculations methods, care should be taken to avoid further increase of CPU time needed for beam shape optimization.

In each step of the beam shape optimization routine only a small number of pencil

beams close to the field edge is switched on or off. Instead of doing a complete re-calculation in each step, a much faster method is to add/remove the dose contribution of each pencil that is switched on/off for each voxel. For this purpose, the dose contribution in voxel *i* from pencil beam *j* for each pencil close to the edge of the field could be stored during the pre-calculation of dose distributions for beams in the initial set.

8.3.5 Simultaneous beam direction and profile optimization

In chapter 6, the importance of non-coplanar beam setup optimization for IMRT in SBRT of liver tumors was demonstrated. The IMRT plans were optimized in a sequential procedure by first using Cycle to generate optimal beam angles for a 3D CRT plan, and then enter these angles into a commercial TPS (XIO, CMS) to generate intensity profiles for an optimal IMRT plan. In this study, for each patient, IMRT plans were generated for both a coplanar and a non-coplanar beam set-up, optimized with Cycle. The two IMRT plans with optimized beam orientations were compared with an IMRT plan for a coplanar, 11 field equi-angular setup. Compared to the latter set-up, optimized non-coplanar set-ups yielded much larger maximum PTV doses ($\sim$30%), while strictly staying within the imposed constraints. Possibly, even higher dose escalations could have been obtained if non-coplanar beam angle optimization and beam profile optimization would have been performed simultaneously, and not sequentially. An indication for suboptimal performance of sequential optimization steps is the observation that for a few patients, IMRT plans based on Cycle optimized coplanar beam set-ups performed (slightly) worse than corresponding plans generated for the 11 field equi-angular setup. In a study by Woudstra et al.[8], it was shown that Cycle integrated with segmented IMRT (i.e., only the intensity in a few pre-defined segments could be modulated) improved treatment planning for esophagus tumors. The IMRT implementation in that study[8] did not include beam shape optimization, which is important for stereotactic treatment.

Currently, Cycle is extended with a new algorithm for segmented IMRT that will include beam segment shape optimization. Planning comparisons will be performed to test the hypothesis that simultaneous optimization of beam angles and profiles will further improve plan quality. In another project in Erasmus MC, beam angle optimization will be combined with a more advanced algorithm for profile optimization. Again, planning comparisons are needed to assess the relative quality of the generated plans.

8.3.6 4D planning with Cycle

Currently, treatment planning is performed on a static 3D-CT data set, and a PTV is constructed to avoid local underdosage of the CTV resulting from residual breathing motion of the CTV and tumor set-up errors. The advent of 4D-CT imaging allows for a more accurate prediction of the position and shape of OARs and CTV as a function of the breathing cycle phase during treatment. The clinical introduction of 4D-CT may result in smaller CTV-PTV margins[9,10].

On the other hand, a 4D CT data set, consisting of *n* 3D-CT data sets corresponding to *n* phases in the breathing cycle, may also be directly used for plan generation in order to include simulated respiratory motion in the optimization process (4D treatment planning)[11,12]. The advantage of 4D planning is that the CTV can be used as planning target instead of the

PTV, potentially leading to a smaller volume of normal tissue receiving a high dose[12]. As explained below, Cycle may be extended with an option for 4D planning.

As for each 4D planning algorithm, a basic requirement for plan generation is access to a patient specific co-registration matrix, determined with rigid or non-rigid registration[13,14], containing for each voxel in each structure (OAR or target) the position in each phase of the breathing cycle. To allow 4D planning with Cycle, for each beam angle in the initial set, separate dose distributions have to be pre-calculated for each of the *n* CT-scans and added using the co-registration matrix and the relative weights of the *n* phases. If beam shape optimization is not required, the current version of Cycle can then be used to generate a 4D treatment plan based on the composite pre-calculated dose distributions.

To include beam shape optimization in 4D planning, Cycle has to be modified to allow calculation of off-axis dose distributions for modified field shapes, for *n* 3D-CT data sets instead of the current single 3D-CT data set. Moreover, dose addition using the co-registration matrix must be repeatedly performed during the optimization process. As a consequence, the calculation time for beam shape optimization might increase by a factor of *n* or more. In section 8.3.4, a method is described to lower the CPU time required for repeated calculations of off-axis dose distributions in the beam shape optimization part, when more advanced and more computation intensive dose algorithms are used. This method can be extended to 4D-planning.

8.4 Clinical issues for SBRT of liver metastases

8.4.1 Dose conformality and geographical tumor miss

To assess conformality of prescription isodoses to 3D PTV contours, the conformality index, CI, was used, which is defined as the ratio between the volume enclosed by the prescription isodose and the volume of the PTV. For CI values close to the ideal value of 1, the average distance between the prescription isodose and the PTV surface is small. For the Cycle optimized non-coplanar 3D-CRT plans (65% strategy) in chapter 4, the CI has an average value of 1.26, while the CI for the clinical plans of these patients was on average 1.32. Timmerman et al. recommend to keep the CI below 1.2, and use 1.4 as maximum limit[15]. Further decrease in CI of the Cycle 3D-CRT plans can be achieved by lowering the Cycle CI constraint level, which will lead to a smaller distance between the PTV and the prescription isodose.

In chapter 3, it was shown that the difference between the minimum PTV dose and the maximum dose at a distance of 2 cm outside the PTV is considerable higher for the optimized non-coplanar plans compared to clinical treatment planning (Tab. 3.5). This suggests that the dose gradient around the PTV is increased for computer optimized non-coplanar plans.

A study by Voroney et al.[16] showed that GTVs contoured on CT images are smaller than GTVs contoured on MRI, and that the distance between the MRI-GTV and the CT-GTV was larger than 5 mm for on average 19% of the GTV surface. Clinical GTV contouring is based on CT images and potential deviations from MRI delineation are not explicitly accounted for in the PTV margin. With the currently applied relatively high CI, plans might be forgiving for (small) inaccuracies in PTV margin. For more conformal plans (i.e., with

a lower CI) the probability of partial geographical tumor miss may increase. Higher dose gradients just around the PTV, will increase the underdosage due to geographical tumor miss. Currently, Erasmus MC is developing a new SBF, allowing MR-imaging in treatment position to improve tumor delineation.

8.4.2 On-line re-planning

In the current treatment protocol, the planning CT-scan is used for contouring of the target and OARs and for treatment planning. Prior to each treatment fraction, a CT is made to determine the required isocenter shift for centering the CTV in the PTV [9]. In this daily image guidance procedure, position changes and deformation of critical organs relative to the planning scan are not considered, which might lead to higher OAR doses than planned, potentially exceeding the applied planning constraints. Since the number of treatment fractions is low, the random component of these inter-fraction changes in OAR position, orientation and shape will not average out.

In an on-going study, OAR doses are retrospectively calculated for each fraction, using the daily CT-scans and applied isocenter shifts. The OARs are contoured on these treatment CT's. Per OAR voxel the total delivered dose can be calculated by adding the dose contributions of the individual fractions. Since OARs might show intra-fraction deformation [13,17], a challenge in this study is the correct co-registration of OAR voxels in each treatment fraction to make proper calculation of the total dose delivered to each OAR voxel possible. Since the biological effect of dose delivered in varying fractions is different from a dose delivered in constant fractions, the addition of fraction doses has to be done in a biological way.

If significant deviations in realized OAR dose from planning dose are observed in this retrospective study, the treatment protocol for future patients might be changed by including daily dose calculations for treatment CT-scans. Unacceptable large calculated OAR doses due to OAR displacements or deformations could then trigger canceling of the daily dose delivery. For the more distant future, a system for daily re-planning based on the treatment CT could then be developed. To avoid large increases in treatment time and patient discomfort, such a system needs a fast re-planning method, i.e. within a couple of minutes.

8.5 Non-coplanar vs. coplanar liver SBRT

In chapters 3 and 6, treatment plans with optimized coplanar and non-coplanar beam setups are compared for 3D-CRT and IMRT, respectively. For both treatment techniques it was concluded that application of non-coplanar beams improves the treatment planning for SBRT of liver tumors. However the observed increase in absolute $D_{PTV,\,99\%}$ due to a non-coplanar setup differed considerably between both studies; 4.5% for the 3D-CRT plans (chapter 3), and 23.2% for the IMRT plans (chapter 6). Possible explanations of this difference are:

- The optimization procedures applied in both studies were different on two points. In chapter 3, for a fixed prescribed maximum tumor dose, the 3D-CRT plan with the highest possible minimum PTV dose within the applied planning constraints was generated. In chapter 6, for each patient, the IMRT plan with the highest possible absolute PTV

dose within the planning constraints was generated, while the ratio $D_{PTV,\,min}$ / D_{isoc} was kept constant at 65%. The second difference is that in chapter 3 the mean liver dose was used as constraint, which was not used for the IMRT plans in chapter 6.

- Application of non-coplanar beam setups is much more advantageous for IMRT treatments than for 3D-CRT treatments.

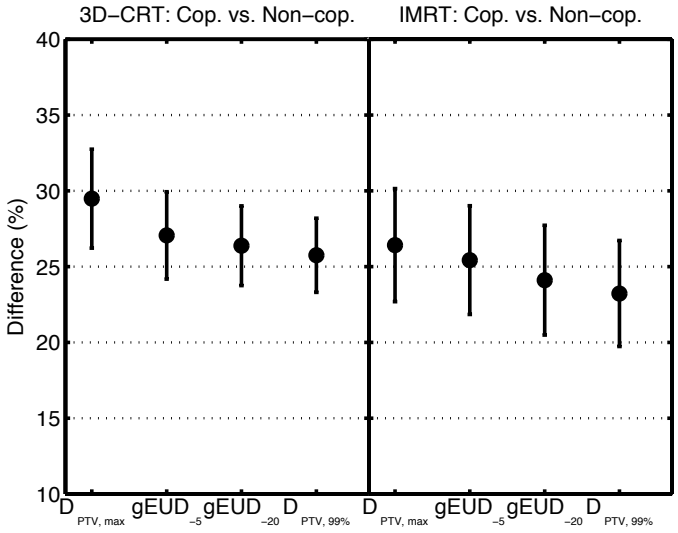

Figure 8.1: Patient group mean differences for the PTV dose parameters $D_{PTV,\,max}$, gEUD(-5), gEUD(-20), and $D_{PTV,\,99\%}$ between optimized coplanar and non-coplanar beam setups for the 3D-CRT and IMRT plans of chapter 6.

In the planning procedure in chapter 6, Cycle is used to first generate 3D-CRT plans with either an optimized coplanar or optimized non-coplanar beam setup. These set-ups are then used to generate IMRT plans with the XIO treatment planning system. Separate comparisons for 3D-CRT and IMRT in delivered PTV doses with coplanar and non-coplanar setups are presented in Fig. 8.1 The dose increase in $D_{PTV,\,99\%}$ for the non-coplanar beam setups is 25.7% for the 3D-CRT plans and 23.2% for the IMRT plans.

Because of the small differences between 3D-CRT and IMRT plans seen in Fig. 8.1, it is concluded that the observed relatively small differences in PTV dose between coplanar and non-coplanar setups in chapter 3 (see above) result from the applied planning procedure that differs from the approach in chapter 6. It seems that application of non-coplanar beams instead of coplanar beams is more advantageous if the goal of the treatment planning procedure is the generation of a plan with the maximally escalated PTV dose within the applied planning constraints, than when the goal is to maximize the PTV dose homogeneity.

Bibliography

[1] Méndez Romero A, Wunderink W, Hussain SM, et al. Stereotactic body radiation therapy for primary and metastatic liver tumors: A single institution phase I-II study *Acta Oncol*. 2006;45:831–837.

[2] Dawson LA, McGinn CJ, Normolle D, et al. Escalated focal liver radiation and concurrent hepatic artery fluorodeoxyuridine for unresectable intrahepatic malignancies. *J Clin Oncol*. 2000;18:2210–2218.

[3] Lu HM, Kooy HM, Ledoux ZH Leber RJ. Optimized beam planning for linear accelerator-based stereotactic radiosurgery *Int J Radiat Oncol Biol Phys*. 1997;39:1183–1189.

[4] MacKenzie MA, Robinson DM. Intensity modulated arc deliveries approximated by a large number of fixed gantry position sliding window dynamic multileaf collimator fields *Med Phys*. 2002;29:2359–2365.

[5] Cheng JC, Wu JK, Huang CM, et al. Radiation-induced liver disease after three-dimensional conformal radiotherapy for patients with hepatocellular carcinoma: dosimetric analysis and implication *Int J Radiat Oncol Biol Phys*. 2002;54:156–162.

[6] Cheng JC, Wu JK, Lee PC, et al. Biologic susceptibility of hepatocellular carcinoma patients treated with radiotherapy to radiation-induced liver disease *Int J Radiat Oncol Biol Phys*. 2004;60:1502–1509.

[7] Hadinger U, Krieger T, Flentje M, et al. Influence of calculation model on dose distribution in stereotactic radiotherapy for pulmonary targets *Int J Radiat Oncol Biol Phys*. 2005;61:239–249.

[8] Woudstra E, Heijmen BJ, Storchi PR. Automated selection of beam orientations and segmented intensity-modulated radiotherapy (IMRT) for treatment of oesophagus tumors *Radiother Oncol*. 2005;77:254–261.

[9] Wunderink W, Méndez Romero A, Vasquez Osorio EM, et al. Target coverage in image-guided stereotactic body radiotherapy of liver tumors *Int J Radiat Oncol Biol Phys*. 2007;68:282–290.

[10] Xi M, Liu MZ, Deng XW, et al. Defining internal target volume (ITV) for hepatocellular carcinoma using four-dimensional CT. *Radiother Oncol*. 2007;84:272–278.

[11] Guckenberger M, Krieger J Wilbert T, Richter A, et al. Four-dimensional treatment planning for stereotactic body radiotherapy *Int J Radiat Oncol Biol Phys*. 2007;69:276–285.

[12] Alasti H, Cho YB, Vandermeer AD, et al. A novel four-dimensional radiotherapy method for lung cancer: imaging, treatment planning and delivery *Phys Med Biol*. 2006;51:3251–3267.

[13] Brock KK, Dawson LA, Sharpe MB, et al. Feasibility of a novel deformable image registration technique to facilitate classification, targeting, and monitoring of tumor and normal tissue *Int J Radiat Oncol Biol Phys*. 2006;64:1245–1254.

[14] Orban de Xivry J, Janssens G, Bosmans G, et al. Tumour delineation and cumulative dose computation in radiotherapy based on deformable registration of respiratory correlated CT images of lung cancer patients *Radiother Oncol*. 2007.

[15] Timmerman RD, Kavanagh BD. Stereotactic body radiation therapy *Curr Probl Cancer*. 2005;29:120–157.

[16] Voroney JP, Brock KK, Eccles C, et al. Prospective comparison of computed tomography and

magnetic resonance imaging for liver cancer delineation using deformable image registration *Int J Radiat Oncol Biol Phys*. 2006;66:780–791.

[17] Kaus MR, Brock KK, Pekar V, et al. Assessment of a model-based deformable image registration approach for radiation therapy planning *Int J Radiat Oncol Biol Phys*. 2007;68:572-580.

Summary

Stereotactic radiotherapy is a treatment technique with a higher accuracy in 3D localization and immobilization of the tumor than for conventional radiotherapy. For stereotactic radiotherapy the dose is delivered in one or a small number of fractions with a high dose per fraction, resulting in a much higher biological effective dose to the tumor. Therefore, stereotactic radiotherapy is well suited for treatment of tumors that are highly insensitive to radiation. For example, a dose delivered in 3 treatment fractions of 20 Gy, as often used for lung tumors has the same biological effect as a dose of 150 Gy delivered in fractions of 2 Gy (assuming α/β=10). Note that in the latter case 75 treatment fractions are needed, which is generally considered too high.

Because of the low number of fractions with high doses, the advantage of a higher inter-fraction repair for normal tissue than for tumor tissue is reduced for stereotactic radiotherapy, potentially increasing the risk on late toxicity for the same anti-tumor effect. This higher chance on late toxicity is counteracted by using more focused dose distributions, and the increment in localization and immobilization precision, which allows for smaller target volumes yielding smaller volumes of normal tissue receiving a high dose. The focused dose distributions are characterized by a high degree of conformality of the prescription isodose to the target volume, a high dose fall-off between target volume and normal tissue, and a minimized dose to the organs at risk. This thesis discusses several techniques for more focused stereotactic irradiation of intra-cranial (chapter 2), and extra-cranial (liver) tumors (stereotactic body radiotherapy, SBRT), chapters 3 to 7.

Small intra-cranial tumors ($<$ 2 cm) are often treated with stereotactic arc therapy. With this technique the dose is delivered to the patient with a number of non-coplanar arcs (i.e. out of the patient's axial plane), for which the gantry rotates during irradiation. The beam is shaped with a cone collimator, resulting in a spherical volume that receives a high dose. In chapter 2, a new method for increasing the conformality of the dose distribution to the tumor, in case of a non-spherical tumor, by partial blocking of the cone collimator with the jaws of the linear accelerator, is presented. Measurement of required input data for the treatment planning system (TPS), for fields smaller than 2 cm, are described, together with correction methods for increased electron disequilibrium and the smoothing effect of the detector. The feasibility of the technique was proven by validation of TPS calculations with point dose measurements on the central beam axis and measurements of off-axis dose distributions. Moreover, the advantage of partial cone blocking in arc therapy for small intra-cranial lesions

was shown in a planning study.

To maximize the conformality of a dose distribution to the target volume and the dose fall-off between the target and healthy tissue, and to optimize sparing of organs at risk (OAR), a SBRT treatment plan generally consists of many non-coplanar and coplanar beams. Many beam combinations are possible, and finding the optimal set is not a trivial task. In clinical practice, this step in the treatment planning process is performed by the technician, using a manual trial-and-error procedure. Chapter 3 describes adaptations to an in-house developed beam direction and beam weight optimization algorithm ('Cycle') for SBRT. Important extensions of Cycle for SBRT were inclusion of beam shape optimization, and inclusion of non-coplanar input beams. To study the impact of plan generation with Cycle, automatically generated plans were compared to clinically applied plans, for a set of previously treated patients with a liver tumor. The Cycle plans were optimized by maximizing the minimum planning target volume (PTV) dose, while strictly adhering to the absolute prescribed tumor center dose, and to the imposed OAR constraints. Both coplanar and non-coplanar Cycle plans were compared with the clinical plan. It was demonstrated that automated beam direction optimization with the extended Cycle algorithm substantially improves the therapeutic ratio for SBRT of liver patients, compared to the clinical plan. Furthermore, the Cycle optimized non-coplanar plans were better than the optimized coplanar plans.

In stereotactic radiotherapy, the dose is prescribed to an isodose that closely surrounds the PTV. For SBRT, often prescription isodoses of 65% or 80% are used. In chapter 4, Cycle was used to generate liver SBRT plans, based on dose prescription at the surrounding 65% isodose, or at the 80% isodose. It was concluded that on average the 65% strategy has a better therapeutic ratio than the 80% strategy.

Radiobiological quantities, such as the gEUD(a), are intended as a measure of the biological effect resulting from an inhomogeneous OAR or target dose distribution. In chapter 5, treatment plans with a maximized PTV gEUD(a) (without limitations on other PTV dose parameters) are generated with Cycle, and compared with the strategies using a 65% or 80% prescription isodose. All plans had to strictly comply with the imposed OAR hard constraints. It was demonstrated that on average, gEUD(a) optimization is superior to conventional strategies with a 65% or 80% isodose that closely surrounds the PTV.

In chapter 6, optimized non-coplanar and coplanar beam set-ups for 3D-CRT plans generated with Cycle, are used as input for an external IMRT optimization system (XiO, CMS) to generate optimized IMRT plans. For both the generation of the coplanar and non-coplanar Cycle 3D-CRT plans, and the IMRT plans, the same optimization procedure was used; maximization of the total PTV dose without violation of the OAR constraints. The coplanar and non-coplanar IMRT plans are compared with an IMRT plan with a non-optimized, 11 equi-angular, coplanar beam set-up. It was concluded that the IMRT plans for the optimized, non-coplanar beam set-ups have substantially higher doses delivered to the PTV than both the IMRT plans based on optimized coplanar beam orientations, and IMRT plans generated for the equi-angular set-up. On average, IMRT plans with an optimized coplanar beam set-up had a slightly higher PTV dose than IMRT plans with the 11 equi-angular beam set-up.

Clinical introduction of improved treatment technology, e.g. daily 4D-CT image guidance for SBRT of liver tumors may allow the use of smaller CTV-PTV margins. In chapter 7, Cycle was used to generate treatment plans with different CTV-PTV margins. These plans were compared with a Cycle plan with the clinical CTV-PTV margin. It was concluded that due to decreases in CTV-PTV margin, a considerable improvement in therapeutic ratio can be achieved.

Samenvatting

Het onderwerp van dit proefschrift is behandelplannen voor stereotactische radiotherapie. Stereotactische radiotherapie is een behandelingstechniek voor het bestralen van tumoren met megavolt fotonen bundels. Deze bestralingstechniek onderscheidt zich van conventionele radiotherapie door een verbeterde geometrische nauwkeurigheid bij zowel de lokalisatie als bij het toedienen van de dosis aan de tumor.

Een tweede onderscheid is dat de stralingsdosis wordt toegediend in een klein aantal fracties met een hoge dosis per fractie. Dit heeft een verhoogde biologische schade aan het tumorweefsel en een hogere kans op tumor controle tot gevolg, met name voor tumoren die relatief ongevoelig voor ioniserende straling zijn. Bijvoorbeeld, een dosis van 60 Gy die in 3 fracties van 20 Gy wordt toegediend, heeft hetzelfde biologische effect als een totale dosis van 150 Gy toegediend in fracties van 2 Gy. In het laatste geval zijn 75 fracties nodig, wat onacceptabel hoog is.

Omdat het toedienen van de dosis in een klein aantal fracties ook een relatief hogere biologische schade aan gezond weefsel geeft, is de mate van focussering van de dosis op de tumor uitermate belangrijk. Belangrijke eigenschappen van een dosis verdeling zijn: de mate waarin de isodose, waarop de dosis wordt voorgeschreven, conform met het doelvolume loopt, een hoge dosis gradiënt tussen het doelvolume en het gezonde weefsel en het voldoen aan de dosis limieten voor de verschillende kritieke organen. In dit proefschrift worden een aantal technische verbeteringen voorgesteld en onderzocht voor meer gefocusseerde dosis verdelingen voor stereotactische radiotherapie voor intra-craniale tumoren, hoofdstuk 2, en voor extra-craniale tumoren, hoofdstuk 3-7.

Voor stereotactische radiotherapie van kleine intra-craniale tumoren ($<$ 2 cm) wordt vaak arc therapie gebruikt waarbij de gantry van de lineaire versneller roteert tijdens het stralen. Vanwege de kegelvormige collimator is de bundel cirkelvormig. Voor tumoren die niet bolvormig zijn zou de dosisverdeling meer conform aan de tumor gemaakt kunnen worden als de bundelvorm aangepast zou kunnen worden door middel van het afblokken van de cirkelvormige velden met de collimator blokken van de lineaire versneller. Metingen van de invoerdata voor het treatment planning systeem (TPS), en de correcties voor gebrek aan elektronen evenwicht en het uitsmeer effect ten gevolge van de afmeting van het detectievolume van de detector zijn beschreven. De beschreven methode is gevalideerd door vergelijking van TPS berekeningen met metingen. Voor twee patiënten werd retrospectief een nieuwe behandelplan gemaakt. Beide plannen waren een verbetering ten opzichte van het oude plan,

waarbij geen afblokking van het veld was gebruikt.

In hoofdstuk 3 wordt de aanpassing van een bestaand computer algorithme voor bundel richting selectie en optimalisatie beschreven om het toepasbaar te maken voor treatment planning voor stereotactische behandeling van levertumoren (stereotactic body radiotherapy, SBRT). De aanpassingen bestonden uit het toevoegen van bundels die niet in het axiale vlak van de patiënt liggen (non-coplanaire bundels) en van optimalisatie van de bundelvorm. Klinisch werden bundelrichting en bundelvorm gekozen door een laborant op basis van ervaring. Vanwege het grote aantal vrijheidsgraden is de kans op een suboptimaal planning resultaat groot. Met het aangepaste algoritme is aangetoond dat de behandelplannen, waarbij bundelhoek optimalisatie is toegepast, beter zijn dan de plannen die klinisch worden gebruikt voor 3D-CRT. Daarnaast is aangetoond dat de plannen met bundelhoek optimalisatie, waarbij ook non-coplanaire bundels mogen worden geselecteerd, beter zijn dan plannen waarbij alleen coplanaire bundels mogen worden geselecteerd.

De dosis voor het planning target volume (PTV) wordt voorgeschreven op de isodose die kort rondom het doelvolume loopt. Sommige instituten gebruiken hiervoor de isodose met 80% van de iso-centrum dosis, terwijl andere instituten hiervoor de 65% isodose gebruiken. In hoofdstuk 4 wordt een vergelijking tussen beide strategieën gemaakt. Daarvoor zijn met Cycle plannen gemaakt met zowel de 65% als de 80% strategie. Het blijkt dat de plannen voor de 65% strategie gemiddeld beter zijn dan die voor de 80% strategie. Grootheden als de gEUD(a) worden gebruikt als maat voor het totale radiobiologische effect van een dosisverdeling in een structuur (kritiek orgaan of doelvolume). In hoofdstuk 5 zijn met Cycle plannen gegenereerd waarbij de gEUD van de PTV werd geoptimaliseerd. Deze plannen zijn vergeleken met de plannen van de 80% en de 65% strategie. Het bleek dat de gEUD strategie in betere plannen resulteerde dan de 80% en de 65% strategie.

In hoofdstuk 6 is de combinatie van IMRT met bundelhoek optimalisatie onderzocht. Hiervoor zijn met Cycle voor elke patiënt twee 3D-CRT plannen gegenereerd; een met een coplanaire en een met een non-coplanaire bundel set-up. De bundelrichtingen van deze plannen zijn ingevoerd in het XIO planning systeem. Met dit systeem is vervolgens een geoptimaliseerd IMRT plan gemaakt. Ook is er voor een bundel set-up met 11 coplanaire bundels met een vaste hoekafstand tussen de bundels een geoptimaliseerd IMRT plan gemaakt. Uit de vergelijking tussen de drie verschillende IMRT plannen bleek, dat de IMRT plannen met een non-coplanaire bundel set-up veel beter waren dan die met een coplanaire bundel set-up. Ook de IMRT plannen met een geoptimaliseerde coplanaire bundel set-up waren gemiddeld beter dan de niet geoptimaliseerde coplanaire plannen.

Klinische introductie van meer geavanceerde technologie, bijvoorbeeld 4D-CT, kan leiden tot kleinere CTV-PTV marges en dus kleinere PTVs. In hoofdstuk 7 zijn voor verschillende CTV-PTV marges met Cycle voor SBRT van lever tumoren 3D-CRT plannen gemaakt, welke zijn vergeleken met het Cycle plan met de klinische CTV-PTV marge. Deze vergelijking toont aan, dat door verkleining van de CTV-PTV marge een aanzienlijke toename in de therapeutische ratio behaald kan worden.

Curriculum vitae

Jacco de Pooter was born on the 16th of november 1977 in Terneuzen. After finishing high school in 1996 he started his university studies in applied physics at the Technical University of Delft. During the master phase he performed a three month trainee ship at Philips research in the field of Fresnel diffraction effects in frontlights for liquid-crystal displays. In 2002 Jacco graduated in the field of optical recording on the subject 'Sub-wavelength optical detection using waveguides' at the TU Delft Optics research group.

Then Jacco became a PhD student at the department of radiation oncology at the Erasmus Medical Center (Daniel den Hoed). His main research subjects were dosimetry and treatment plan optimization for stereotactic radiotherapy. The present thesis is the result of this PhD project. At the start of 2007, he continued his career at the dutch national institute for primary standards, NMi van Swinden laboratory. Jacco is married with Lycia. They have two children, Simon en Mathias.

List of Publications

[1] JA de Pooter, HJ Cornelissen, JJM Braat, Fresnel diffraction effects in the frontlight for a liquid-crystal display *Applied Optics* 2002;**41**:5230-7

[2] JA de Pooter, M Essers, PJCM Nowak, C de Pan, BJM Heijmen, PC Levendag, Stereotactic arc therapy for small elongated tumors using cones and collimator jaws; dosimetric and planning aspects *Med Phys*. 2004;**31**:3444 - 51

[3] A Méndez Romero, W Wunderink, SM Hussain, JA de Pooter, BJM Heijmen, PCJM Nowak, JJ Nuyttens, RP Brandwijk, C Verhoef, JNM Ijzermans, PC Levendag. Stereotatic radiotherapy for primary and metastatic liver tumors: a single institution phase I-II study, *Acta Oncol*. 2006;**45**:831-7

[4] JA de Pooter, A Méndez Romero, WPA Jansen, PRM Storchi, E Woudstra, PC Levendag, BJM Heijmen, Computer optimization of non-coplanar beam set-ups improves stereotactic treatment of liver tumors *Int J Radiat Oncol Biol and Phys*. 2006;**66**:913 - 26

[5] JA de Pooter, W Wunderink, A Méndez Romero, PRM Storchi, BJM Heijmen, PTV dose prescription strategies for SBRT of metastatic liver tumors *Radiother Oncol*. 2007;**85**:260-6

[6] BJM Heijmen, JA de Pooter, A Méndez Romero, W Wunderink, E Woudstra, PR Storchi, PC Levendag, Computer generation of fully non-coplanar treatment plans for SBRT of liver tumours based on gEUD optimisation *Proceedings of the 15th International conference on the use of computers in radiation therapy, Toronto, Canada*. 2007:333-37

[7] LA de Prez, JA de Pooter, The new NMi orthovolt x-ray absorbed dose to water primary standard based on water calorimetry *Phys. Med. Biol*. 2008;**53**:3531-42

[8] S Molinelli, JA de Pooter, A Méndez Romero, W Wunderink, MG Cattaneo, R Calandrino, BJM Heijmen, Simultaneous tumour dose escalation and liver sparing in Stereotactic Body Radiation Therapy (SBRT) for liver tumours due to CTV-to-PTV margin reduction *Radiother Oncol*. 2008;**87**:432 - 8

[9] JA de Pooter, A Méndez Romero, W Wunderink, PRM Storchi, BJM Heijmen, Automated non-coplanar beam direction optimization improves IMRT in SBRT of liver metastasis *Radiother Oncol. Accepted for publication*

Dankwoord

Een proefschrift schrijven doe je niet in je eentje. In de loop der jaren hebben veel mensen direct of indirect hier aan bijgedragen door samenwerking in onderzoek of gewoon door hun interesse te tonen in het werk. Al deze mensen wil ik hiervoor van harte bedanken. In het bijzonder wil ik de volgende personen noemen.

Als eerste wil ik mijn promotor Ben Heijmen bedanken. Zijn vermogen om op een andere manier tegen onderzoeksresultaten aan te kijken, zijn kritische vragen en zijn bereidheid om tijd voor je te nemen, hebben niet alleen veel bijgedragen aan dit proefschrift maar het heeft mij ook gevormd als onderzoeker.

Pascal Storchi en Evert Woudstra wil ik bedanken voor de basis die zij al hadden gelegd met Cycle. Vanuit deze basis mocht ik verder werken. Daarnaast kon ik veel van hun ervaring en kennis van treatment plan optimalisatie gebruik maken. Hierdoor is Cycle een essentieel onderdeel geworden van dit proefschrift.

Marion Essers wil ik bedanken voor de directe begeleiding in de eerste anderhalf jaar van mijn onderzoek. Haar enthousiasme voor klinisch fysisch onderzoek heeft mij erg gemotiveerd en heeft veel bijgedragen aan het eerste artikel. Peter Levendag wil ik bedanken voor de stimulerende gesprekken, met name in het begin van het promotie traject. Ook wil ik hem en de andere leden van de promotiecommissie bedanken voor het beoordelen van dit proefschrift.

Connie de Pan wil ik bedanken voor de bijdrage aan het eerste artikel. Door jouw hulp kreeg ik vlot inzicht in de klinische treatment planning voor intra-craniële stereotactie en kon ik me snel alle ins en outs van het XKnife planning systeem eigen maken. In het kader van het eerste artikel wil ik ook Peter Nowak bedanken voor zijn inbreng in de klinische achtergrond voor intra-craniële stereotactie.

De basis voor de fysische kant van het eerste artikel wordt gevormd door een grote hoeveelheid metingen. Erik Loef en Ben Göbel hebben een grote bijdrage geleverd aan deze metingen. Dank voor jullie meedenken en de tijd die jullie er ook 's avonds in hebben willen steken.

Alejandra Méndez en Wouter Wunderink bedankt voor de samenwerking in de 'lever' groep. Jullie inbreng op de artikelen en de discussies over de SBRT behandeling waren boeiend en motiverend. Wim Jansen bedankt voor jouw inbreng in het tweede artikel. Jouw idee van toepassen van Cycle voor lever plannen licht aan de basis van dit artikel.

Also many thanks to Silvia Molinelli. It was a pleasure to cooperate with you in the

research on the influence of decreasing CTV-PTV margins. You got used to Cycle very quickly, which speed up the research considerably.

Op de afdeling fysica heb ik me alle jaren goed thuis gevoeld. Naast het boeiende werk en de prettige sfeer was er ook ruimte voor gezelligheid in de vorm van de jaarlijkse SOEP. Veel dank ben ik ook schuldig aan de automatiseringsgroep, vragen of problemen met XIO CadPlan, Virgo of welk systeem dan ook, ze werden altijd opgelost. Martijn Hol wil ik bedanken voor de tijd als kamergenoot, waarin we naast het werk ook de politiek en de sportwereld konden bespreken.

Tot slot wil ik mijn ouders bedanken voor hun liefdevolle steun. Lang voordat ik nog maar aan promoveren dacht, waren jullie al bezig met mij te motiveren, mijn vragen te beantwoorden, en mij op te voeden. Pa en Ma, bedankt dat jullie er al die tijd voor mij waren. Dezelfde liefdevolle steun ontvang ik ook thuis van Lycia. Samen met onze jongens ben je een grote stimulans voor mij.